

Heavy metals and persistent organic pollutants: New developments.

EMEP/MSC-E Technical Report 4/2012

DRAFT



EMEP/MSC-E Technical Report 4/2012

August 2012

Heavy Metals and Persistent Organic Pollutants: New Developments.

Shatalov V., Ilyin I., Gusev A., Rozovskaya O., Sokovykh V.,
Travnikov O., Vulykh N., Wiberg K. and Cousins I.

DRAFT

Meteorological Synthesizing Centre - East
Krasina pereulok, 16/1
123056 Moscow
Russia
Tel.: +7 495 981 15 67
Fax: +7 495 981 15 66
E-mail: msce@msceast.org
Internet: www.msceast.org

CONTENTS

INTRODUCTION	5
PART I. HM MODELLING	7
Chapter I.1. DEVELOPMENT OF ADJOINT APPROACH FOR THE ASSESSMENT OF HM ENVIRONMENTAL CONTAMINATION	8
I.1.1. Formulation of adjoint model	8
I.1.2. Testing of adjoint model results by the transport of Pb over EMEP domain	12
I.1.3. Optimization of measurement-to-calculation agreement with the help of emission scenarios	16
Chapter I.2. TESTING WET DEPOSITION SCHEME FOR THE CZECH STATIONS	19
Chapter I.3. EVALUATION AND MODIFICATION OF WIND RE-SUSPENSION SCHEME	25
PART II. POP MODELLING	39
Chapter II.1. INVESTIGATION OF DEGRADATION OF POPS IN PARTICLE-BOUND FORM	40
II.1.1. Kinetics of heterogenic reactions	40
II.1.2. Chemical composition of atmospheric aerosol	55
Chapter II.2. ADJUSTMENT OF EMISSION DATA FOR MODELLING	64
II.2.1. Temporal variability of POP emissions	64
II.2.2. Congener composition of emissions	71
REFERENCES	87
Annex A. B[A]P DEGRADATION PRODUCTS	95
Annex B. OBSERVEF OC MASS CONCENTRATIONS	100

INTRODUCTION

The work on the refinement of model approaches to evaluation of environmental contamination by POPs is carried out by MSC-E permanently. The present report is aimed at the description of the activities on the refinement of models, input data for modelling (particularly, emission data) and the development of complex monitoring/modelling/emission approach carried out in 2012.

The report is divided into two parts concerning assessment of environmental contamination by heavy metals (HMs) and persistent organic pollutants (POPs), respectively. This division is to some extent conditional since the results obtained for one of these two pollutant groups can be applied in future for the other. For example, adjoint modelling approach, which is now elaborated for HMs, will be further developed for the application to POP assessment.

The work on elaboration of complex monitoring/modelling/emission approach is continued in the current year by elaboration of adjoint model for HMs. The formulation of this model and testing the agreement between predictions of direct and adjoint models is described in I.1.1 and I.1.2. Section I.1.3 contains an example of application of adjoint model to the analysis of agreement between measurement and model results. For the demonstration of such analysis the comparison of calculations of Pb transport and deposition in 2007 with measurements at EMEP site Kosetice (CZ3) are used. The comparison was performed by the optimization procedure worked out by MSC-E.

Chapter I.2 contains the evaluation of wet deposition scheme for HMs used in MSCE-HM model on the basis of results obtained for the Czech Republic in the course of the EMEP Case Study on heavy metal pollution assessment for individual countries started in 2009. For the evaluation eight priority background regional stations with co-located measurements (i.e., measurements of concentrations both in air and in precipitation) were used. The Chapter contains sensitivity study for calculated values of wet deposition with respect to in-cloud and below-cloud scavenging parameters. Further steps of investigation of HMs wet removal from the atmosphere can be aimed at modification of vertical distribution of the pollutant in the atmosphere. In particular, another approach to distribute emissions along vertical in the model can be applied. Besides, modification of the model by introduction of convective mixing process can be considered.

Evaluation and testing of wind resuspension scheme used in the MSCE-HM model is considered in Chapter I.3. Inclusion of wind re-suspension process in modelling of heavy metal transport and deposition favoured improving of modelling results for the EMEP region as whole. In particular, it helped reducing significant underestimation of modelled concentrations in air and wet deposition of lead and cadmium compared to the observed values. However, at some cases the use of wind re-suspension scheme leads to overestimation of the observed concentrations in air. It was demonstrated that wind-driven re-suspension of dust particles to the atmosphere from the agricultural lands, adapted in the model, is overestimated. Investigations described in the Chapter allowed selecting optimal set of parameters for updating model wind re-suspension scheme.

Chapter II.1 is devoted to the review of the investigations of B[a]P degradation in the atmosphere due to heterogenic reactions (namely, oxidation and nitration) taking place at aerosol surface. The Chapter contains the description of rate constants for the above reactions found in the literature (Section II.1.1). Since reaction rates strongly depend on chemical nature of aerosol-carrier, the review of the data on environmental levels and chemical composition of atmospheric aerosol was carried out (Section II.1.2). At present the problem of determination of spatial distribution of organic carbon composition in aerosols is not completely solved. In particular, large uncertainties in modeling of the levels of organic compounds in the atmosphere are connected with secondary organic aerosol. So,

further investigations on kinetics of heterogenic reactions between PAHs and ozone/nitrous atmospheric compounds and on chemical composition of atmospheric aerosol are needed.

Finally, Chapter II.2 is aimed at the adjustment of emission data used for modeling. Two issues are considered in the Chapter: temporal variations of emissions and congener composition of complex chemical mixtures. Temporal variations of emissions can essentially affect environmental pollution by some pollutants such as PAHs and PCDD/Fs, whose emissions from residential heating are essential. Due to the seasonal variability of degradation rates, temporal variations of emissions can affect not only monthly but also annual means of air concentrations of the above pollutants. Section II.2.1 describes possible approach to evaluation of temporal variability of emissions from residential heating on the example of B[a]P. Further, congener composition of complex chemical mixtures' emissions can be of extreme importance for environmental modelling. In particular, model evaluation of total toxicity of PCDD/F mixture requires simulating the transport of 17 toxic (2,3,7,8 - substituted) PCDD/F congeners separately to take into account differences in their physical-chemical properties leading to the corresponding differences in their fate in the environment. Section II.2.2 presents possible approach to determination emission congener composition by inverse modelling approach on the basis of available measurements of PCDD/F congener composition of atmospheric concentrations.

Part I.

HM MODELLING

Chapter I.1.

Development of adjoint approach for the assessment of HM environmental contamination

The evaluation of sensitivity of POP pollution to the values of emissions at various locations is an essential part of the general analysis of contamination in the European region. In particular, the necessity of such evaluation arises in the course of the analysis of discrepancies between measurement data and model calculations or for the investigation of source contributions to the contamination in the given country/region. The sensitivity of any **target parameter** P characterizing the pollution (such as air concentration or deposition in a given grid cell, concentration of a pollutant averaged over the country/region and certain period, etc.) with respect to emissions in a given grid cell is defined as the value of this parameter originated by unit emissions in the considered grid cell.

If the sensitivities of a target parameter P are known for each grid cell, then the value of this parameter generated by arbitrary emission distribution can be calculated as the sum of emission values multiplied by the corresponding sensitivities over all grid cells with non-zero emissions. The set of sensitivities of the given parameter for all grid cells is known as the **influence function** for this parameter. For brevity, we restrict ourselves by consideration of averages of air concentrations over given regions and time periods.

Several methods of approximate evaluation of the influence function are known. First (and the simplest) method is based on the calculation of densities of trajectories of air masses arriving to the considered region within the selected time period. This method was implemented for the evaluation of the contamination by B[a]P in the EMEP region in [Ilyin *et al.*, 2010]. Earlier this approach was successfully implied for evaluation of radioactivity pollution from Chernobyl accident [Persson *et al.*, 1987]. In particular, it was found that for correct evaluation of influence function it is necessary to include in the calculations at least degradation process of B[a]P. However, such an approach does not allow taking into account such important process as atmospheric eddy diffusion (see the discussion in [Robertson, 2004]).

To include all transport mechanisms in the evaluation of the influence function adjoint (dual) equation approach can be used. This approach is based on the fact that the influence function for the given target parameter satisfies the so-called adjoint equation. Applications of adjoint approach to environmental problems were first outlined by [Marchuk, 1986; Uliasz, 1987]. Further this approach was applied for various pollutants by a lot of authors (see, e.g., [Hakami *et al.*, 2005; Villani *et al.*, 2010; Baklanov *et al.*, 2011] and others).

I.1.1. Formulation of adjoint model

Here the problem of calculation of atmospheric transport and deposition of heavy metals over the EMEP domain is considered (direct problem). Model description of the problem used at present in MSC-E takes into account the following processes:

- atmospheric advection;
- diffusion in the vertical direction;
- wet and dry deposition of the pollutant considered.

Mathematical formulation of this problem is as follows.

Main equation has the form:

$$\frac{\partial c}{\partial t} + \text{div}(c\vec{v}) - \frac{\partial}{\partial z} \left(K_z \frac{\partial c}{\partial z} \right) + \alpha c = e, \quad (1)$$

Where c is the pollutant air concentration (kg/m³);

\vec{v} is three-dimensional distribution of the wind speed (m/s);

K_z is the coefficient of vertical turbulent diffusion (m²/s);

α is the coefficient of removal from the atmosphere due to wet deposition (1/s);

e is emission flux to the atmosphere (kg/m³/s).

The equation is considered on the time period from 0 to T in three-dimensional domain over the EMEP region with upper boundary changing in space and time according to meteorological conditions. In fact, the model is formulated in sigma-coordinates which automatically determine the upper boundary of the domain. Below the EMEP domain is denoted as D_{EMEP} , and upper boundary as $z(x, y, t)$.

To complete the statement of the direct problem initial and boundary conditions are to be set.

Initial condition for equation (1) is given at $t = 0$:

$$c|_{t=0} = c_0, \quad (2)$$

where $c_0(x, y, z)$ is initial spatial distribution of the atmospheric concentration of the pollutant.

It is assumed that the value of pollutant concentration at the upper boundary of the calculation domain equals zero:

$$c|_{z=z(x, y, t)} = 0. \quad (3)$$

The boundary condition at the lower boundary $z = 0$ has the form:

$$K_z \frac{\partial c}{\partial z} + v_d c \Big|_{z=0} = 0 \quad (4)$$

describing the process of dry deposition of the pollutant with deposition velocity v_d .

Boundary conditions at the lateral boundary B_{EMEP} of the EMEP domain should be put on the part of this boundary at which wind velocity is directed inside D_{EMEP} . This part will be further denoted as $D_{\text{EMEP}}^{\text{in}}$, and the rest part as $D_{\text{EMEP}}^{\text{out}}$. It should be taken into account that these parts depend on time. Then boundary conditions on the lateral boundaries are written in the form

$$c|_{B_{\text{EMEP}}^{\text{in}}} = c_b, \quad (5)$$

where c_b are known values of boundary concentrations.

Equation (1) with conditions (2) – (5) forms the full formulation of the direct problem.

It often happens that some integral characteristics of pollution (**target parameters**) are of particular interest together with spatial distribution of air concentrations. These may be concentration averages over particular regions and time periods, wet and dry deposition mass deposited over particular regions during specified time periods, etc. Mostly, such characteristics can be expressed via concentrations by:

$$P = \int_0^T dt \int_{D_{EMEP}} dx dy \int_0^{z(x,y,t)} \chi(x,y,z,t) \cdot c(x,y,z,t) dz, \quad (6)$$

where $\chi(x,y,z,t)$ is a function determining the target parameter which will be referred below as the *density of the target parameter*. For example, if $\chi(x,y,z,t) = (T \cdot V)^{-1}$ inside some domain with volume V and zero outside this domain, formula (6) defines average concentration over the domain for the period from 0 to T . Such characteristics can be calculated directly from concentration field if the latter is calculated for the given emission distribution. However, if one is interested, for example, by the sensitivity of the given characteristic to emission distribution, for calculations of the considered characteristic the direct problem should be solved for each particular emission distribution separately. The same concerns to the case when optimization of the agreement between measurements and model predictions is considered.

There is a way to avoid repeated solving of the direct problem for various emission distributions by calculating the so-called influence function $\psi(x,y,z,t)$ for the given target parameter P such that the value of this parameter can be calculated as an integral:

$$P = \int_0^T dt \int_{D_{EMEP}} dx dy \int_0^{z(x,y,t)} \psi(x,y,z,t) \cdot e(x,y,z,t) dz \quad (7)$$

provided that initial concentrations c_0 and boundary concentrations c_b equal zero (more general formula is given below). Such function can be calculated with the help of so-called adjoint problem and allows calculating the given characteristic P for any emission distribution in a simple manner. It should be however stressed that to consider another characteristic requires repeated solving of the dual problem.

The aim of this section is to derive the expression for the adjoint problem including its main equation, initial and boundary conditions. To do that, we multiply equation (1) by (arbitrary at the moment) function ψ and integrate the result from 0 to T and over the EMEP domain D_{EMEP} . Below the integrals of all five terms in equation (1) are considered separately. The aim of the following calculations is to derive main equation and initial and boundary conditions for ψ such that formula (7) takes place. The integral of the first term on the left in (1) is

$$\int_0^T dt \int_{D_{EMEP}} dx dy \int_0^{z(x,y,t)} \psi \frac{\partial c}{\partial t} dz = - \int_{D_{EMEP}} dx dy \int_0^{z(x,y,t)} c_0 \psi \Big|_{t=0} dz - \int_0^T dt \int_{D_{EMEP}} dx dy \int_0^{z(x,y,t)} c \frac{\partial \psi}{\partial t} dz \quad (8)$$

under the assumption that $\psi|_{t=T} = 0$ and taking into account initial condition (2) for concentrations.

Using the Gauss formula, integral of the second term on the left in (1) can be rewritten in the form:

$$\begin{aligned}
\int_0^T dt \int_{D_{EMEP}} dx dy \int_0^{z(x,y,t)} \psi \cdot \text{div}(c\bar{v}) dz = & - \int_0^T dt \int_{D_{EMEP}} dx dy \int_0^{z(x,y,t)} c \cdot (\bar{v}, \nabla) \psi dz + \\
& + \int_0^T dt \int_{B_{EMEP}^{in}} ds \int_0^{z(x,y,t)} c_b \cdot \psi(\bar{v}, \bar{n}) \Big|_{B_{EMEP}^{in}} dz \quad (9)
\end{aligned}$$

under the assumption that $\psi \Big|_{B_{EMEP}^{out}} = 0$. Here ds is area element along lateral EMEP boundary and \bar{n} is the external normal to this boundary.

Integration by parts with respect to z variable allows reducing the integral of the fourth term on the left in (1) to the form:

$$\int_0^T dt \int_{D_{EMEP}} dx dy \int_0^{z(x,y,t)} \psi \frac{\partial}{\partial z} \left(K_z \frac{\partial c}{\partial z} \right) dz = \int_0^T dt \int_{D_{EMEP}} dx dy \int_0^{z(x,y,t)} c \frac{\partial}{\partial z} \left(K_z \frac{\partial \psi}{\partial z} \right) dz \quad (10)$$

under the assumptions: $\psi \Big|_{z=z(x,y,t)} = 0$ and $K_z \frac{\partial \psi}{\partial z} + v_d \psi \Big|_{z=0} = 0$.

The integrals of the last term on the left and of the only term on the right do not require transformations. Collecting equations (8) – (10) together, we obtain:

$$\begin{aligned}
\int_0^T dt \int_{D_{EMEP}} dx dy \int_0^{z(x,y,t)} c \left\{ -\frac{\partial \psi}{\partial t} - (\bar{v}, \nabla) \psi - \frac{\partial}{\partial z} \left(K_z \frac{\partial \psi}{\partial z} \right) + \alpha \psi \right\} dz = & \int_0^T dt \int_{D_{EMEP}} dx dy \int_0^{z(x,y,t)} \psi e dz + \\
& \int_{D_{EMEP}} dx dy \int_0^{z(x,y,t)} c_0 \psi \Big|_{t=0} dz - \int_0^T dt \int_{B_{EMEP}^{in}} ds \int_0^{z(x,y,t)} c_b \cdot \psi(\bar{v}, \bar{n}) \Big|_{B_{EMEP}^{in}} dz \quad (11)
\end{aligned}$$

Now if, in addition to the above conditions, the function ψ satisfies the equation:

$$-\frac{\partial \psi}{\partial t} - (\bar{v}, \nabla) \psi - \frac{\partial}{\partial z} \left(K_z \frac{\partial \psi}{\partial z} \right) + \alpha \psi = \chi, \quad (12)$$

where χ is the density of the considered parameter (see formula (6)), then formula (11) determines the values of the parameter P via emission e , boundary c_b and initial c_0 data directly avoiding solving the direct problem:

$$P = \int_0^T dt \int_{D_{EMEP}} dx dy \int_0^{z(x,y,t)} \psi e dz + \int_{D_{EMEP}} dx dy \int_0^{z(x,y,t)} c_0 \psi \Big|_{t=0} dz - \int_0^T dt \int_{B_{EMEP}^{in}} ds \int_0^{z(x,y,t)} c_b \cdot \psi(\bar{v}, \bar{n}) \Big|_{B_{EMEP}^{in}} dz \quad (13)$$

Initial and boundary conditions for the solution of the adjoint problem derived above are

$$\psi \Big|_{t=T} = 0, \quad (14)$$

$$\psi|_{z=z(x,y,t)} = 0, \quad (15)$$

$$K_z \frac{\partial \psi}{\partial z} + v_d \psi|_{z=0} = 0, \quad (16)$$

and

$$\psi|_{B_{EMEP}^{out}} = 0. \quad (17)$$

It should be understood that, since initial data for equation (12) is given at $t = T$ instead of $t = 0$, this equation should be solved in the inverse time from T to 0. This is the first difference between equations (1) and (12). The second difference is that the second terms on the left are of opposite signs in (1) and (12) and have different forms. To eliminate this difference, equation (12) can be rewritten as

$$-\frac{\partial \psi}{\partial t} - \text{div}(\psi \bar{v}) - \frac{\partial}{\partial z} \left(K_z \frac{\partial \psi}{\partial z} \right) + (\alpha + \text{div} \bar{v}) \psi = \chi, \quad (18)$$

Boundary and initial conditions (14) – (16) have the same form as for the direct problem.

So, it can be seen that the direct problem can be used for solving the dual problem with the following modifications:

- solving the problem in the inverse time;
- changing the sign of all velocities to the opposite one;
- substituting $\alpha + \text{div} \bar{v}$ instead of α .

Taking this into account, the direct model with the above modifications was applied for solving the dual problem. Of course, uncertainties arising from replacing exact problem by its discrete analogue can lead to uncertainties in calculating the chosen characteristic with the help of the dual approach, and the accuracy of the discrete analogue of formula (13) should be examined. This will be performed in the next section.

I.1.2. Testing of adjoint model results by the transport of Pb over EMEP domain

Calculation results

For illustration of the results that can be obtained by the adjoint model and for testing the applicability of adjoint approach the following model runs were performed:

1. The run of dual model for meteorology data of 2009 with monthly averages of Pb air concentrations in cell (72,50) as target parameters (the cell is that containing Kosetice station).
2. The run of the direct model with emissions of six European countries separately (Belgium, the Czech Republic, Germany, Finland, Italy and Poland). These countries make different

contributions to the concentrations in the considered cell due to their location and emission totals.

The result of calculations by the dual model is the set of influence functions for monthly averages of air concentrations at Kosetice station for all months of 2009. Examples of spatial distribution of influence coefficients (influence function) in the surface atmospheric layer for monthly averages in April and June are shown in Fig. 1.

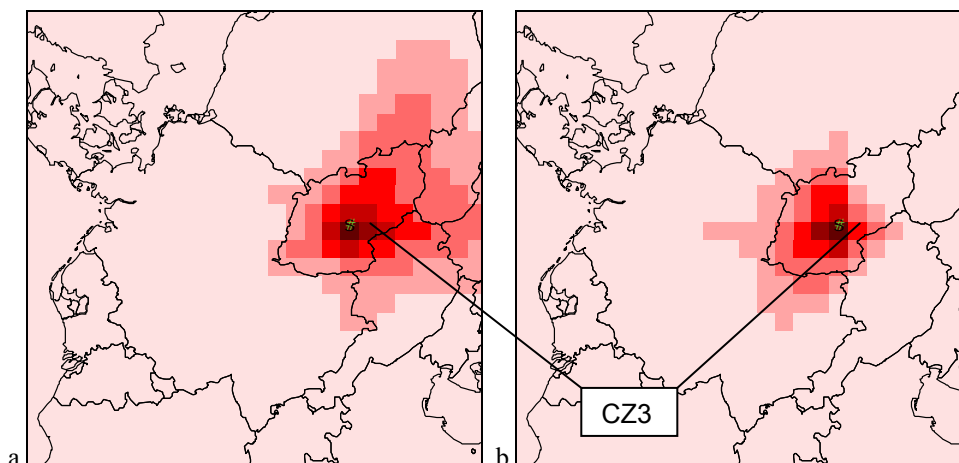


Fig. 1. Influence function for April (a) and June (b)

After calculating the influence functions for monthly means concentration levels with any given emission distribution can be calculated in a very simple manner. For example, spatial distribution of German emissions (to the surface atmospheric layer) is shown in Fig. 2.

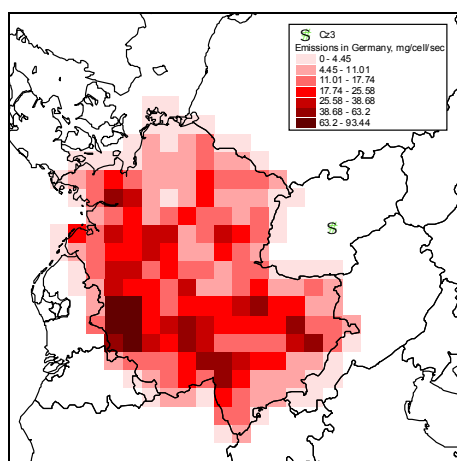


Fig. 2. Spatial distribution of emissions of Pb in Germany in 2009 used in calculations, mg/cell/sec

Multiplying emission values by influence coefficients in each grid cell we obtain contributions of emissions of each grid cell to the monthly averages of air concentrations at Kosetice station (Fig. 3).

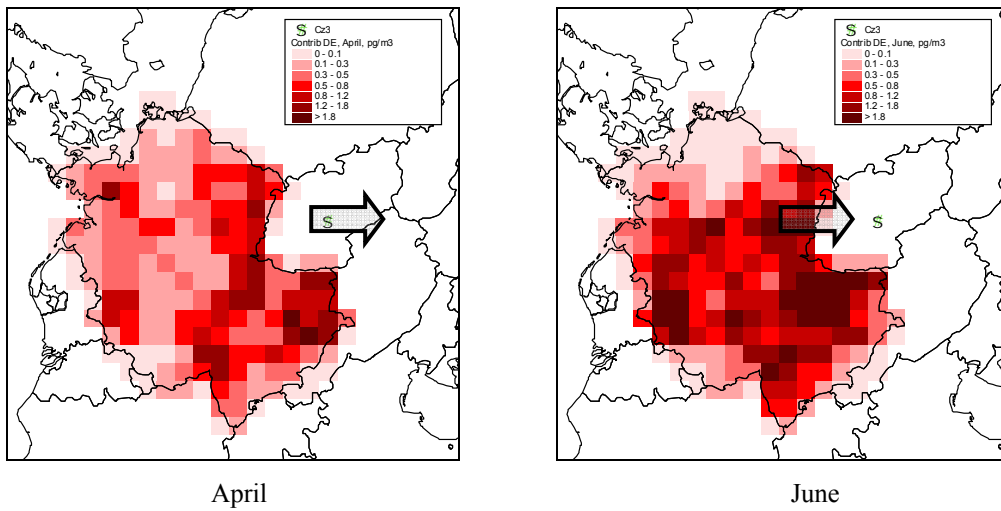


Fig. 3. Contributions from German sources to air concentrations at Kosetice, pg/m^3

Further, spatial distribution of Polish emissions (to the surface atmospheric layer) is shown in Fig. 4.

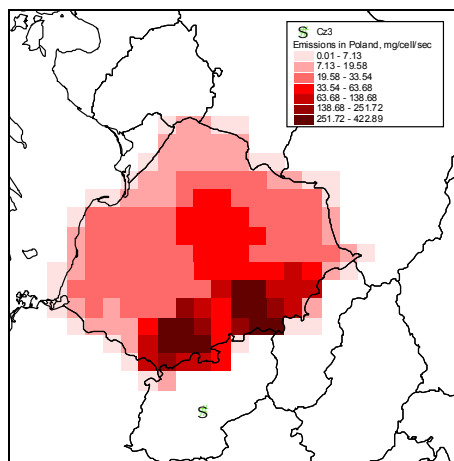


Fig. 4. Spatial distribution of emissions of Pb in Poland in 2009 used in calculations, $\text{mg}/\text{cell}/\text{sec}$

The contributions of Polish emissions of each grid cell to the monthly averages of air concentrations at Kosetice station calculated on the basis of influence function are given in Fig. 5.

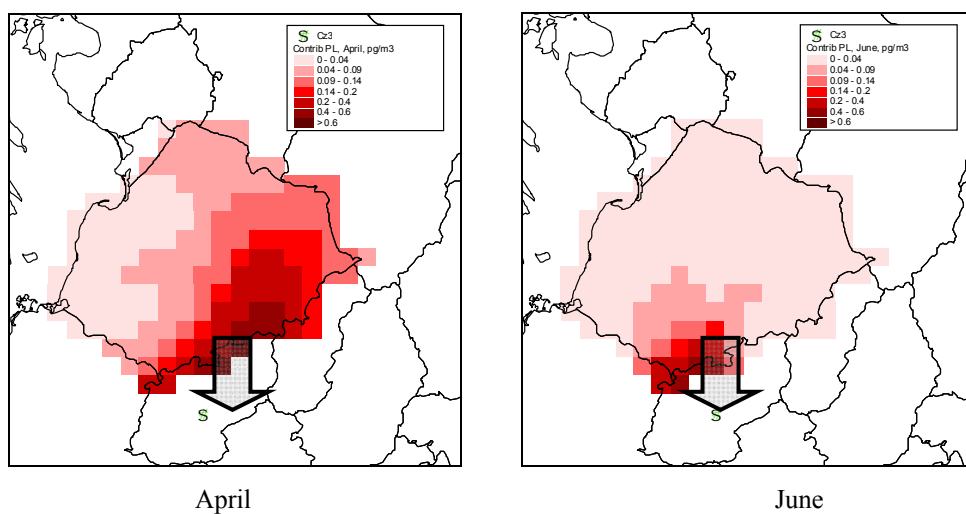


Fig. 5. Contributions from German sources to air concentrations at Kosetice, pg/m^3

Testing of the adjoint model

To test the adjoint model, the values of the calculations of monthly and annual averages of air concentrations obtained by the direct model were compared with the evaluation of these concentrations via the influence function calculated by the adjoint model using formula (7) above. The following figure compares contributions of the considered countries to air concentrations in Kosectice on the annual basis *calculated* by the direct model with those *estimated* with the help of influence function.

The contributions are in the range from 0.0006 ng/m³ for Finland to 0.53 ng/m³ for Poland. The range of differences between model calculations and estimates with the help of the influence function is 2% – 30%. Maximum differences calculated for Belgium (20%) and Finland (29%). For the rest countries the differences do not exceed 20%.

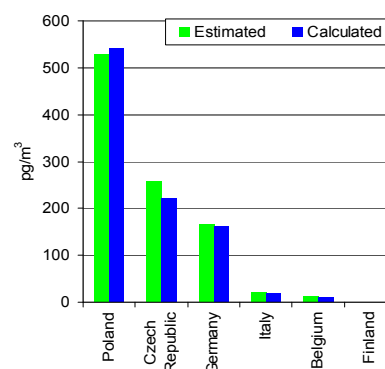


Fig. 6. Contributions of various sources to air concentrations in Kosectice (Pb, 2009), annual averages

Comparison on a monthly basis

Contributions of the considered countries to monthly means of air concentrations at Kosectice are shown by plots in the Fig. 7.

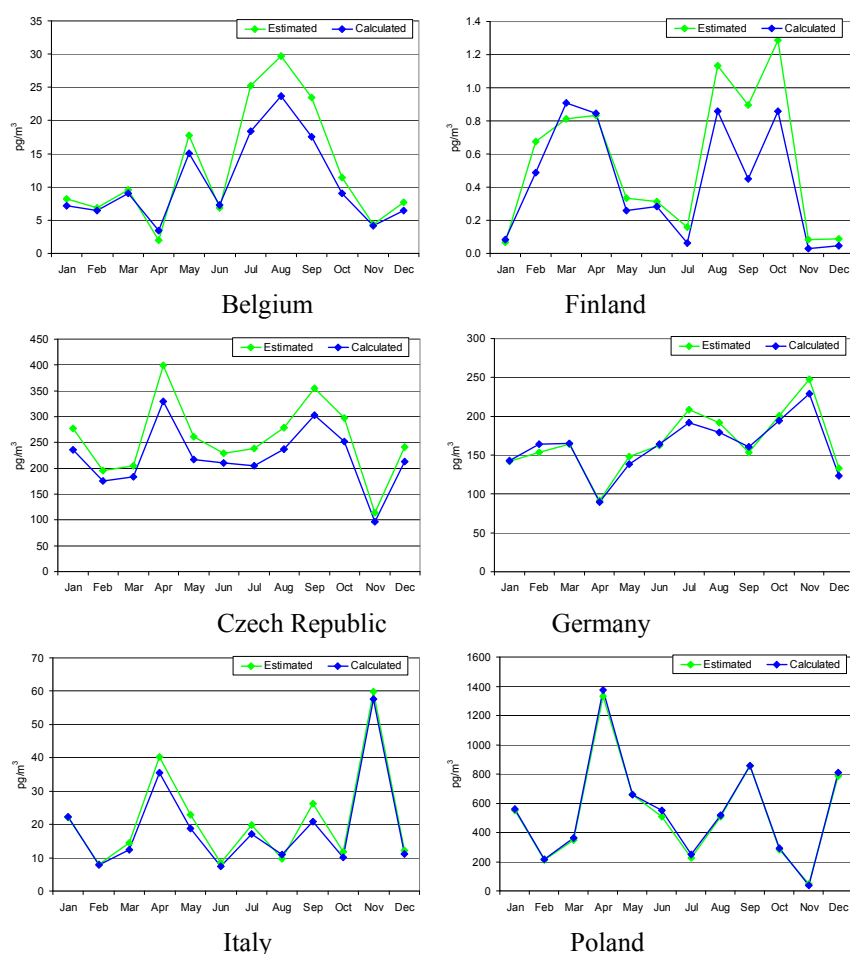


Fig. 7. Contributions of the considered countries to monthly means of air concentrations at Kosectice

Possible reasons of discrepancy may be splitting by processes and uncertainties in calculation of vertical wind velocity. In any case, the considered comparison shows that the values of influence function obtained by running the adjoint model can be applied to the optimization of the agreement between measurements and model calculations by constructing emission scenarios. The example of such application is considered in the next section.

I.1.3. Optimization of measurement-to-calculation agreement with the help of emission scenarios

As explained in Section I.1.2, contributions of various emission sources to the contamination at the given location can be calculated on the basis of the corresponding influence function and emission spatial distribution. This data can be used for the construction of emission scenarios for optimization of the agreement between model calculations and measurement data at particular monitoring sites.

Here the optimization procedure is demonstrated by the analysis of agreement between measurements and model results at Kosetice site in 2007 on the monthly basis. Influence functions for monthly means of Pb air concentrations at Kosetice were calculated by the above described adjoint model. The values of influence function in the cell (i, j) in the month m are denoted by $\gamma_{ij,m}$. Further, emissions used in modeling are split into four groups: emissions from anthropogenic sources $e_{ij,m,anthr}$ and emissions due to re-suspension from bare soils, urban areas and arable soils ($e_{ij,m,bare}$, $e_{ij,m,urban}$, and $e_{ij,m,arable}$, respectively). Using this information, contributions of emissions of each group in each grid cell to the concentrations at Kosetice site in the month m can be calculated as products of the influence function values by the values of the corresponding emissions:

$$\begin{aligned} c_{ij,m,anthr} &= \gamma_{ij,m} \cdot e_{ij,m,anthr}, & c_{ij,m,urban} &= \gamma_{ij,m} \cdot e_{ij,m,urban}, \\ c_{ij,m,bare} &= \gamma_{ij,m} \cdot e_{ij,m,bare}, & c_{ij,m,arable} &= \gamma_{ij,m} \cdot e_{ij,m,arable}. \end{aligned} \quad (19)$$

Total concentration at the considered site in month m can be then evaluated as a sum of all contributions over all grid cells.

The optimization of emissions is carried out by multiplication of emissions at each grid cell by a *correction coefficient* $\alpha_{ij,g}$ (being one and the same for each month but different for different source groups). Here the index g stands for source group, $g = 1, \dots, 4$ for emissions from anthropogenic sources, bare soil, urban areas and arable lands, respectively. Taking into account that the contribution of the emissions in a given cell to the concentration is directly proportional to the emission value, the concentration c_m^{calc} at Kosetice site in the month m is then given by:

$$c_m^{calc} = \sum_{g=1}^4 \sum_{i,j} \alpha_{ij,g} \cdot \gamma_{ij,m} \cdot e_{ij,m,g}. \quad (20)$$

Further, if c_m^{meas} is monthly means of air concentrations measured at Kosetice in the month m , the quadratic error between measurements and model prediction can be calculated as:

$$QE = \sum_{m=1}^{12} \left(c_m^{meas} - \sum_{g=1}^4 \sum_{i,j} \alpha_{ij,g} \cdot \gamma_{ij,m} \cdot e_{ij,m,g} \right)^2. \quad (21)$$

The optimization procedure is the optimal choice of correction coefficients for each grid cell and each of source groups for minimizing the value of quadratic error (21).

It should be taken into account that the above optimization procedure can be ill-conditioned due to the possibility of usage grid cells with very small contributions together with large values of correction coefficients. To avoid this, two regularizing conditions are used:

- Only grid cells with concentration contributions exceeding a threshold level are used in optimization. The threshold levels are chosen depending on source group.
- The values of correction coefficients are searched within the given range (also dependent on a source group).

The threshold levels and ranges of correction coefficients are chosen so that the results of optimization are reasonable.

The described optimization procedure is realized with the use of steepest descent method in the domain determined by the chosen ranges of correction coefficients. Besides, it is possible to perform optimization with additional restriction of conservation of emission totals in all European countries.

The results of optimization for the following ranges of correction coefficients:

- anthropogenic sources – from 0.5 to 2;
- other sources (re-suspension) – from 0.1 to 10

are presented in Fig. 8. The ranges of correction coefficients used approximately correspond to the expected range of uncertainties of emissions of corresponding source groups.

It is seen that the agreement between measurements and modeling results is essentially refined by the application of adjustment procedure. Correlation coefficient between measurements and calculations have been increased from 0.74 to 0.89. The range of measurement-to-calculation factor became from 1.07 to 1.52 compared with the range from 1.03 to 2.00 for initial (non-optimized) calculations.

It is also interesting to analyze the influence of different source groups on refining the agreement between measurements and calculations. To reveal this influence, optimization procedure was applied for correction anthropogenic and re-suspension sources separately with same ranges of correction coefficients. The result of optimization procedure changing anthropogenic emission only (at maximum 2 times) is shown in Fig. 9. For optimization due to anthropogenic emission only correlation coefficient between model results and measurements is enlarged to 0.77 only and the range of measurement-to-calculation ratio becomes from 1.11 to 1.56. It can be seen also that the refinement of the agreement takes place mainly from May to December whereas in the period from January to April no essential improvement takes place. The agreement in April became even worse.

If only re-suspension emission sources are optimized, the result is quite different (see Fig. 10). For this case correlation coefficient has been increased up to 0.86, and range of measurement-to-calculation factor became from 1.06 to 1.46. It is seen also that the improvements conditioned by changes in re-

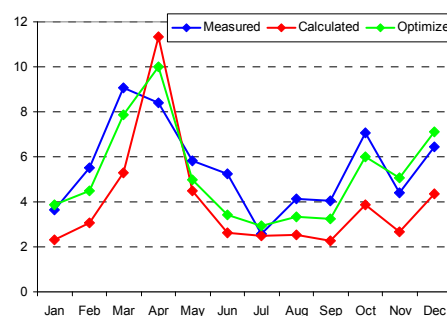


Fig. 8. Results of optimization procedure for Pb concentrations in 2007.

suspension flux occur mainly in the period from January to May, whereas in other months the refinement is worse.

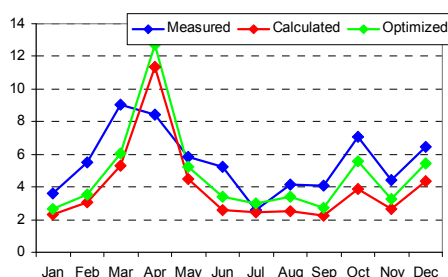


Fig. 9. Results of optimization procedure for Pb concentrations in 2007 with correction of anthropogenic emissions only.

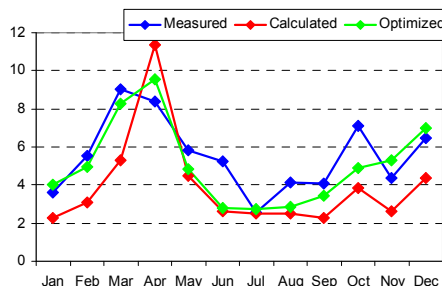


Fig. 10. Results of optimization procedure for Pb concentrations in 2007 with correction of emissions due to re-suspension only.

So, the refinement of both anthropogenic emissions and emissions from re-suspension leads to the improvement of the agreement between measured and calculated monthly averages throughout the entire year and leads to the best results.

It is also interesting to see spatial distribution of correction coefficients showing the rates of enlarging/diminishing concentrations (see Fig. 11). It is seen that maximum values of correction coefficients are obtained for some locations in Black Triangle and in several cells in Poland, Austria and the Czech Republic.

The considered optimization process enlarges, in particular, anthropogenic emissions in countries. It is also interesting to analyze if corrections of spatial distributions of emissions without enlarging emission totals in countries can lead to the refinement of measurement-to-calculation agreement. Fig. 12 demonstrates the results of such optimization procedure in which changing of emissions in particular cells up to 10 times is allowed. In general, the results of this optimization are similar to that considered above when optimization of all emission groups was performed. The results are slightly worse (for example, correlation coefficient obtained by corrections of spatial distribution only is 0.86 against 0.89 for optimization spatial distribution and emission totals). However, the results show that one can restrict himself by refinement of spatial distribution of anthropogenic emissions without essential loss of accuracy.

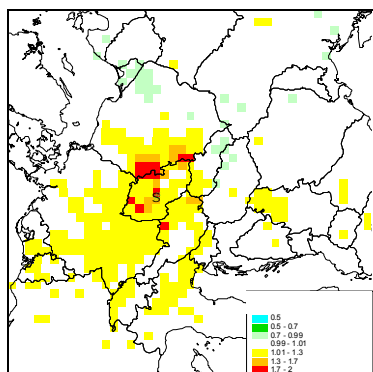


Fig. 11. Spatial distribution of correction coefficients for anthropogenic emissions.

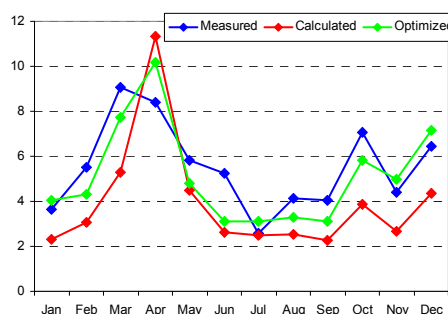


Fig. 12. Results of optimization procedure for Pb concentrations in 2007 (change of spatial distribution only).

Chapter I.2.

TESTING WET DEPOSITION SCHEME FOR THE CZECH STATIONS

EMEP Case Study on heavy metal pollution assessment for individual countries started in 2009. The main objective of the study is to improve assessment of pollution levels in the EMEP domain on the base of the integrated analysis of factors affecting quality of the assessment including emissions, measurements, and modelling with fine (e.g., 5x5 km, 10x10 km) spatial resolution in individual countries [Ilyin *et al.*, 2011]. Several countries were involved into this activity. Here testing model description of wet deposition scheme will be performed on the basis of the data obtained from experts from the Czech Republic.

We recall that eight priority background regional stations with co-located measurements (i.e., measurements of concentrations both in air and in precipitation) were selected for the detailed analysis of pollution levels in the country. Analysis of modelling results calculated with 5-km spatial resolution demonstrated that annual mean air concentrations were reproduced relatively well compared to measurements. Relative bias does not exceed 1% for the totality of stations and it ranges from -22% to +42% for individual stations. NRMSE varies from 0.7 to 1.4. Moreover, the transition from 50-km to 5-km resolution resulted to some improvement of the model performance in terms of comparison with observed values (see the above cited report).

However, annual mean wet deposition fluxes were largely underestimated at a number of priority stations selected for the analysis. At station Bily Kriz the underestimation made up 40%, at station Na Lizu - about 30%. At other stations the underestimation varied from factor 2.2 to 6 (Fig. 13). At the same time, the comparison of annual precipitation amounts observed at stations and simulated by meteorological driver, do not differ much. At station Bily Kriz the modelled precipitation are below the observed one by about 30%, and at Rudolice v Horach – by 22%. For other stations the difference between the observed and modelled precipitation is within $\pm 15\%$ limits. Therefore, relatively small difference in precipitation amounts cannot be a reason explaining the underestimation of the observed wet deposition fluxes.

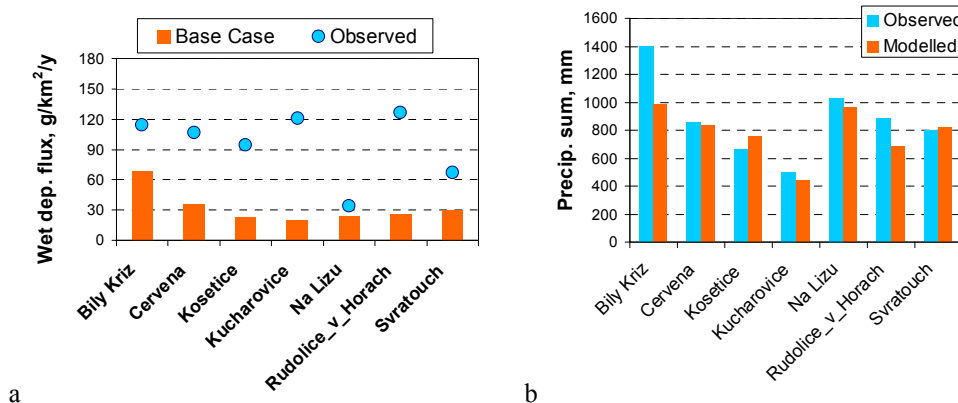


Fig. 13. Modelled vs. observed annual wet deposition fluxes (a) and precipitation amounts (b) in 2007

Comparison of weekly time series of modelled and observed wet deposition fluxes revealed that in some periods the model reproduces the observed wet deposition fluxes satisfactorily well, while in the other periods significant underestimation is found. For example, at station Bily Kriz the observed wet deposition was reasonably well reproduced in the beginning and the middle of the year, while in the end of the year the underestimation of the observed fluxes is high (Fig. 14). Similar situation is noted for station Cervena.

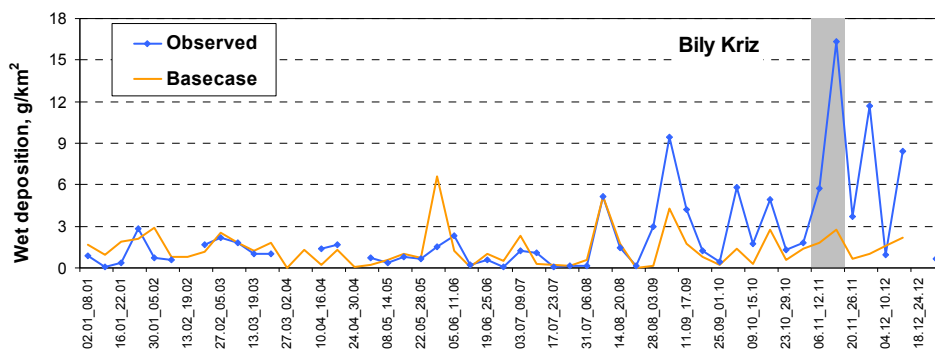


Fig. 14. Time series of modelled and observed weekly wet deposition flux of Cd at station Bily Kriz in 2007

At some stations (e.g., Kosetice, Kucharovice, Rudolice v Horach) the situation is different: underestimation occurs in particular periods scattered across the entire year. In these periods the modelled deposition is lower than the observed one by an order of magnitude. Significant underestimations can be caused by a number of reasons, such as uncertainties of the model parameterizations, measurement issues, influence of local sources and uncertainties of anthropogenic emissions in some regions.

In order to investigate if parameterization of modelled wet deposition can lead to significant underestimation of the observed wet deposition fluxes special sensitivity study was carried out. Wet scavenging process in the model is split in two processes: in-cloud and below-cloud scavenging. Coefficients determining scavenging of a pollutant by precipitation in clouds and below clouds were multiplied by factors 5 and 10 and the model was run again. The results based on the increased wet scavenging parameters were compared with original modelling results (so-called base case) and with observations.

Response of the model to changes of scavenging parameters is demonstrated in Fig. 15 for the priority stations. The 5-times increase of below-cloud scavenging results in much smaller increase of annual wet deposition (Fig. 15a): modelled wet deposition increased up to 20%. The 5-times increase of in-cloud scavenging led to more explicit response of the model. Wet deposition increased up to 46%. At some stations the increase of scavenging led even to some decrease of deposition. Most likely, it is caused by stronger removal of the pollutant on the way from its sources to stations. The stronger response to the increase of in-cloud removal (Fig. 15b) compared to below-cloud scavenging is explained by the fact that in-cloud scavenging encompasses the entire column of the troposphere (up to top of clouds) while below-cloud scavenging takes place only below clouds bottom and hence involves only few lower model layers. The 10-fold increase of either in-cloud or below-cloud scavenging led to rise of wet deposition just somewhat higher than that caused by 5-fold increase. Most likely, even at 5-time increase most of cadmium is removed from the atmosphere during rain events, and thus further increase of the scavenging in the model does not produce more wet deposition.

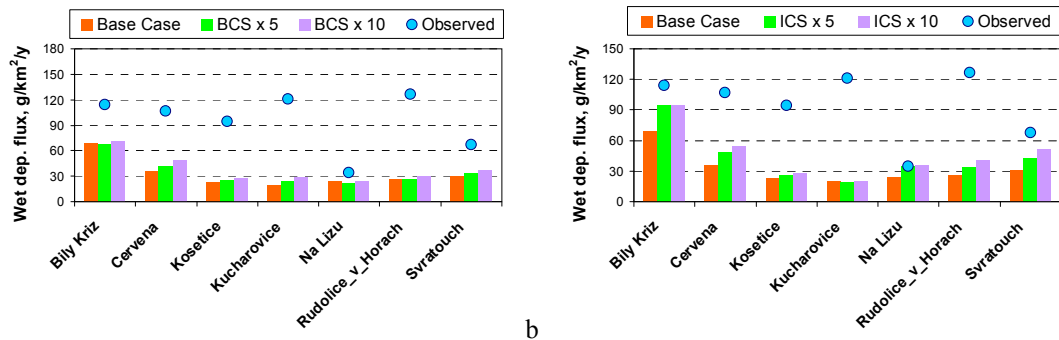


Fig. 15. Observed annual wet deposition fluxes of Cd at Czech monitoring stations and modelled fluxes based on numerical tests with increase of below-cloud scavenging (a) and in-cloud scavenging (b)

Magnitude of discrepancies between modelled and observed deposition varied considerably for different periods and different monitoring stations. For example, weekly wet deposition fluxes were relatively well reproduced by the model at station Bily Kriz in the beginning and middle of year 2007, while in the end of the year the model significantly underestimated the observed fluxes. The increase of in-cloud scavenging favoured improving agreement between modelled and measured fluxes in the end of the year, but it led to overestimation of the observations in the beginning and middle of the year (Fig. 16). Distinct response of modelled wet deposition on the increase of wet scavenging is indicated also for stations Cervena, Na Lizu and Svatouch.

At some other stations, e.g., Kucharovice, the increase of wet scavenging does not result to adequate changes of modelled wet deposition flux (Fig. 17). The difference between modelled and observed wet deposition fluxes in some periods remains at level of order of magnitude. Similar situation is noted for Kosetice, Rudolice v Horach.

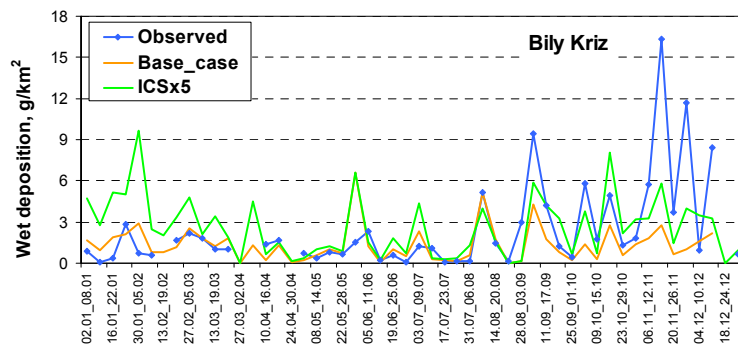


Fig. 16. Time series of observed weekly wet deposition flux of Cd at station Bily Kriz in 2007 and modelling results (base case and 5-times increased in-cloud scavenging)

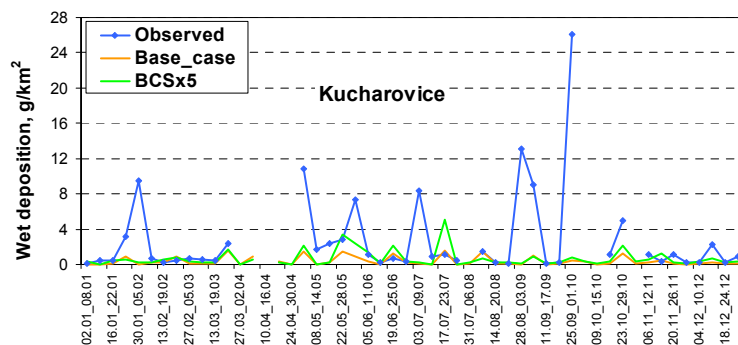


Fig. 17. Time series of observed weekly wet deposition flux of Cd at station Kucharovice in 2007 and modelling results (base case and 5-times increased in-cloud scavenging)

Similar to Kucharovice station, wet deposition fluxes observed at station Kosetice exhibit several peaks, which are not reproduced by the model (Fig. 18). The increase of scavenging parameters allows increasing of modelled wet deposition in some periods, but it is not enough to explain the peaks. For example, in the period from 4 to 10 of September modelled deposition are 6.6 times below than the observed ones. The increase of in-cloud scavenging favoured rise of calculated wet deposition 2.2 times. However, even increased wet deposition are still below the observed values.

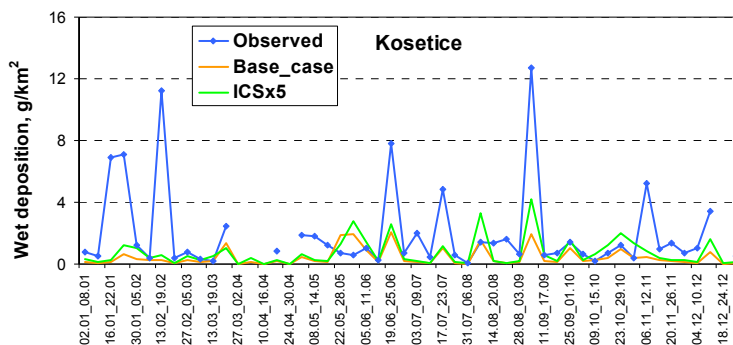


Fig. 18. Time series of observed weekly wet deposition flux of Cd at station Kosetice in 2007 and modelling results (base case and 5-times increased in-cloud scavenging)

Since some of peaks of cadmium fluxes may be connected with measurement issues, cadmium time were compared with the time series of wet deposition of sulphur. Sulphur presents in the environment in much larger quantities and hence its measurements are less complicated compared to cadmium. As seen (Fig. 19), in some periods normalized wet deposition of cadmium and sulphur are very close. This fact can make us to suggest that these peaks are ‘real’ and explained by elevated levels of pollution caused by e.g., long-range transport from emission sources releasing large quantities of cadmium and sulphur, or by influence of local sources. In some other periods, however, normalized levels of sulphur are much lower than those of cadmium. Quality check of cadmium measurements at these peaks is needed.

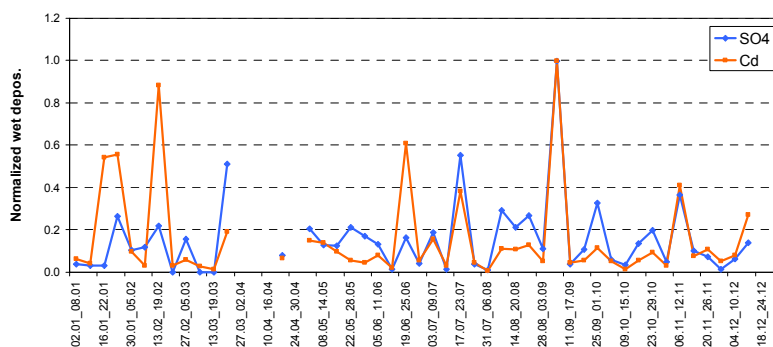


Fig. 19. Normalized observed weekly wet deposition fluxes of sulphate and cadmium at station Kosetice in 2007

Monitoring at Czech stations is carried out on weekly basis. Therefore, it is necessary to select a number of weekly episodes for more detailed analysis. First of all, the periods with significant underestimation of observed wet deposition fluxes were selected. However, one of possible reasons of the discrepancies between modelled and observed wet deposition can be difference between precipitation amounts simulated by MM5 and those observed at monitoring stations. Although annual sums of modelled and observed precipitation do not differ much (Fig. 13b), the weekly sums can differ considerably. In order to avoid uncertainties linked with differences of precipitation amounts, the

episodes where relative difference between modelled and observed precipitation is within $\pm 30\%$ limits were selected for the further analysis.

The further step was investigation of vertical distribution of wet scavenging simulated by the model. For this purpose information on vertical distribution of various parameters responsible for calculations of wet scavenging were derived. First of all, mass of cadmium removed by wet deposition at each model layer was calculated for each station and for different episodes. As seen from the Fig. 20a, most of cadmium is removed by wet scavenging from the third and fourth model layer (around 200 – 400 m above ground). At the same layers maximum mass of cadmium in air in this period is indicated (Fig. 20b). Vertical profile of condensed water in the atmosphere (sum of liquid and frozen water content) indicates location of clouds where in-cloud scavenging occurs. In the considered period at Bily Kriz the peak of cloud water takes place at the 5th model layer (around 700 m) (Fig. 20c).

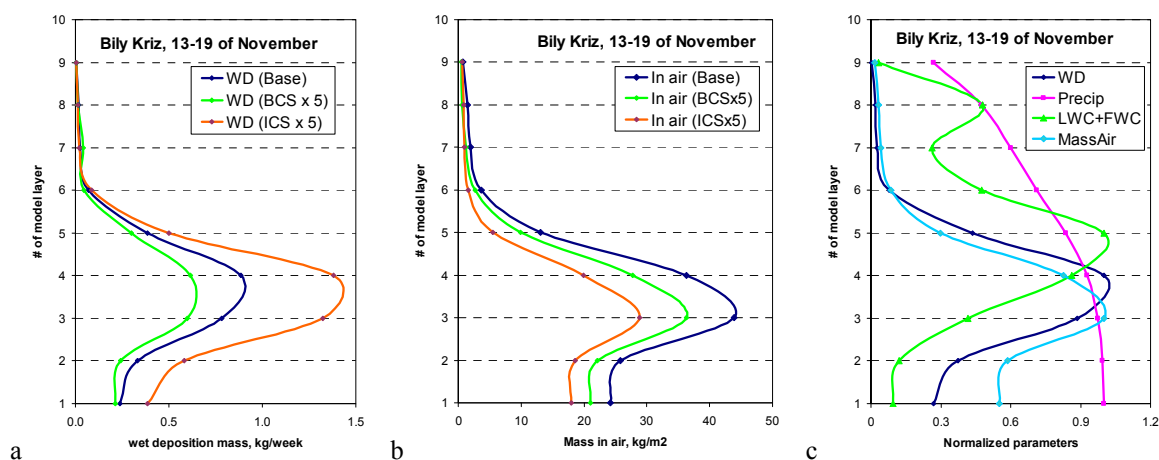


Fig. 20. Vertical profiles of wet deposition originated at each model layer (a) and time-averaged mass of cadmium at model layers (b) calculated with base-case wet scavenging and 5-time increased wet deposition. (c): vertical profiles of normalized precipitation amounts at each model layer (precip), liquid and frozen water content (LWC+FWC), cadmium mass in air (MassAir) and wet deposition (WD) calculated using base-case scavenging parameters. The parameters related to station Bily Kriz, for period 13-19 of November.

The 5-time increase of in-cloud scavenging coefficient leads to the increase of wet deposition 1.2 – 1.8 times at lower six model layers. At other layers the contribution to wet deposition flux was minor. However, the increase of below-cloud scavenging resulted to unexpected decline of wet deposition flux. A number of model tests with various magnitude of increase of below-cloud scavenging also demonstrated the decline of wet deposition as below-cloud scavenging increases (Fig. 21). Most likely, the increase of wet deposition caused stronger removal of pollutants on the way from the sources to the station. Therefore, air with smaller concentrations approached the station and thus smaller amount was washed out in spite of the increase of below-cloud scavenging coefficient.

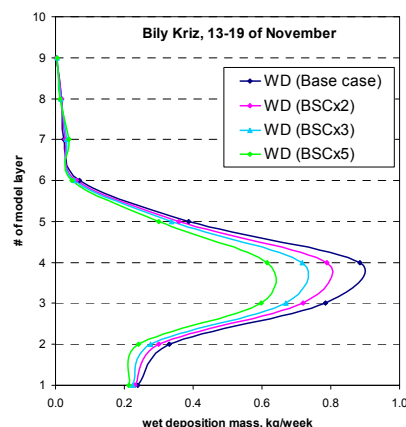


Fig. 21. Vertical profiles of wet deposition originated at each model layer derived from base-case calculations and tests with 2, 3 and 5-times increase of below-cloud scavenging for station Bily Kriz, period 13-19 of November

Another example of analysis of vertical distribution was undertaken for station Kosetice, for the period 4 – 10 of September. Maximum cadmium mass removed by wet deposition takes place at 5th model layer (around 700 m) (Fig. 22a) as well as local maximum of water content (Fig. 22c). Another maximum of water content occurs at the eighth model layer (more than 2 km), but mass of cadmium in air is low at this layer and thus its contribution to wet deposition is not high.

Increase of below-cloud scavenging results to increase of wet deposition flux in layers below cloudiness (Fig. 22a), namely first – fourth layers. In the upper layers deposition declined. The increase of in-cloud scavenging results to more pronounced increase of wet deposition compared to that of below-cloud cloud scavenging. Modelled mass of cadmium in air declines due to rise of wet scavenging (Fig. 22b).

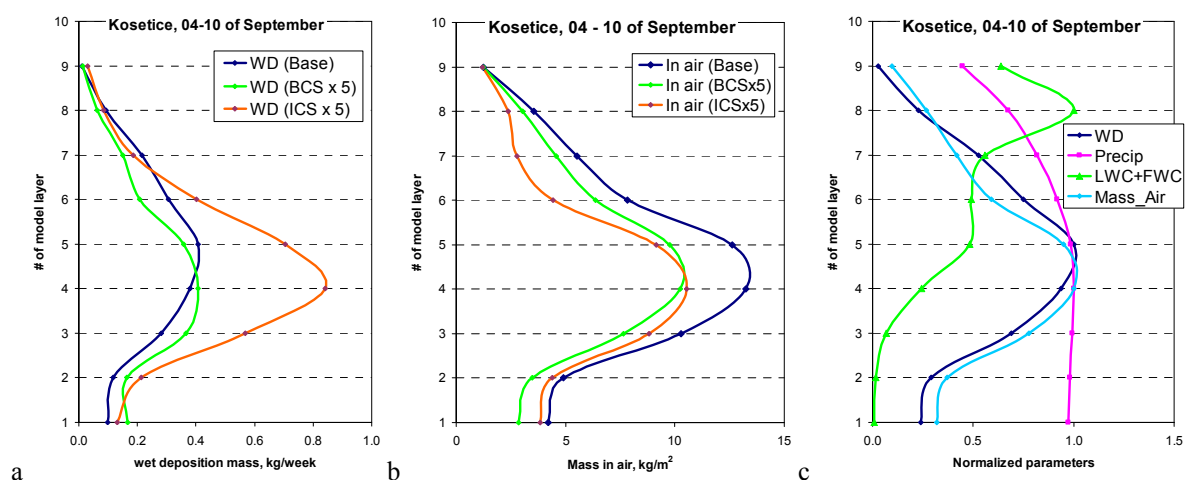


Fig. 22. Similar to Fig. 20, but for the period from February 13 to 19 at Kosetice station

The main preliminary conclusions which follow from the above results are:

- The increase of in-cloud or below-cloud scavenging results to some increase of cadmium wet deposition flux. However, this increase is insufficient to overcome significant underestimation of the observed wet deposition.
- According to the model parameterizations, in-cloud scavenging of cadmium seems to be more efficient compared to below-cloud scavenging.
- Most of cadmium in air (in terms of mass) as well as its wet deposition over the Czech stations are concentrated in the third – fifth layers.

It is assumed in the model that cadmium is emitted in the three lower model layers. However, the experiments demonstrate that the most of cadmium is removed by wet scavenging from upper model layers. Therefore, the further steps aimed at investigation of cadmium wet removal over the Czech Republic and improvement of the modelling results will be directed to modification of vertical distribution of the pollutant in the atmosphere. In particular, another approach to distribute emissions along vertical in the model can be applied. Besides, modification of the model by introduction of convective mixing process can be considered.

Chapter I.3.

EVALUATION AND MODIFICATION OF WIND RE-SUSPENSION SCHEME

Anthropogenic economical activity causes releases of heavy metals to the atmosphere. However, in addition to direct anthropogenic emissions, heavy metals can enter the atmosphere with dust particles, re-suspended from the underlying surfaces. In order to take into account heavy metals entering the atmosphere because of this process, wind re-suspension scheme was developed and implemented in the MSCE-HM model [Gusev *et al*, 2006b; Ilyin *et al*, 2007].

Inclusion of wind re-suspension process in modelling of heavy metal transport and deposition favoured improving of modelling results for the EMEP region as whole. In particular, it helped reducing significant underestimation of modelled concentrations in air and wet deposition of lead and cadmium compared to the observed values. However, at some stations and in particular short-term episodes the use of wind re-suspension scheme sometimes leads to decline of the model performance, namely, in overestimation of the observed concentrations in air. This situation took place both in the EMEP region, and at local scales in the framework of country-specific case studies. Therefore, MSC-E initiated revision of re-suspension scheme.

Particles can enter the atmosphere by anthropogenic emissions, gas-to-particles conversion, nucleation etc. Wind re-suspension is therefore one of numerous processes responsible for aerosol input to the atmosphere. In order to evaluate wind re-suspension scheme specific situations when this process is dominating are considered. The evaluation was based on dust storm episode which took place in end of March, 2007, in Ukraine and was associated with atmospheric transport of dust particles through the central and the western part of Europe [Birmilli *et al*, 2008, Bessagnet *et al.*, 2008]. Unlike numerous dust storm episodes originated in desert regions of Africa [e.g., Chen *et al*, 2011; Marticorena *et al*, 2010; McKendry *et al*, 2007; Sodemann *et al*, 2006] or eastern Asia [Kim *et al*, 2004; Shimizu *et al*, 2004; Xu *et al*, 2004], the source of dust release and monitoring stations recorded elevated particle concentrations were located in the same modelling domain.

In 23rd – 24th of March, 2007, a cyclone was located over the Mediterranean region, while anticyclone was situated over Scandinavia. Strong pressure gradient between these two systems conditioned strong surface winds with velocities up to 15 m/s and gusts up to 25 m/s [Birmilli *et al*, 2008]. These synoptic conditions associated with long period of dry weather and lack of vegetation in the agricultural regions of the eastern part of Ukraine caused re-suspension of soil dust particles and their atmospheric transport in the north-western direction. The plume of these particles was detected at numerous measurement stations in the central Europe (Germany, Poland, Austria, the Czech Republic), recorded peak concentrations of PM₁₀ in 24-25 of March. Some smaller peaks were observed at stations in the Netherlands, the United Kingdom and the north of France [Birmilli *et al*, 2008, Bessagnet *et al.*, 2008].

Most of stations measuring particulate matter report their results as concentrations of particles which diameter less or equal to 10 μm or 2.5 μm (PM₁₀ and PM_{2.5}, respectively). Therefore, MSCE-HM model was adopted to simulate transport and deposition of PM_{2.5} and of so-called coarse fraction. This coarse fraction PM_{coarse} includes particles which diameter is within 2.5 – 10 μm limits. Concentrations of PM₁₀ are calculated as a sum of PM_{2.5} and PM_{coarse}.

Atmospheric lifetime of a particle largely depends on its size. Hence, to simulate transport and deposition of PM_{2.5} and PM_{coarse} it is necessary to know their mass median diameters (MMD). The MMDs are derived from the particle size distribution within the considered size ranges. MMDs for air concentrations of PM_{2.5} and PM_{coarse} produced by wind re-suspension are not known a priori. To

determine the MMDs re-suspension and atmospheric transport was simulated for 17 particle bins within 0 – 20 μm range for the period from 1st of March to 15th of April. These bins were defined as follows: six bins were taken for size range from 0 μm to 3 μm with 0.5 μm step, eight bins for 3-11 μm range with 1 μm step and 3 bins for 11 – 20 μm range with 3 μm step.

MMD for PM_{2.5} particles, simulated for the period from 1st of March - 15th of April varies from 1.2 to 1.45 μm over most of EMEP countries (Fig. 23a). Relatively high MMD is noted for the Central Asian region, south-east of European part of Russia and the eastern part of Ukraine because in these regions re-suspension of soil dust is mostly occurs in this period. Besides, relatively high MMD is noted for the western and south-western parts of Europe. It is caused by the influence of particles coming from sea spray.

Similar to P_{2.5}, spatial variability of MMD for coarse particles is not high (Fig. 23b). It ranges between 5.4 and 6.8 μm over most part of EMEP countries. Eastern Ukraine, south-east of European part of Russia and Central Asia are the regions where MMD is relatively high, which is explained by the fact that these regions are sources of re-suspended dust particles. Since larger particles are removed more easily from the atmosphere, the contribution of larger particles is higher in source regions and hence MMD is higher.

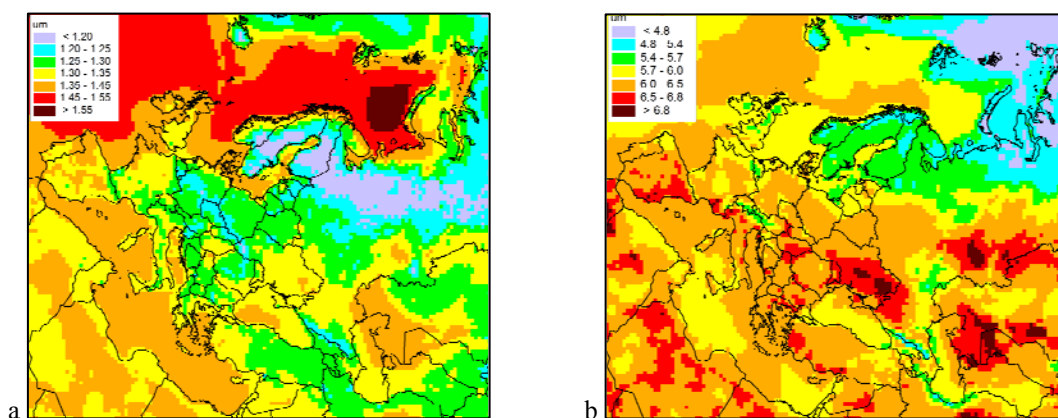


Fig. 23. Calculated mass median diameters for PM_{2.5} (a) and PM_{coarse} (b) averaged over period from 1st of March - 15th of April

Figure 24 demonstrates examples of temporal variability of MMD at three gridcells: in the source region (point UKR1), in the central part of Europe (station DE44, Germany) and in region remote from re-suspension sources (station NO1, Norway). As seen from the figure, variability of MMDs both for PM_{2.5} and for PM_{coarse} is not high.

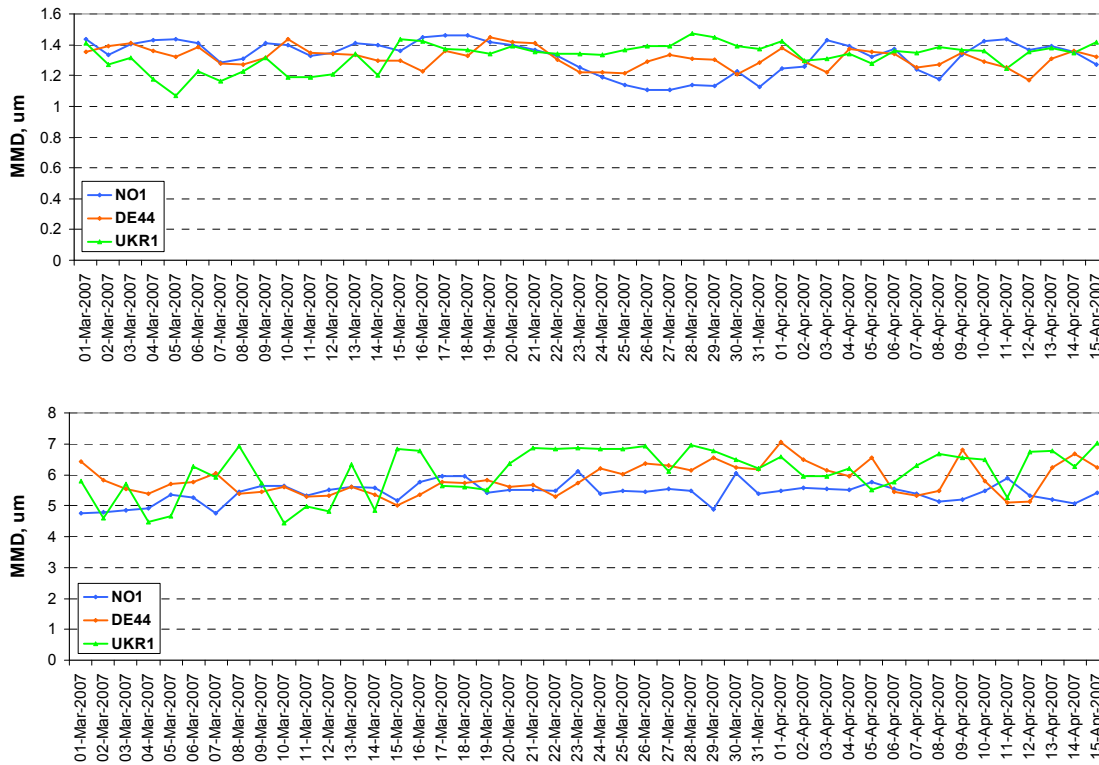


Fig. 24. Calculated time series of MMDs for MP_{2.5} (upper) and PM_{coarse} (lower) at sample points in remote regions (station NO1, Norway), in central part of Europe (station DE44, Germany) and in region of re-suspension origin (UKR1, Ukraine)

Since spatial and temporal variability of MMD for PM_{2.5} and PM_{coarse} is not high, MMD values, averaged over European land part of the EMEP region, were derived for the further use in the model calculations. Estimated MMD for PM_{2.5} is 1.3 μm , and for PM_{coarse} - 6.3 μm (Fig. 25).

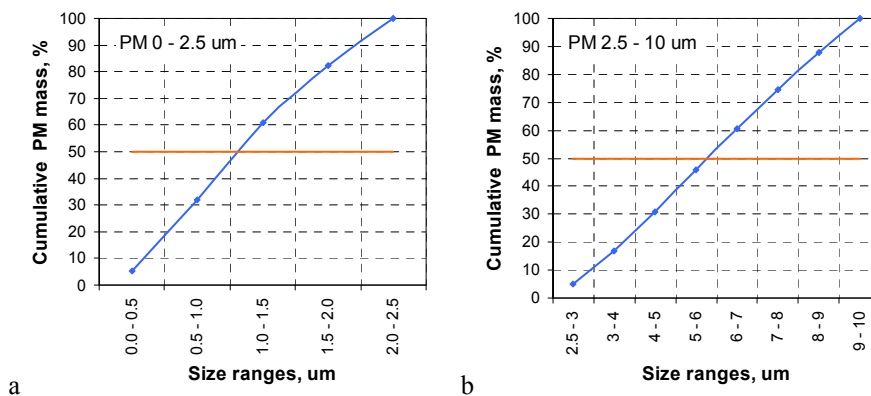


Fig. 25. European-mean cumulative size distribution of PM based on model calculations driven by wind re-suspension. Red line indicates particle size corresponding to median of mass

Information on PM measurements used in testing of wind re-suspension scheme is available from EMEP stations and from national monitoring programmes. For example, peak PM₁₀ concentrations in 24th – 26th of March were recorded at 302 stations in Germany and 69 stations in the Czech Republic. First of all, stations with hourly measurements were selected for the analysis (Fig. 26a). Besides, since the main PM component for the model testing is PM_{coarse}, we selected stations where

PM2.5 and PM10 are measured simultaneously, so that concentrations of PM_{coarse} can be calculated. Therefore, as much as 14 stations from Germany, 22 stations from the Czech Republic and 5 British stations (with one EMEP station among them) were selected for further analysis (Fig. 26b).

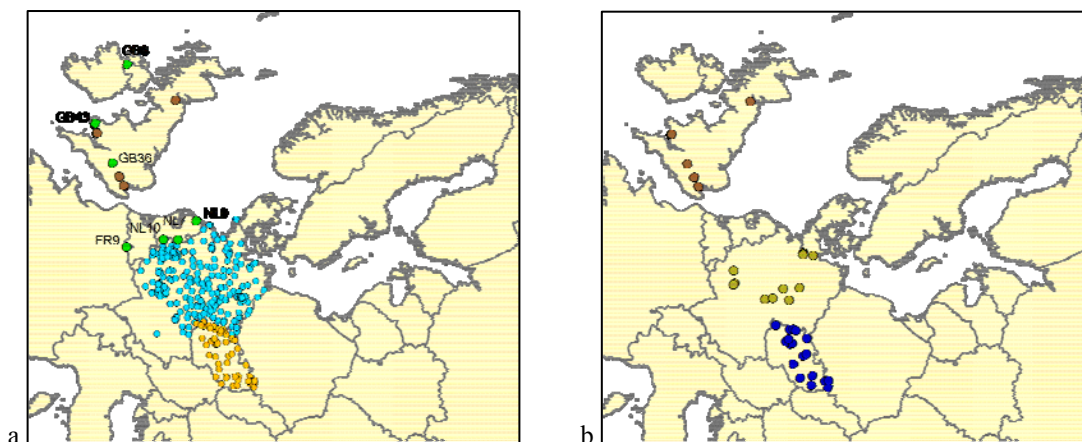


Fig. 26. Stations measured PM10 (a) and both PM10/ PM2.5 (b) where peak concentrations in 24 – 26th of March were recorded

Preliminary comparison of modelled and measured concentrations of PM_{coarse} at some of these selected stations demonstrates that the modelled concentrations do not always exhibit peak in the considered period. The reason for this is the fact that plume of re-suspended dust particles generated by the model likely does not fully coincide with the real observed plume. Figure 27 depicts daily mean concentrations simulated by the model for 24th of March and maximum concentrations of PM10 measured at the German and Czech stations in the same day. As seen from the figure, the zone of maximum modelled concentrations is located somewhat northward relative to zone of maximum observed concentrations. This inconsistency is likely explained by uncertainties of meteorological data or by their relatively rough (6 hours) temporal resolution for this particular task.

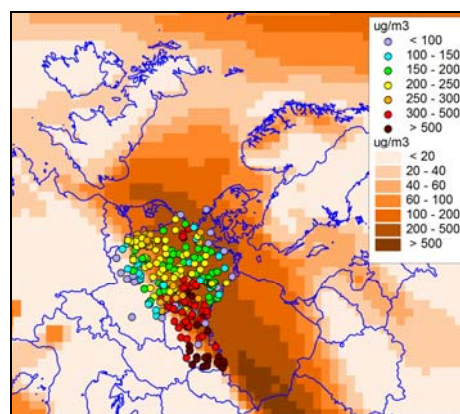


Fig. 27. Calculated daily mean concentrations (shaded) and observed daily maximum concentrations (circles) in March 24th, 2007

The task is to test wind re-suspension scheme from viewpoint of mass of dust particles released to the atmosphere by this process. Therefore, the stations where the model does not reproduce the peaks were also omitted from the analysis.

MSCE-HM model was applied to perform modelling of PM2.5 and PM_{coarse} concentrations for the end of March, using MMDs for these size ranges described above and the selected stations for comparison of modelled and observed concentrations. Contributions of various surface categories to calculated concentration of PM were established. These categories include barren/deserts, agricultural, urban, and sea surfaces. Besides, contribution of anthropogenic sources was also included. However, it is worth noting that the model takes into account transport and deposition of particles, and does not consider process of aerosol dynamics such as gas-to-particle conversion, nucleation, coagulation etc. Therefore, the contribution of anthropogenic sources to overall concentration represents the result of only atmospheric transport and deposition and, thus, it is likely underestimated.

As seen from Fig. 28, the largest contribution to PM modelled concentrations at the selected stations, averaged over the period from 21st to 26th of March is made by agricultural lands. The contribution for PM10 concentrations varies from about 50% to more than 90%. Similar contributions are noted for PM_{coarse} and PM2.5. Contributor of the second importance is sea salt. Its role is relatively important at British stations and some German stations located nearby sea coast. It also follows from the figure that the model tends to overestimate measured PM10 and PM_{coarse} concentrations.

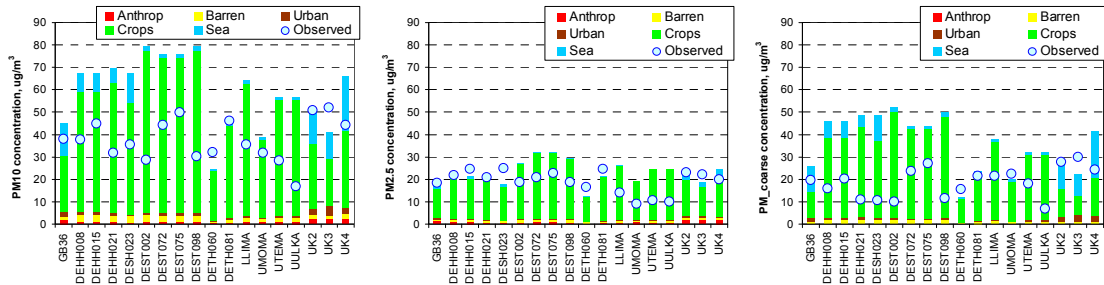


Fig. 28. Contribution of various sources to PM concentrations in the period from 21st to 26th of March, 2007

Examples demonstrating the temporal variability of PM source contributions to overall modelled concentration are presented for stations DETH060 (Germany) and Harwell (the United Kingdom) (Fig 29 and 30). As seen, peak concentrations of PM10 at the German station were reproduced relatively well in the period from 9:00 to 21:00 of 24th of March, but the second peak in 26th of March, generated by the model, was not supported by measurements (Fig. 29a). Concentrations of the coarse fractions were also reproduced relatively well: Both peaks were captured by the model. PM2.5 concentrations were typically underestimated in the period from 24th to 26th of March (Fig. 29b). It is not surprising because the model does not include processes of aerosol dynamics which are responsible for formation of most part of fine particles. However, the peaks of PM2.5 concentrations were overestimated by the model. For the British station peak concentrations of both PM2.5 and PM_{coarse} were overestimated (Fig. 30).

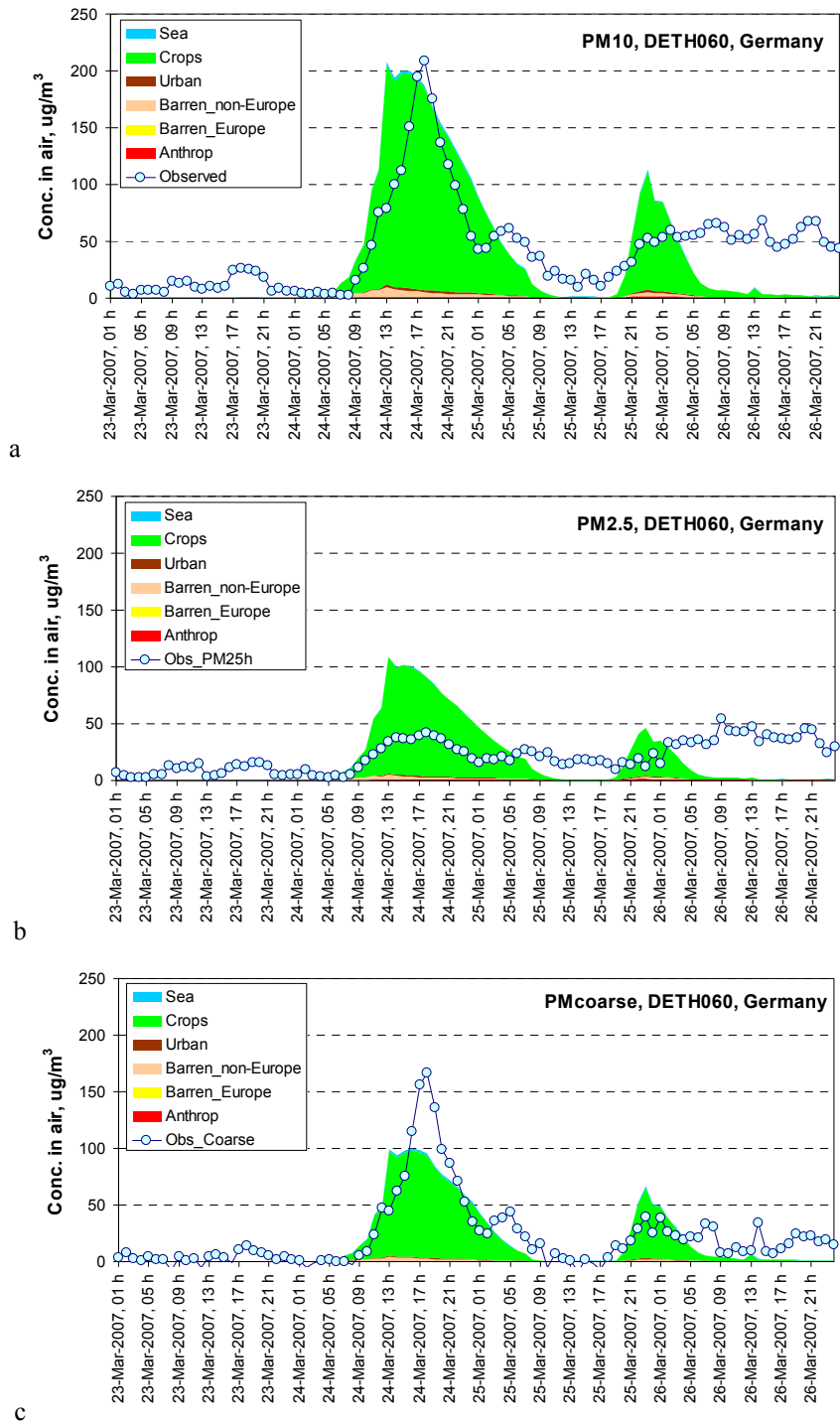


Fig. 29. Observed concentrations of PM₁₀(a), PM_{2.5}(b) and PM_{coarse} (c) at station DETH060, Germany, and contribution of various PM emission sources to corresponding modelled concentrations.

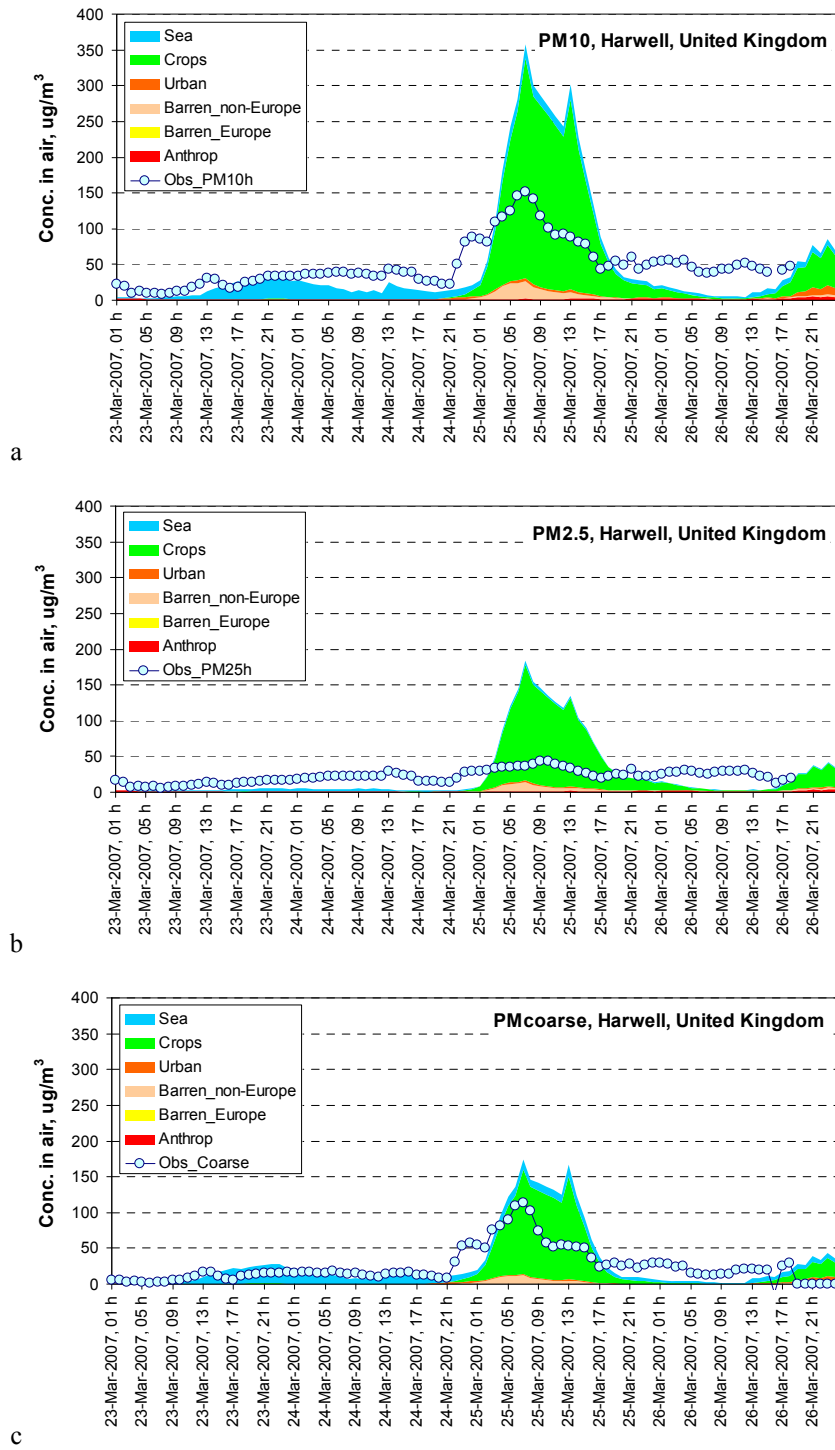


Fig. 30. Observed concentrations of PM10(a), PM2.5(b) and PMcoarse (c) at station Harwell, the United Kingdom, and contribution of various PM emission sources to corresponding modelled concentrations.

The purpose of the study is to test if the model wind re-suspension scheme generates reasonable amount of dust. It can be done by analysis of peak of PM concentrations measured at stations and produced by the model. Therefore, the further analysis is focused on the peak. Two parameters of the peak were considered. The first one is maximum concentration measured or modelled in the period when the peak takes place. The second one is averaged concentration in peak period. It is an average value in 24-hour period with peak. This period is defined so that the maximum concentration falls on the middle of this period (Fig. 31). This averaged value can be considered as a characteristic of mass of PM passing through the monitoring station. It is important to note that modelled and measured peaks do not always coincide in time. The comparison of modelled and measured PM concentrations reveals that as a rule the difference between modelled and observed peaks is 1 – 2 hours.

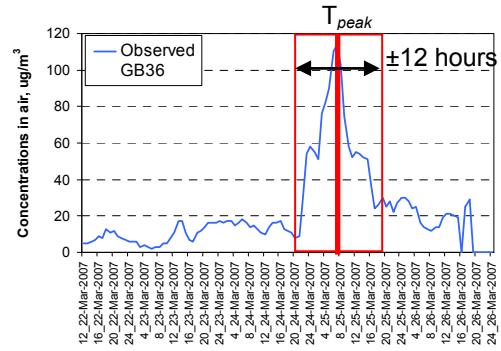


Fig. 31. Selection of time period for the analysis. Example for station GB36 (Harwell, the United Kingdom)

The criteria employed in the analysis are mean relative bias, Pearson correlation coefficient and normalized root mean square error. For the base case simulations (simulations based on current version of re-suspension scheme) the statistical indexes are summarized in Table 1. Diagrams for individual stations are shown in Fig. 32. As it follows from the table and from the figures, the model significantly overestimates the observed 24-hour averaged concentrations. Observed concentrations of PM_{coarse} overestimated more than twice, PM_{10} – about 2.5 times and $PM_{2.5}$ – almost three times. Besides, it is important to note that the highest overestimation is obtained for fine particles ($PM_{2.5}$) which take part in long-range transport more readily compared to coarse particles.

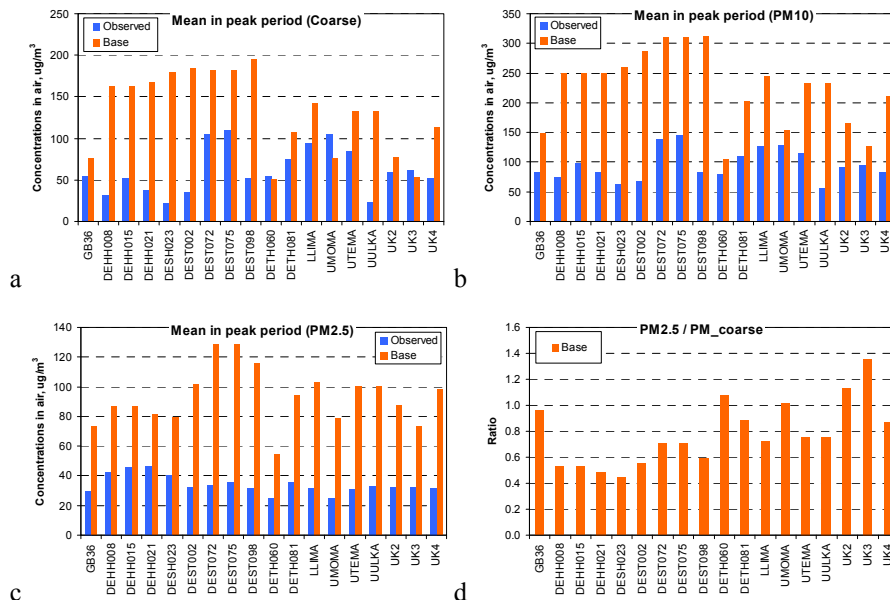


Fig. 32. Modelled (base case) and observed concentrations of PM_{coarse} (a), PM_{10} (b), and $PM_{2.5}$ (c) averaged for the peak period, and ratio of modeled $PM_{2.5}$ to PM_{coarse} concentrations (base case)

Table 1 . Statistical indicators of comparison of observed and modeled (base case) concentrations of PM

PM	Obs	Mod	Rel. Bias	Rc	NRMSE
Coarse	62.0	132.4	114	-0.11	1.42
PM10	96.1	225.3	134	0.16	1.46
PM2.5	34.1	93.0	173	0.08	1.77

Since the major contributor of PM concentrations is re-suspension from agricultural lands, the further modifications were focused on decreasing of re-suspension of this type of surface. Moreover, it would be important to decrease the contribution of PM2.5 to particulate matter concentrations. A number of numerical experiments aimed at these two purposes were undertaken.

Parameterization of wind re-suspension of particles is described in detail in MSC-E reports [Gusev *et al.*, 2006b; Ilyin *et al.*, 2007]. In the model this process is described as combination of saltation (horizontal movement of soil aggregates driven by wind stress) and sandbaling (impaction of soil by saltating aggregates and further ejection of smaller particles). Wind suspension of particles occurs when wind stress exceeds a certain threshold value, which, in turn, depends on wetness of soil, existence of sheltering roughness elements on the soil, atmospheric parameters (e.g., air density). Vertical flux of re-suspended mass of dust depends on size distribution of soil aggregates and availability of loose soil material on the soil surface.

Meteorological parameters are generated by MM5 meteorological driver, and soil wetness is parameterized according to approach described in [Fécan *et al.*, 1999]. Modification of these factors was not involved in the numerical tests. Other factors, such as availability of loose soil material, effect of sheltering by roughness elements and size distribution of soil aggregates were investigated.

Availability of loose soil material is described by constant K . For example, for sandy desert soils abundant with loose soil material, this constant is around unity [Gomes *et al.*, 2003] and $K = 1$ was accepted in the model. For agricultural lands $K = 0.1$ was assumed. Density of sheltering roughness elements is characterized by frontal area index λ . According to field measurements, this parameter varies from 0.001 to 0.2 [Marticorena *et al.*, 2006, Shao and Yang, 2005]. In current model version $\lambda = 0.002$ for agricultural lands. Size distribution of re-suspending particles is determined by soil texture, i.e. relative content of clay, sand and silt. In the current version of the model the $1^\circ \times 1^\circ$ data of International Satellite Climatology Project (ISLSCP) interpolated to the 50x50 km model grid are used. Alternative source of soil texture data, involved in numerical tests, is Harmonized World Soil Database (HWSD). These data are more contemporary and their spatial resolution is higher (around 1x1 km) compared to ISLSCP.

Maps of soil, silt and clay content in the EMEP region, derived from ISLSCP and HWSD soil data bases are demonstrated in Fig. 33. First of all, it is clear that HWSD-based data are more mosaic because of higher spatial resolution of the source data, compared to ISLSCP. In general, spatial distributions of soil components derived from these two databases are similar. However, there are some regional differences. For example, in HWSD clay content is lower in the central and southern parts of Europe, and sand content – in deserts of Africa and Central Asia, compared to ISLSCP. On the other hand, content of sand in the northern part of Europe in HWSD is higher than that in ISLSCP.

List of experiments and brief description of changed parameters is available in Table 2 .

Table 2. List of numerical tests and short description of modified parameters of re-suspension scheme

Model run	Parameters
Base case run	All parameters are unchanged ($\lambda = 0.002$, $K=0.1$, ISLSCP soil data)
Test 1	$K = 0.05$
Test 2	$\lambda = 0.02$
Test 3	$\lambda = 0.005$
Test 4	$\lambda = 0.01$
Test 5	$\lambda = 0.006$
Test 6	$\lambda = 0.007$
Test 7	Soil texture from HWSD
Test 8	Like in test 5, but soil texture from HWSD
Test 9	Like in test 6, but soil texture from HWSD
Test 10	Particle size distribution of [Kok, 2011b], soil texture from HWSD
Test 11	Like in test 10, but $K = 0.03$
Test 12	Like in test 10, but $K = 0.02$
Test 13	Like in test 10, but $K = 0.05$
Test 14	Like in test 10, but $K = 0.01$

Here K – constant reflecting possibility of the limitation of soil aggregates supply because of depletion of loose material on the surface. λ – frontal area index, characterizing density of sheltering roughness elements.

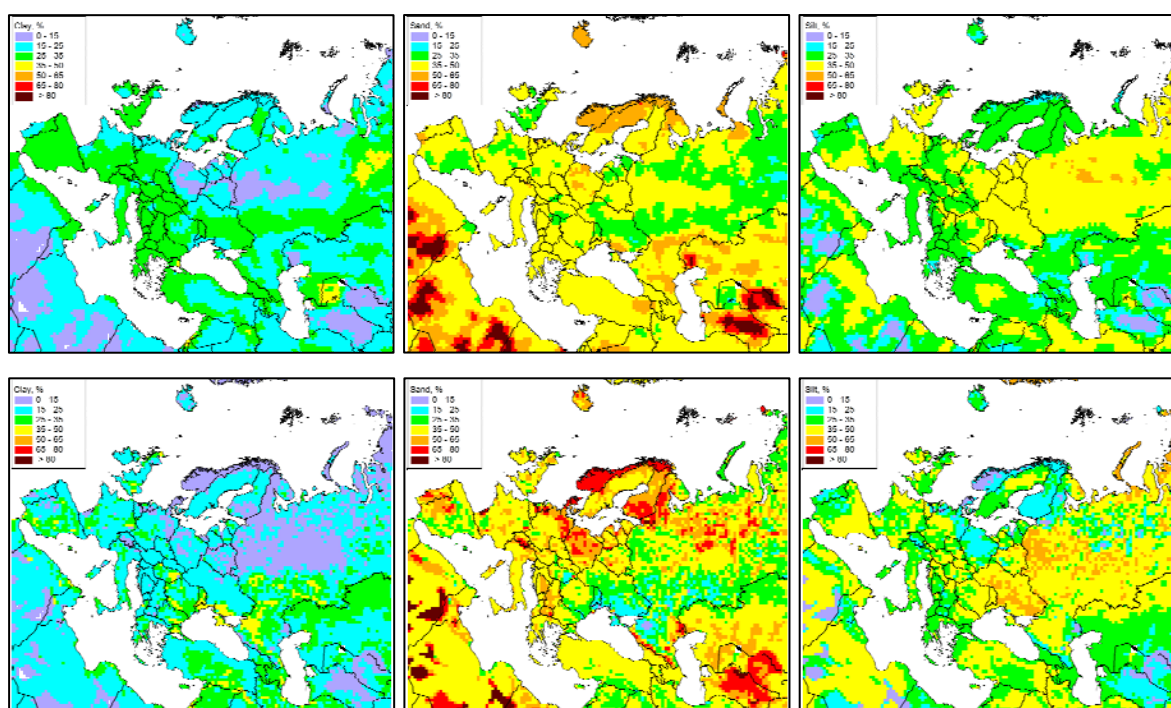


Fig. 33. Maps of content of clay (left), sand (middle) and silt (right) according to ISLSCP (top) and HWSD (bottom) soil data bases

Statistical indicators for each of these tests are summarised in Table 3. As seen, the use of twice smaller constant K (Test 1) results to 1.9 times decrease of PM concentrations (Fig. 34). However, reduction of his parameter does not affect size distribution of re-suspending particles. Indeed, the ratios of $PM_{2.5}$ to PM_{coarse} concentrations for the base case and for test 1 are very alike for the selected stations (Fig. 34). Therefore, even if the modelled concentration of coarse fraction of PM becomes close to the observed one (Relative bias is 14%), $PM_{2.5}$ is still overestimated.

Table 3. Statistical results of numerical tests

PM _{coarse}																
Tests	Obs	Base	1	2	3	4	5	6	7	8	9	10	11	12	13	14
Average	62.0	132.4	70.9	20.8	81.6	44.9	71.2	62.5	140.4	71.6	61.9	298.9	96.4	150.8	69.2	14.1
RB,%		113.5	14.4	-66.4	31.6	-27.6	14.8	0.8	126.4	15.5	-0.2	382.1	55.5	143.3	11.5	-77.3
SP. Corr:		-0.11	-0.14	-0.23	-0.11	-0.13	-0.11	-0.11	0.18	0.18	0.18	0.18	0.12	0.15	0.09	0.30
NRMSE:		1.46	0.64	0.81	0.73	0.58	0.63	0.57	1.48	0.52	0.48	4.11	0.82	1.66	0.53	0.88
PM10																
Tests	Obs	Base	1	2	3	4	5	6	7	8	9	10	11	12	13	14
Average	96.1	225.3	119.8	28.9	127.9	65.3	109.4	94.5	230.0	107.7	91.7	378.2	128.0	199.8	92.0	55.9
RB,%		134.5	24.7	-69.9	33.1	-32.0	13.9	-1.7	139.3	12.1	-4.6	293.6	33.2	108.0	-4.3	-41.8
SP. Corr:		0.16	0.13	-0.07	0.14	0.10	0.14	0.13	0.31	0.30	0.29	0.30	0.27	0.29	0.24	0.14
NRMSE:		1.50	0.46	0.75	0.53	0.44	0.40	0.34	1.52	0.34	0.30	3.13	0.50	1.22	0.31	0.50
PM2.5																
Tests	Obs	Base	1	2	3	4	5	6	7	8	9	10	11	12	13	14
Average	34.1	93.0	48.9	8.1	46.3	20.5	38.3	32.0	89.6	36.1	29.8	79.3	31.6	49.0	22.8	41.8
RB,%		172.6	43.3	-76.3	35.8	-39.9	12.2	-6.2	162.7	5.8	-12.5	132.6	-7.4	43.7	-33.0	22.7
SP. Corr:		0.08	0.09	0.14	0.06	0.06	0.06	0.06	0.17	0.17	0.18	0.05	0.06	0.03	0.10	0.42
NRMSE:		1.82	0.54	0.78	0.47	0.45	0.30	0.25	1.71	0.25	0.25	1.42	0.25	0.54	0.39	0.37

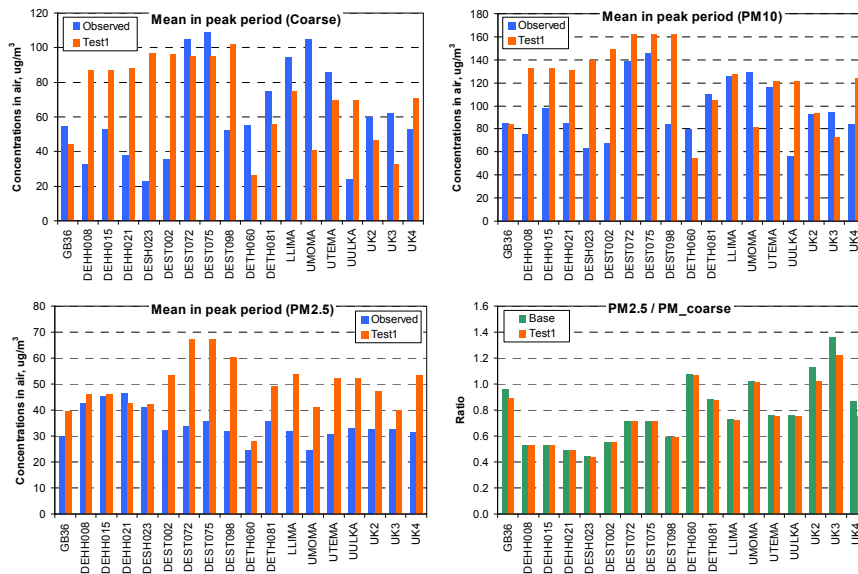


Fig. 34. Modelled (test 1) and observed concentrations of PM_{coarse}(a), PM10(b), and PM2.5(c) averaged for the peak period, and ratio of modeled PM2.5 to PM_{coarse} concentrations (test1 and base case)

Tests from 2 to 6 were focused on variation of frontal area index parameter λ . Threshold friction velocity depends on this parameter. According to current parameterization, the higher friction velocity is, the higher is the probability of ejection of finer particle mode from soils. Therefore, variation of λ will affect both mass of re-suspended particles and distribution between its coarse and fine fractions. Among this group of tests the test number 6 looks most successful from viewpoint of statistical indexes (Table 3). Besides, the fraction of fine particles (PM2.5) in air is declined at all stations compared to the base case (Fig. 35).

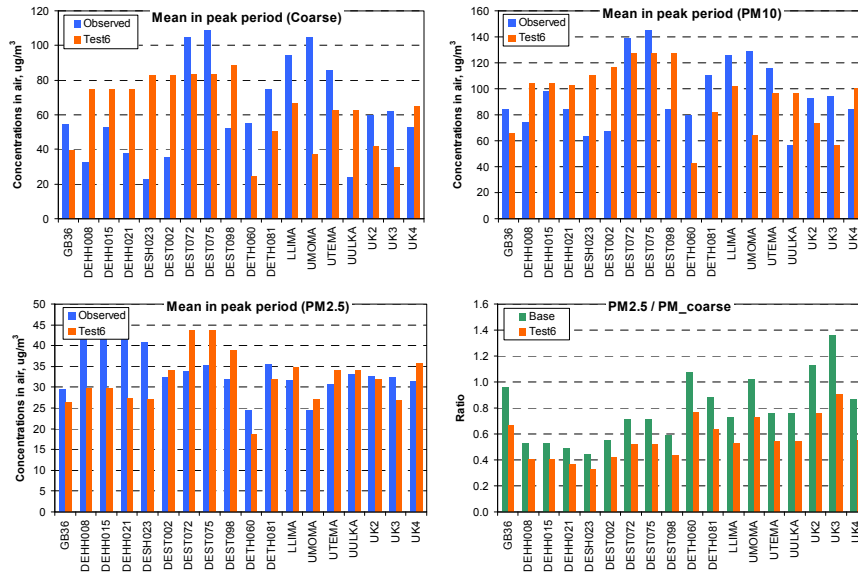


Fig. 35. Modelled (test 6) and observed concentrations of PM_{coarse} (a), PM_{10} (b), and $PM_{2.5}$ (c) averaged for the peak period, and ratio of modeled $PM_{2.5}$ to PM_{coarse} concentrations (test 6 and base case)

Tests numbered 7, 8 and 9 have the same set of input parameters, as in base case run, tests 5 and 6, respectively. The only exception is data on soil texture. In these tests the HWSD data were used instead of ISLSCP applied for other tests. The use of HWSD data lead to higher spatial correlation between modelled and measured 24-hour PM concentrations (Table 3). The lowest relative bias (almost zero) and NRMSE for PM_{coarse} is achieved in test 9 (Fig. 36). For PM_{10} and $PM_{2.5}$ these statistical indexes are also lower than in the other tests. Compared to the base case run, the ratio between $PM_{2.5}$ and PM_{coarse} concentrations is smaller. In means that the parameters introduced in test 9 favour reduction of overestimated fine fraction of modelled $PM_{2.5}$ concentrations caused by re-suspension. The parameters of this test can be applied for modification of currently used parameterization of wind re-suspension of dust and particle-bound heavy metals.

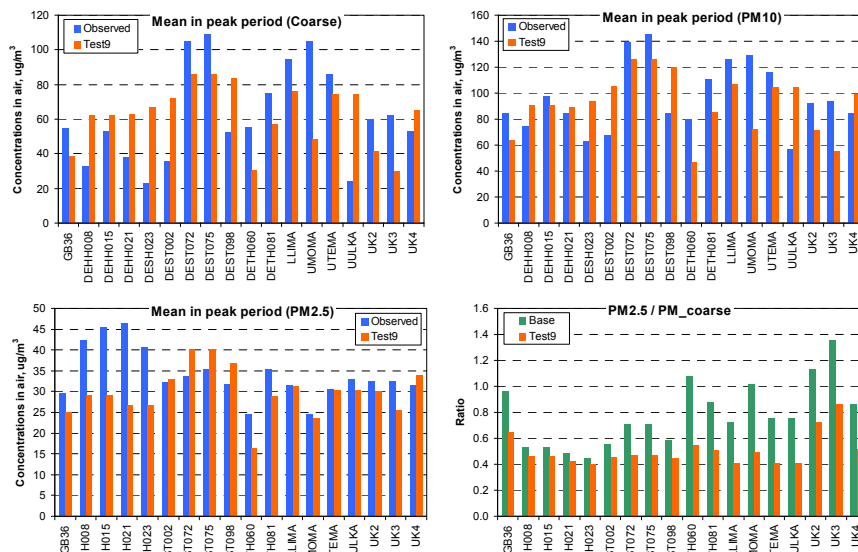


Fig. 36. Modelled (test 9) and observed concentrations of PM_{coarse} (a), PM_{10} (b), and $PM_{2.5}$ (c) averaged for the peak period, and ratio of modeled $PM_{2.5}$ to PM_{coarse} concentrations (test 9 and base case)

Currently used wind re-suspension scheme states that fraction of re-suspended coarse and fine particles depends on friction velocity [Alfaro and Gomes, 2001]. Similar assumption is adapted by other researches, e.g., [Shao et al., 2011]. However, there is an alternative viewpoint suggested by [Kok, 2011a], assuming that particle size distribution (PSD) does not depend on friction velocity. In paper [Kok, 2011b] parameterization of PSD of re-suspended dust is described. The complete re-suspension scheme including this particle size distribution is not yet available, according to our knowledge. Therefore, experimental model runs were performed based on combination of two approaches. Total mass of dust re-suspended by wind is calculated following assumptions adapted in currently used scheme. PSD of this mass is assumed according to [Kok, 2011b]. It should be stressed that, although the experiment involving approach of [Kok, 2011b] is useful, but it is not fully correct, because calculation of total mass of re-suspended particles is carried out using approaches which implicitly assume dependence of size distribution on friction velocity.

These are experiments from 10th to 14th. In the test 10 the parameters of the scheme were the same as in the base case run, except for soil texture data and assumption of PSD. It resulted to significant (2.3 times) increase of coarse, and some (15%) decrease of fine fraction concentrations compared to the base case (Fig. 37). Since the base case concentrations of PM are already overestimated compared with measurements, the mass of PM particles emitted in test 10 should be decreased. This decrease is achieved by modifying the parameter K , which prescribes availability of soil aggregates for re-suspension. The results obtained in test 13 seem to be most reasonable from viewpoint of statistical indicators among tests 10 – 14 (Table 3).

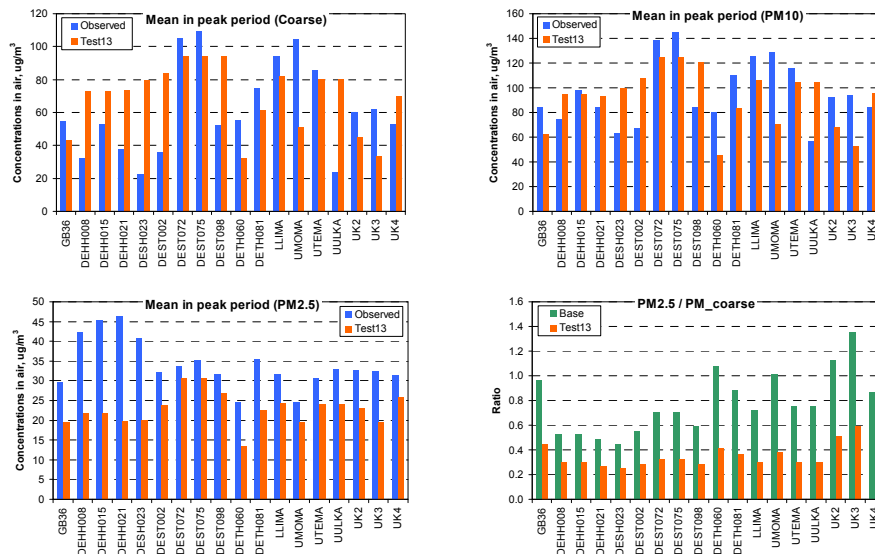


Fig. 37. Modelled (test 13) and observed concentrations of PM_{coarse} (a), PM_{10} (b), and $PM_{2.5}$ (c) averaged for the peak period, and ratio of modeled $PM_{2.5}$ to PM_{coarse} concentrations (test 13 and base case)

Examples of time series of PM_{coarse} and $PM_{2.5}$ concentrations observed at some stations and simulated in several tests are shown in Fig. 38 and 39, respectively. As seen, in the base case simulations peak values are generally overestimated by the model. At some stations (e.g., UTEMA) the modelled peak is lower than the observed one, but the modelled peak is “broader” compared to measured one. Modifications of the re-suspension make the peaks much closer to the observed value.

Modifications of the wind re-suspension scheme lead also to more realistic temporal dynamic of $PM_{2.5}$ concentrations. Unlike PM_{coarse} , $PM_{2.5}$ observed concentrations either do not exhibit any peak in the considered period, or this peak is low. Whereas in the base case calculations the peak concentrations of $PM_{2.5}$ are overestimated, the results based on modified scheme are much closer to the observations.

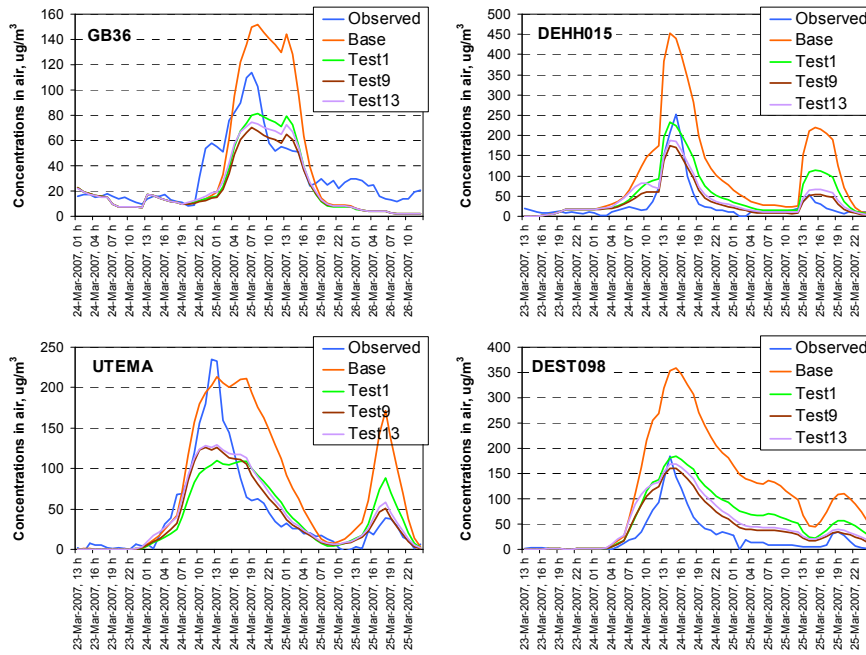


Fig. 38. Examples of observed and calculated concentrations of PMcoarse at some monitoring stations

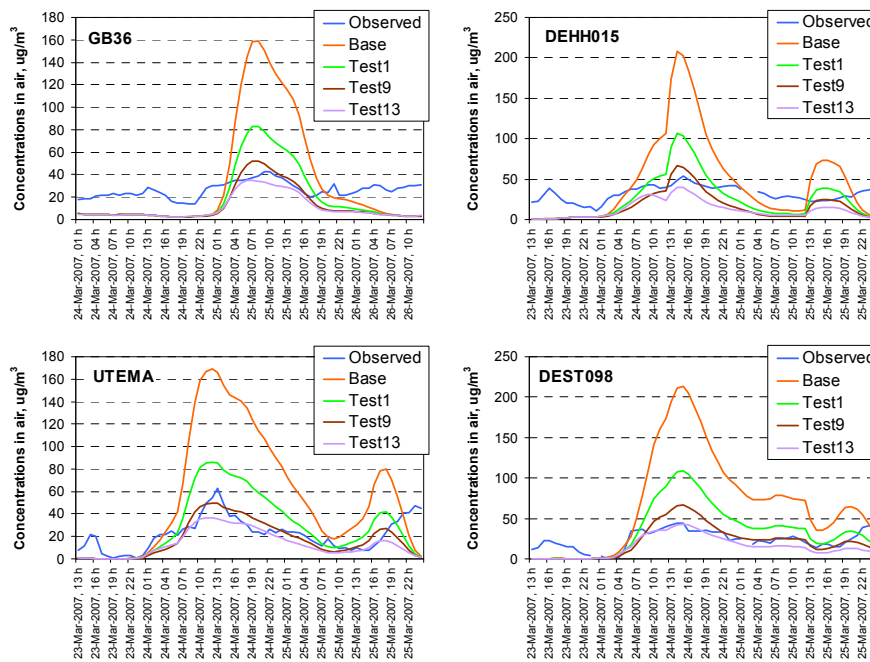


Fig. 39. Examples of observed and calculated concentrations of PM_{2.5} at some monitoring stations

Conclusions and further steps

This investigation demonstrated that wind-driven re-suspension of dust particles to the atmosphere from the agricultural lands, adapted in the model, is overestimated. A number of numerical experiments allowed examining sensitivity of the modelling results to some parameters controlling mass of re-suspended particles and their size distribution. Modelled concentrations of aerosol particles were compared against observations carried out in episode of significant re-suspension and atmospheric transport of dust from eastern Ukraine to the central and the north-western parts of Europe. Optimal set of parameters was selected to update model wind re-suspension scheme.

Part II. POP modelling

Chapter II.1.

INVESTIGATION OF DEGRADATION OF POPS IN PARTICLE-BOUND FORM

II.1.1. Kinetics of heterogenic reactions

Degradation in the atmosphere is one of the most important environmental processes for evaluating PAH contamination levels. Since all four indicator PAH compounds (B[a]P, B[b]F, B[k]F and IP) exist in the atmosphere mostly in the particle-bound form, degradation of PAHs on particles is an important process that should be taken into account in modelling of PAH fate in the environment. Here the investigation of this process is performed for B[a]P since for this compound more information is available.

In [Gusev *et al.*, 2006a,b] a parameterization of B[a]P degradation on particles based on averaged information on atmospheric reactants and aerosol chemical composition was proposed. It was shown that even such rough parameterization of B[a]P particulate degradation allows essentially improve the agreement between measurements and model predictions on the level of monthly averages.

The processes of B[a]P degradation in the atmosphere are governed by chemical nature of B[a]P itself, by the atmospheric concentrations of main reactants such as OH-radical, ozone, NO_x, N₂O₅ and others, and by concentrations and chemical composition of atmospheric aerosol. However, both reactants concentrations and aerosol chemical composition are subject to strong spatial variations, so that the proposed scheme does not describe seasonal variations of pollution in different parts of Europe in the full extent. To further improve the description of particulate degradation of B[a]P it is reasonable to examine reactions of B[a]P with particular atmospheric pollutants, mainly with ozone and nitrogen oxides.

The consideration of the theory of chemical reactions including PAHs and, in particular, B[a]P was carried out in a lot of papers and monographs. Here we mention only the classical monographs [Harvey, 1991; Finlayson-Pitts and Pitts, 2000]. This section is aimed at the review of the theory of chemical interactions between particle-bound B[a]P and gaseous atmospheric reactants. This class of reactions is known as heterogenic ones. Reaction rates and reaction products for this class are dependent on a number of factors such as ambient temperature, moisture, reactants concentrations and chemical composition of particles-carriers.

In addition, important feature of B[a]P degradation in the atmosphere is that reactions with the above atmospheric reactants not only reduce B[a]P content in the atmosphere but also lead to formation of degradation products that are different for interactions with different atmospheric reactants and may be even more harmful than B[a]P itself [Organic chemistry of the atmosphere, 1991]. In particular, this relates to oxy- and nitro-derivatives of B[a]P.

Heterogenic reactions of B[a]P with ozone.

A number of experimental studies show the ability of B[a]P to photochemical and/or chemical oxidation under the conditions close to the environmental ones [Pitts *et al.*, 1986; Kamens *et al.*, 1988; Calvert *et al.*, 2002, and others]. The most common reaction with ozone that is characteristic for all polycyclic aromatic hydrocarbons is electrophilic substitution. This reaction leads to formation of different oxy-derivatives of PAHs such as quinones, phenols, dihydrodioles and oxides [Calvert *et al.*, 2002, Toxicological Profile for polycyclic aromatic hydrocarbons, 1995].

Oxygenated polycyclic aromatic hydrocarbons are considered to be the second compound class identified for combustion processes. They are known to have carcinogenic, neoplastigenic, tumorigenic and mutagenic properties. The sources of these pollutants could be both primary (from direct emissions) and secondary (as oxidative products of the corresponding PAHs) [Lazzati, 2009]. Particular attention should be paid to B[a]P diones due to their harmful effects to human health. The atmospheric concentrations of these compounds are well-correlated with those of B[a]P, which can be indicative of their secondary origin.

The scheme of interaction of B[a]P with the atmospheric ozone together with main reaction products taken from [Calvert *et al.*, 2002] is presented in Fig. 1. Basic characteristics of degradation products are summarized in Table A1 in Annex A.

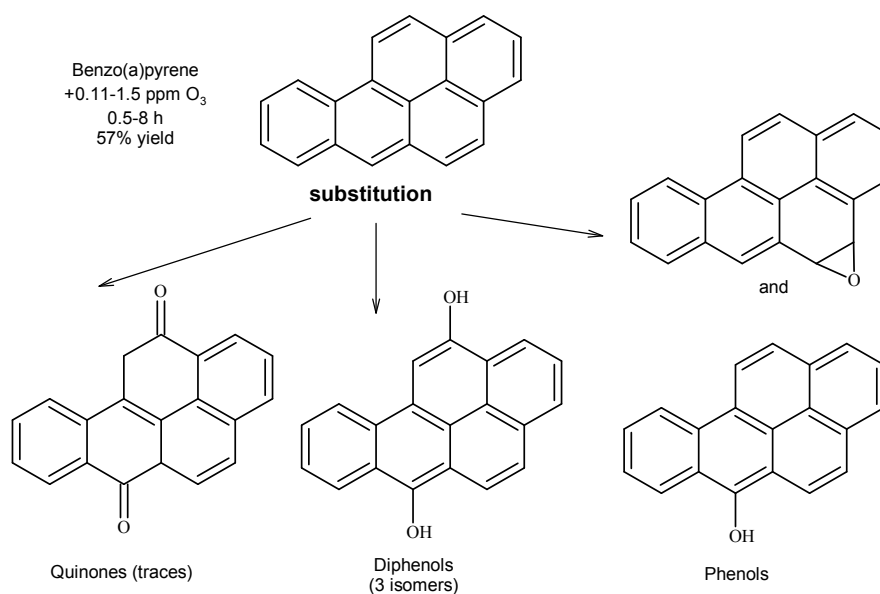


Fig. 1. The scheme of interaction of B[a]P with the atmospheric ozone together with main reaction products [Calvert *et al.*, 2002]

In addition to oxidation, break or separation of one of carbocycles initiated by ozone can lead to formation of such compounds as benzanthrone, benzanthronedicarboxylic acid and others [Calvert *et al.*, 2002]. So, the interaction of ozone with B[a]P sorbed on particle surface can result to the formation of complex mixtures of B[a]P oxi-derivatives. As an example, B[a]P sorbed on glass fiber filter exposed to ozone at concentration of 1 ppm form first dialdehydes and dicarboxylic and ketocarboxylic acids by ring-opening mechanism with parallel formation of B[a]P diones [Finlayson-Pitts and Pitts, 2000]. These compounds are of particular importance due to their harmful effects on human health. Mutagenic properties of the mixture of B[a]P oxy-derivatives can be conditioned also by the presence of benzo[a]pyrene-4,5-oxide.

Unfortunately, just few works on determination of B[a]P oxidation products in the atmosphere are found in literature. These works are mainly aimed at the examination of concentrations of PAH oxy-derivatives in urban atmosphere. So, in the spring of 1996 measurements of oxy-PAHs in a garden near business centre of Boston, USA were carried out [Allen, 1997]. Benzo[a]pyrene-6,12-dione was found in the aerosol sample at concentration of 96 pg/m³.

In the course of measurements of a number of oxy-B[a]P in the atmosphere in Munich in 1997 the following main analytically detected compounds were Benzo[a]pyrene-1,6-dione, Benzo[a]pyrene-3,6-

dione и Benzo[a]pyrene-6,12-dione [Koeber *et al.*, 1999]. In winter time (February 1997) highest concentrations (from 20 to 334 pg/m^3) were found for Benzo[a]pyrene-1,6-dione. The B[a]P concentrations in this period varied from 0.3 to 2.8 ng/m^3 . The ratio Benzo[a]pyrene-1,6-dione: Benzo[a]pyrene-3,6-dione: Benzo[a]pyrene-6,12-dione in February was 1:0.8:0.5. In summer time (July 1997) maximum concentrations (353 pg/m^3) were detected for Benzo[a]pyrene-3,6-dione; Benzo[a]pyrene-6,12-dione was not found. The investigation of oxy-PAHs in the atmosphere of Munich showed that concentrations of B[a]P diones is determined by photochemical conditions rather than B[a]P concentrations.

Summer measurements of concentrations of B[a]P and its oxy-derivatives in Milan are described in [Lazzati, 2009]. Here the same diones as in [Koeber *et al.*, 1999] were found with following concentrations:

from 67 to 430 pg/m^3 for Benzo[a]pyrene-1,6-dione;

from 0,056 to 294 pg/m^3 for Benzo[a]pyrene-3,6-dione;

from 0 to 174 pg/m^3 for Benzo[a]pyrene-6,12-dione

This is somewhat higher than summer concentrations in Munich but similar in order of magnitude.

The relation between the three detected components is displayed in Fig. 2. The comparison of concentrations of B[a]P diones in daytime and nighttime shows lower B[a]P degradation rate in dark time. All concentrations of B[a]P diones are well-correlated with ozone concentrations (r^2 from 0.47 to 0.58). For B[a]P-6.12-dione the correlation with solar radiation levels is high enough ($r^2 = 0.44$).

The results obtained by [Lazzati, 2009] manifest that oxidation of B[a]P is governed not only by ozone concentrations but also by solar radiation intensity.

The interaction between B[a]P and gaseous atmospheric reactants is investigated over 30 years. These investigations were stimulated by disclosure of the decay of B[a]P concentrations at filters especially for long sampling periods. In particular, in [Pitts *et al.*, 1986] it was shown that B[a]P losses on glass fiber filter can be from 20% to 90% at ozone concentration level of 200 ppb.

The investigation of kinetics of heterogenic reaction between B[a]P sorbed on particles of different nature and ozone was carried out in a lot of papers [Alebić-Juretić A., 2000; Pöschl *et al.*, 2001, Kwamena *et al.*, 2004, Kahan *et al.*, 2006, Perraudin E. *et al.*, 2007, Shiraiwa *et al.*, 2011 and others].

One of possible reaction mechanisms for heterogenic reaction between B[a]P and ozone could be Langmuir –Hinshelwood mechanism (Fig. 3) used in [Pöschl *et al.*, 2001, Kwamena *et al.*, 2004, Kahan *et al.*, 2006, Shiraiwa *et al.*, 2011, Zhou *et al.*, 2011]. According to this mechanism, the rate of a heterogeneous reaction is controlled by the reaction of the adsorbed molecules, and that all adsorption and desorption pressure are in equilibrium. Both molecules are supposed to be adsorbed at the aerosol surface and the adsorbed molecules undergo a bimolecular reaction between compounds A (ozone in our case) and B (B[a]P in our case):

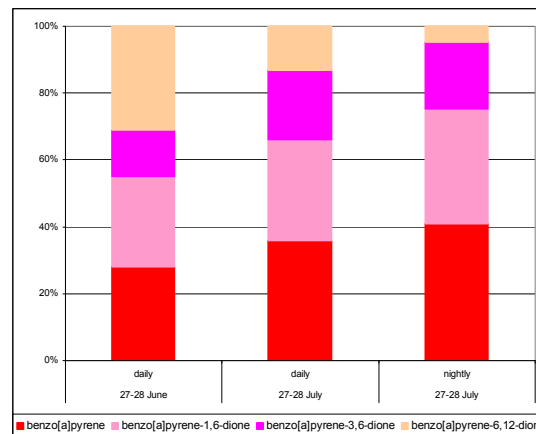
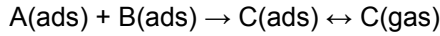
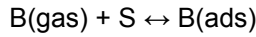
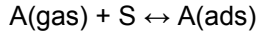


Fig. 2. B[a]P and its oxy-derivatives in the atmospheric air in Milan [Lazzati, 2009]



Thus, reaction rate depends on concentrations of two adsorbed substances A and B.

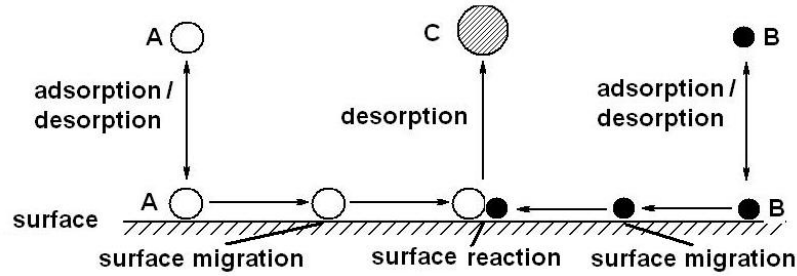
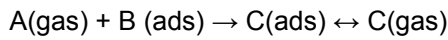
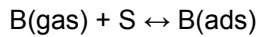


Fig. 3. Langmuir-Hinshelwood Mechanism (heterogeneous catalysis proceeds at a surface)

Another type of interaction is described by Rideal-Eley mechanism. In this mechanism, proposed in 1938 by D. D. Eley and E. K. Rideal, only one of the molecules adsorbs and the other one reacts with it directly from the gas phase, without adsorbing:



According to this mechanism, linear dependence between pseudo-first order rate constant and ozone concentrations in the atmosphere was obtained in [Alebić-Juretić *et al.*, 1990 and Wu *et al.*, 1984].

According to [Pöschl *et al.*, 2001], pseudo-first order rate constant for the interaction between B[a]P adsorbed on soot particles and ozone concentrations in the atmosphere is given by

$$k_1 = k_{2S} \frac{[SS]_S K_{O_3} [O_3]}{1 + K_{O_3} [O_3]} = k_{\max} \frac{K_{O_3} [O_3]}{1 + K_{O_3} [O_3]}, \quad (1)$$

where Langmuir –Hinshelwood mechanism was used.

Here k_{2S} is the second-order reaction constant between B[a]P and ozone adsorbed on soot particles, cm^2/s ,

$[SS]_S$ is the surface concentration of adsorption sites, cm^{-2} ,

K_{O_3} is the Langmuir adsorption equilibrium constant for ozone, cm^3 ,

$[O_3]$ is volume ozone concentration in the atmosphere, cm^{-3} .

The product $k_{\max} = k_{2S} \times [SS]_S$, s^{-1} , is maximum value of pseudo-first order rate constant achieved at high ozone concentrations.

Similar relation was obtained by [Kwamena *et al.*, 2004] for calculation of pseudo-first order rate constant for reaction between atmospheric ozone and B[a]P adsorbed on acelaic acid aerosol. Fig. 4 illustrates the dependency of pseudo-first order reaction rate on ozone concentration and air humidity obtained in this paper.

In particular, the experiment confirms the influence of air humidity to reaction rate of interaction between B[a]P and ozone. For acelaic acid being a surrogate substance for organic aerosol reaction rate constant increases with the increase of humidity. Besides, it is seen that the dependence of pseudo-first order reaction rate on ozone concentrations is non-linear. However, non-linearity takes place at very high ozone concentrations which are not achieved in the environment.

Table 1 summarizes the values of coefficients in (1) used for calculation of pseudo-first order reaction rate obtained in papers [Pöschl et al, 2001, Kwamena et al, 2004 and Zhou et al., 2011].

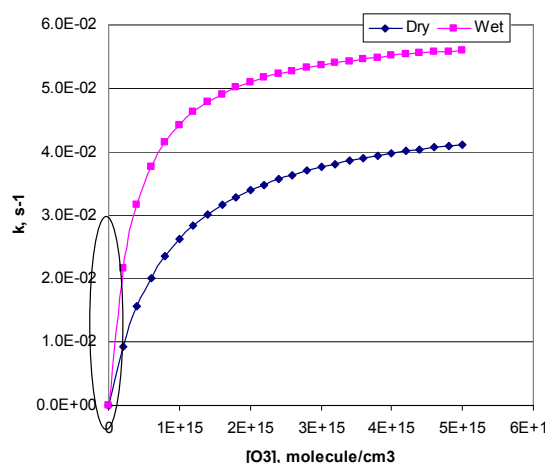


Fig. 4. Dependence of pseudo-first order rate constant on ozone concentrations and air humidity obtained by [Kwamena et al., 2004]

Table 1. Rate constants of heterogenic reactions between B[a]P and ozone on the basis of Langmuir-Hinshelwood mechanism, experiment data.

Solid surface in experiment	K_{O_3} (10^{-13}) cm^3	k_{max}, s^{-1}	humidity, %	References
soot	2.8 ± 0.2	0.015 ± 0.001	0-25	Pöschl et al, 2001
octanol thin films	36	0.0055 ± 0.0002		Kahan et al, 2006 cited from Zhou et al., 2011
azelaic acid aerosols	0.028 ± 0.014	0.060 ± 0.018	~72	Kwamena et al, 2004
	0.012 ± 0.0004	0.048 ± 0.008	<1	
ammonium sulfate	0.21 ± 0.005	0.032 ± 0.002		Zhou et al., 2011
ammonium sulfate+ bis (2-ethylhexyl) sebacate)	0.004 ± 0.0005	0.051 ± 0.002		
ammonium sulfate+eicosane ($C_{20}H_{42}$)	0.139 ± 0.098	0.012 ± 0.002		

At present ozone concentrations in continental region are thought to be from 20 to 40 ppb ($40 - 80 \mu g/m^3$ or $5 \times 10^{11} - 1 \times 10^{12}$ molecules per cm^3). Higher levels of ozone concentrations (50 – 80 ppb) are characteristic for clean regions downwind from cities. In urban and adjacent regions ozone concentrations are even higher (100 – 200 ppb and more). According to the data of Chemical Coordinating Centre of EMEP ozone levels measured at EMEP monitoring network are mainly not more than 50 ppb ($100 \mu g/m^3$) [Hjellbrekke and Fjæraa, 2009].

It is worth noting that model experiments described in literature are focused at determination of rate constants for reaction with ozone alone and use concentration ranges essentially exceeding the levels observed in the atmosphere. From this it can be concluded that at realistic ozone concentrations the dependence of the first-order rate constant on ozone concentrations can be viewed as a linear one (as marked in Fig. 4).

The first-order rate constant for reaction between B[a]P and ozone can be also calculated on the basis of volume ozone concentration and second-order rate constant. On the basis of experimental investigation of ozone/B[a]P interaction second-order rate constants were obtained for graphite, silicagel and soot particles, see Table 2.

Table 2. Second-order rate constants of heterogenic reactions between ozone and B[a]P adsorbed on particles of various types (chemical composition).

Particle type	Second-order rate constants, cm ³ /molecule-s		
	Calvert et al., 2002	Perraudin et al., 2007	Cazaunau et al., 2010
Graphite		$(5.3 \pm 1.5) \times 10^{-17}$	
Wood soot (wood smoke)	1.6×10^{-17}		
Silicagel		$(1.4 \pm 0.3) \times 10^{-16}$	$(2.1 \pm 0.5) \times 10^{-15}$

For typical range of ozone concentrations (0 – 200 ppb) the dependence of pseudo-first order rate constants on ozone concentrations calculated on the basis of literature data (Tables 1 and 2) is shown in Fig. 5.

As follows from the dependencies presented in Fig. 5, most intensive reaction takes place at mineral particles containing ammonium sulfate. Reaction rate constant at silicagel particles obtained by [Perraudin et al., 2007] is 4 – 5 times lower. The comparison of reaction rate constants at ammonium sulfate and silicagel calculated using second-order rate constants reported in [Cazaunau et al., 2010] leads to the conclusion that most fast reaction takes place at silicagel particles. Since reaction rates obtained for particles of one and the same chemical composition (silicagel) obtained by different researchers differ by more than one order of magnitude (15 times), additional work is required for choosing the value of reaction rate constant. At particles with other chemical composition B[a]P oxidation reaction is slower (excluding results of [Pöschl et al, 2001; Bedjanian and Nguyen, 2010]).

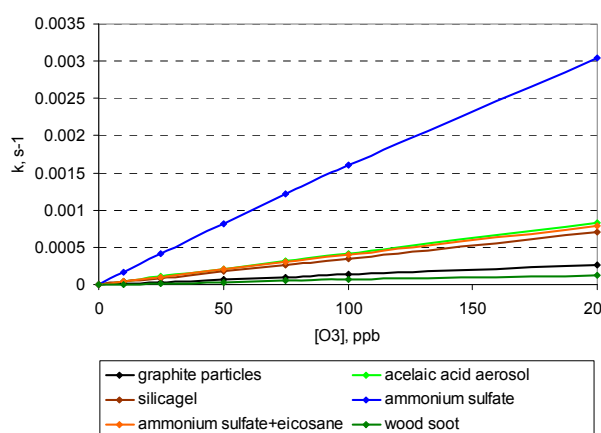


Fig. 5. Dependence of pseudo-first order rate constant for B[a]P/ozon reaction at aerosol particles of various chemical composition.

For aerosols containing organic substance only (azelaic acid) or for mineral aerosol coated by organic film (e. g. ammonium sulfate with eicosan film) rate constants of oxidation decrease in comparison with reactions at ammonium sulfate. However, these rates are sufficiently close to those for silicagel particles according to [Perraudin et al., 2007]. Coating of ammonium sulfate by bis(2-ethylhexyl)sebacate film reduces oxidation reaction 4 times.

For particles containing elemental carbon (graphite and soot) reaction rates constants is considerably less (2.5 – 5 times) than for silicagel particles according to [Perraudin et al., 2007], and 40 – 80 times less than rate constants for silicagel particles reported by [Cazaunau et al., 2010].

Table 3 shows pseudo-first order rate constants for B[a]P oxidation calculated for 50 ppb ozone concentrations calculated on the basis of literature data.

Table 3. Calculated pseudo-first order rate constants of reaction between B[a]P and ozone adsorbed on aerosol particles with different composition at ozone concentrations of 50 ppb.

Solid surface in experiment	Pseudo-first order rate constant, s ⁻¹	Half-life, min	Remarks	References
silicagel	4.8 × 10 ⁻⁴	12	partial surface coverage	<i>Alebić-Juretić et al., 2000</i>
	1.5 × 10 ⁻⁴	40	complete surface coverage	
silicagel	1.8 × 10 ⁻⁴	66		<i>Perraudin et al., 2007</i>
silicagel	2.6 × 10 ⁻³	4,4		<i>Cazaunau et al., 2010</i>
silicagel	1.04 × 10 ⁻⁵	1111		<i>Wu et al., 1984</i>
soot aerosol particle	3.9 × 10 ⁻³	3		<i>Pöschl et al, 2001</i>
soot (wood smoke)	3.3 × 10 ⁻⁵	354		<i>Calvert et al., 2002</i>
laboratory generated kerosene soot*	6.8 × 10 ⁻³	1.7		<i>Bedjanian and Nguyen, 2010</i>
graphite	6.7 × 10 ⁻⁵	174		<i>Perraudin et al., 2007</i>
azelaic acis aerosols	7.2 × 10 ⁻⁵	160	dry (relative humidity <1%)	<i>Kwamena et al., 2004</i>
azelaic acis aerosols	2.1 × 10 ⁻⁴	55	wet (relative humidity 72%)	
1-octanol film (film coated particle matter)	2.5 × 10 ⁻⁶	4691 (3,3 дня)		<i>Kahan et al., 2006</i>
ammonium sulfate (AS)	8.1 × 10 ⁻⁴	14		<i>Zhou et al , 2011</i>
ammonium sulfate+ bis (2-ethylhexyl) sebacate (AS+BES)	6.1 × 10 ⁻⁵	188		
ammonium sulfate+eicosane (C ₂₀ H ₄₂)	2.1 × 10 ⁻⁴	56		

* obtained at temperature 290° K and ozone concentrations 1.3 × 10¹² molecules/cm³ ≈ 50 ppb

Interaction between B[a]P and ozone at particles consisting only of mineral substances (sodium chloride, ammonium sulfate and silicagel) is characterized by pseudo-first order rate constants between 4.0 × 10⁻⁶ to 2.6 × 10⁻³ s⁻¹. For particles consisting totally of elemental carbon (graphite and soot) experimentally obtained pseudo-first order rate constants range from 3.3 × 10⁻⁵ to 3.9 × 10⁻³ s⁻¹.

Values of reaction rate constants obtained in papers [*Pöschl et al, 2001; Bedjanian and Nguyen, 2010*] essentially (by one or two orders of magnitude) exceed those obtained by other researchers. Based on these values one can conclude that B[a]P adsorbed on soot particles possesses maximum reaction ability with respect to ozone.

As it was shown in [*Zhou et al., 2011*] the presence of a film of liquid organic substance (bis (2-ethylhexyl) sebacate – BES) on the surface of an ammonium sulfate particle (AS) slightly decreases the reactivity of B[a]P and is described by Langmuir-Hinshelwood mechanism (Fig. 6). Relatively low value of rate constant for AS + EC system in comparison with AS and AS + BES systems demonstrate suppression of B[a]P reactivity by a film of solid substance such as eicosan (EC).

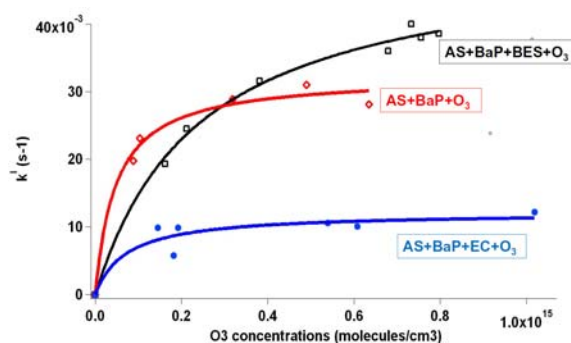


Fig. 6. Pseudo-first-order rate coefficients as a function of gas-phase ozone concentration. The data are fit with Langmuir-Hinshelwood mechanism [*Zhou et al., 2011*].

The conclusion of the above cited paper is “The heterogeneous reactivity of BaP was reduced substantially by a thin (4–8 nm), solid EC coating and entirely suppressed by thick (10–80 nm) coatings, presumably because of slow diffusion through the organic layer. Although the heterogeneous reactivity of surface-bound PAHs is extremely rapid in the atmosphere, this work is the first to experimentally demonstrate a mechanism by which the lifetime of PAHs may be significantly prolonged, permitting them to undergo long-range transport to remote locations” [Zhou *et al.*, 2012].

The attempts to use mechanisms of heterogenic oxidation of particle-bound B[a]P by ozone in a global 3D model are carried out in [Friedman and Selin, 2012]. The authors compared three possible parameterization of oxidation process:

- i. an O₃ reaction rate constant (k_{O_3}) for B[a]P on soot particles from [Pöschl *et al.*, 2001];
- ii. a k_{O_3} for B[a]P dissolved in octanol from [Kahan *et al.*, 2006];
- iii. a k_{O_3} for B[a]P on wet acelaic acid aerosols from [Kwamena *et al.*, 2004]

As a result it was found that B[a]P concentrations calculated by the model strongly depend on the scheme of reaction between B[a]P and ozone. On-particle oxidation schemes were tested for BC-phase BaP only (for consistency with the Pöschl scheme which only applies to soot). It was found that:

- The Pöschl scheme reduces both mid-latitude non-urban and Arctic BaP concentrations on average by more than 30 times, causing large underestimates of observed concentrations.
- The Kahan scheme does not substantially reduce concentrations for either the mid-latitude nonurban stations or Arctic stations.
- At mid-latitude nonurban sites, the Kwamena scheme reduces average concentrations by a factor of 6, improving the match to observations, similar to [Mattias *et al.*, 2009] who also used the Kwamena scheme. In the Arctic, however, concentrations are reduced by 10X, which weakens the match to observations and reduces the seasonal variation.

The authors conclude that “In general, however, the Kwamena scheme brings observed and modeled concentrations closest together, and has little effect on the B[a]P which is already well simulated by the model. We conclude that on-particle oxidation has a substantial effect on BaP concentrations, and that a rate intermediate to the Kahan and Kwamena scheme best matches existing data constraints.” As a result, ozone oxidation of B[a]P adsorbed on particles was not included in any of the standard simulations.

In [Mattias *et al.*, 2009] chemical transport model CMAQ was used for calculations of B[a]P concentrations in Europe. However, inclusion of particle-bound B[a]P degradation due to interaction with ozone has led to a reduction of the modeled air concentration by approx. a factor 5.

In [Kwamena *et al.*, 2007] using the scheme of B[a]P oxidation on organic particles [Kwamena *et al.*, 2004 and Kahan *et al.*, 2006] within Multimedia Urban Model in the urban environment it was found that reactions on surface films are dominant heterogeneous reactions with gas phase ozone. The losses of B[a]P adsorbed on particles exceed 75%.

Summarizing the above considerations it can be concluded that at present it is hard to use one of the considered rate constants in MSC-E models since:

- reaction rate constants for particle-bound B[a]P with ozone depend on chemical composition of the atmospheric aerosol, which is subject to essential spatial and temporal variability;

- there are considerable differences in the values of rate constants for reactions between particle-bound B[a]P and ozone obtained by different researchers for particles of one and the same chemical composition (such as silicagel and soot);
- research results show that rate constants for the considered reaction depend on air humidity, however experimental data for the whole range of humidity in the atmosphere as well as the data on temperature dependence of rate constants are absent.

So, the presence of organic compounds in the atmospheric aerosol essentially influences the process of B[a]P oxidation by ozone. However, for accurate parameterization of this process in modeling further research on kinetics of heterogenic reactions between particle-bound B[a]P and ozone including temperature dependence of reaction rates is needed.

Heterogenic B[a]P reactions with atmospheric nitrogen compounds.

Similarly to Oxy-PAHs, nitrated polycyclic aromatic hydrocarbons (Nitro-PAHs) can be either directly emitted from combustion sources (vehicle exhaust; industrial emissions and emissions from domestic residential heating/cooking and wood burning [EHC 229: *Selected Nitro-and Nitro-oxyPAHs*, 2003]) or by chemical reaction with atmospheric reactants. The structure and main characteristics of various nitro-derivatives of B[a]P are presented in Table A2 in the Annex A.

Since there are powerful anthropogenic sources of nitro-PAHs, measurements of these compounds are aimed mainly at the determination of nitro- and dinitropyrenes and and nitrofluorenes. It is found that 1-nitropyrene is a “marker” nitro-PAH for diesel exhaust, and 2-nitrofluoranthene is the major particle-associated nitro-PAH [Reisen and Arey, 2005]. The number of published data on concentrations of B[a]P nitro-derivatives is limited. In the literature mainly the data on 6-Nitrobenzo[a]pyrene are presented.

According to [Matsushita and Iida, 1986], in the atmosphere over Tokyo concentrations of 6-Nitrobenzo[a]pyrene were 0.27 ng/m³. Later investigations [Shii et al., 2000] report the range of concentrations of this pollutant from 0.2 to 0.47 ng/m³. At business centre in downtown of Kanazawa 6-Nitrobenzo[a]pyrene concentrations were found to be 2.3 pg/m³ [Araki et al., 2009]. Higher concentration levels were detected in the atmosphere over Tieling city in China according to the results of measurements at three locations in the period from June 2003 to May 2004 annual averages of concentrations varied in the range from 30.9 to 56.2 pg/m³ [Tang et al., 2009].

In Europe measurements of nitro-PAH concentrations were performed under the program Pollution des Vallées Alpines (POVA). The program included several field campaigns and associated 3D modeling [Brulfert et al, 2005]. As part of the POVA research program, two intensive campaigns were performed in winter 2002-2003 and summer 2003 [Albinet et al., 2008]. The results obtained are displayed in Table 4.

Table 4. Concentrations of 6-Nitrobenzo[a]pyrene in the atmospheric air over Europe.

Sampling location	Location type	Sampling period	Concentrations, pg/m ³	References
France				
Clos de l'Ours	Suburban Alt - 1034 m	Winter 2002-2003	13.0	<i>Albinet et al., 2008</i>
		summer 2003	0.1	
Les Bossons	Road side Alt - 1042 m	Winter 2002-2003	4.3	
		summer 2003	0.9	
Plan de l'Aiguille	Altitude Alt -2263 m	Winter 2002-2003	0.1	
		summer 2003	0.2	
Argentière	Rural Alt -1250 m	Winter 2002-2003	0.2	
		summer 2003	0.1	
Tigny	Rural Alt -441 m	Winter 2002-2003	6.5	
		summer 2003	0.3	
Orelle	Suburban Alt -1134 m	summer 2003	1.0	
Modane	Suburban Alt -1094 m	Winter 2002-2003	5.4	
		summer 2003	1.4	
Sollières	Rural Alt -1373 m	Winter 2002-2003	9.2	
		summer 2003	0.9	
Marseille, 5 avenues	Urban	July 2004	5.9	<i>Albinet et al., 2007</i>
city La Penne sur Huveaune	Sub-urban	July 2004	0.9	
Village Plan d' Aups, ca 30 km of Marseille	rural	July 2004	0.0	
Italy				
Montelibretti, ca 30 km of Rome	Rural	September 2005	36/42*	<i>Cicinato et al., 2008</i>
		October 2005	68/68	
		November 2005	71/92	
		January 2005	11/14	

* associated to PM₁₀ /associated to PM_{2.5}

The comparison of B[a]P and 6-Nitrobenzo[a]pyrene concentrations at particles of size 2.5 and 10 µm obtained in measurements in semi-rural area Montelibretti located 30 km NE of Rome [*Cicinato et al., 2008*] shows that B[a]P concentrations in winter time essentially (by an order of magnitude or more) exceed those of its nitro-derivative whereas in autumn time their ratio diminishes to 3 times.

The concentrations of B[a]P dinitroderivative 3,6-Dinitrobenzo[a]pyrene was detected on atmospheric aerosol particles in winter period in Santiago at 0,002 ng/m³ [*Sera et al., 1991*].

Various types of urban dust were examined with respect to the content of wide spectrum of nitro-PAHs by [*Bamford et al., 2003*]. The results of this work demonstrate that in dust samples the content of 6-Nitrobenzo[a]pyrene essentially exceeds that of other nitroderivatives – 1-Nitrobenzo[a]pyrene and 3-Nitrobenzo[a]pyrene. Thus, it can be concluded that in the atmosphere only one of possible B[a]P nitroderivatives – 6-Nitrobenzo[a]pyrene is mostly detected.

The mechanism of formation of this compound proposed by [Cazaunau et al., 2010] is presented in Fig. 7.

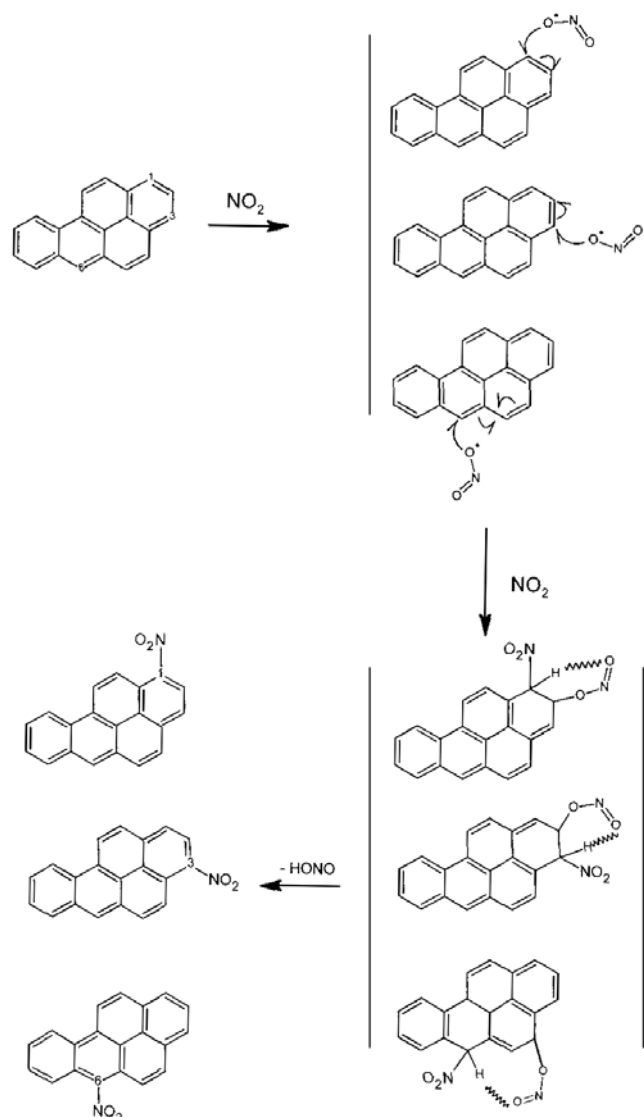


Fig. 7. The mechanism of heterogenic nitration of B[a]P according to [Cazaunau et al., 2010].

As mentioned above, the presence of B[a]P nitro-derivatives in the atmosphere is conditioned by two reasons: direct (anthropogenic) emission and in situ formation involving parent PAHs and nitrating species ($\text{OH} + \text{NO}_2$; NO_3^- ; HNO_3) with isomerically different products.

The atmospheric part of nitrogen cycle includes a number of nitrogen-containing compounds being able to take part in nitration of polycyclic aromatic hydrocarbons. The nitrogen cycle is schematically displayed in Fig. 8.

The presence of NO_2 in the atmosphere leads to a number of gaseous reactions. So, under photolysis

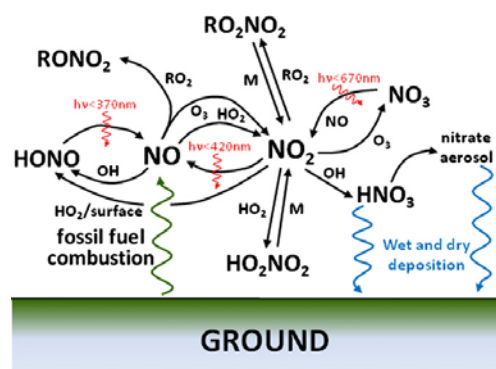
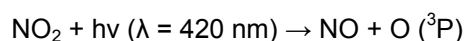
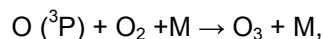


Fig. 8. Schematic representation of the nitrogen cycle [PORG, 1997].

conditions O₃ is formed from the following reaction:

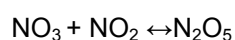
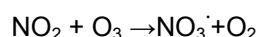


followed by

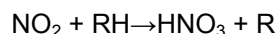


where M is a third molecule that stabilizes the excited intermediate before it dissociates back into reactants [Finlayson-Pitts and Pitts, 1997]

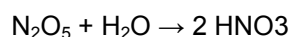
Under dark condition with NO₂ and O₃ in our laboratory system, N₂O₅ and NO₃ radical are most probably the reactive species from the following reaction sequences [Atkinson, 1991; Wayne et al., 1991].



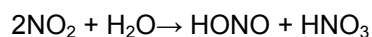
NO₃-radical easily reacts with volatile organic compounds resulting in the appearance of nitric acid:



Nitric acid can also be formed from N₂O₅ in the nighttime as a result of hydrolysis at wet surfaces and aerosol particles:



NO₂ can be hydrolyzed at the surface of soot (heterogenic reaction) with formation of nitric and nitrous acids:



The kinetic details regarding this reaction are not conclusive, but the reaction is likely first order in NO₂ [Finlayson-Pitts et al., 2003; Ziemba et al., 2010].

Thus, a wide spectrum of atmospheric reactants is involved in formation of PAH nitro-derivatives in the atmosphere: OH and NO₃ radicals, NO₂ and HNO₃. Reaction rates depend strongly on the nature and composition of particles on which B[a]P is adsorbed.

There is much less information on rates of reactions with nitrogen compounds compared with those with ozone. Only reaction rates on silicagel (mineral aerosol) and several types of elemental carbon were found in literature. Second order rate constants for B[a]P interaction with NO₂ are given in Table 5.

Table 5. Second-order rate constants for B[a]P reactions with NO₂.

Particle composition	Second-order rate constants, cm ³ /molecule s			
	Calvert et al., 2002	Perraudin et al., 2007	Cazaunau et al., 2010	Guo and Kamens, 1991
Silicagel		$(9.3 \pm 2.3) \times 10^{-15}$	$(5.8 \pm 1.4) \times 10^{-16}$	
Grafite		7.7×10^{-17}		
Wood soot	3.7×10^{-18} ⁽¹⁾			5.1×10^{-19}
	6.2×10^{-19} ⁽²⁾			

⁽¹⁾ – low PAH particle loading

⁽²⁾ – high PAH particle loading

Second-order rate constants for reactions between particle-bound B[a]P and various atmospheric nitrogen compounds (NO₂, NO₃-radical, N₂O₅, HNO₃) presented in the monograph [Calvert *et al.*, 2002] are close to those obtained by [Guo and Kamens, 1991] whereas more recent investigations [Perraudin *et al.*, 2007 and Cazaunau *et al.*, 2010] differ from the above data by several order of magnitude.

Experiments on determination of values of rate constants for reactions between B[a]P and NO₂ show that the fastest reaction takes place on silicagel surface (a surrogate for mineral aerosol compound). It is worth noting that the results reported by different authors [Perraudin *et al.*, 2007, Cazaunau *et al.*, 2010] for reactions on silicagel differ essentially (about 16 times). Reactions on carbon-containing aerosol (graphite) are much slower than on silicagel (with the difference at least one order of magnitude). The most slow reaction rates obtained for B[a]P adsorbed on soot (see Table 5).

Formation of nitro-derivatives and the decrease of concentrations of B[a]P adsorbed on particles with different chemical composition was also investigated for other nitrating agents – nitric acid (HNO₃) and nitrogen pentoxide (N₂O₅). The obtained rate constants are shown in Table 6.

Table 6. Second-order rate constants for B[a]P reactions with other gaseous atmospheric nitrogen compounds.

Particle composition	Second order rate constants, cm ³ /molecule	
	HNO ₃ [Calvert <i>et al.</i> , 2002]	N ₂ O ₅ [Kamens <i>et al.</i> , 1990]
wood soot	3.4×10^{-19}	4.7×10^{-18}
diesel soot		2.9×10^{-17}

In spite of the fact that the presence of HNO₃ fastens nitration, for the case when it is adsorbed at carbon-containing medium (as during smog events) the reaction is essentially slower than on silicagel. This is confirmed by small value of rate constant for the reaction between B[a]P and nitric acid (see Table 6). The reaction with N₂O₅ in the nighttime is somewhat faster but the comparison of the corresponding rate constant with that on silicagel shows that this process seems not to be most essential in formation of B[a]P nitroderivatives. The presence in the atmosphere various gaseous nitrogen compounds and the comparison of experimentally determined reaction rates allows concluding that B[a]P mostly reacts with nitrogen dioxide than with N₂O₅ or HNO₃.

Further, pseudo-first order rate constants for heterogenic reaction between B[a]P and nitrogen dioxide were also experimentally determined (see Table 7).

It should be taken into account that the investigations were performed with levels of nitrogen dioxide essentially exceeding those in the real atmosphere. So, according to European monitoring data, the range of average NO₂ multi-annual concentrations for the period from 1999 to 2008 is 12.4 – 135.5 µg/m³ which correspond to 3.1×10^{11} – 3.4×10^{12} molecules/cm³ or 6.5 – 70.9 ppb [Guerreiro *et al.*, 2010], see Table 7.

As follows from the data presented in Table 7, the range of values of rate constants for reactions between nitrogen dioxide and B[a]P adsorbed on particles containing elemental carbon is rather wide and can amount to three orders of magnitude.

Table 7. Pseudo-first-order rate constants for reactions with NO₂ and B[a]P adsorbed on carbon-containing particles and silicagel.

Solid surface in experiment	Concentrations NO ₂ , molecules/cm ³	Pseudo-first order rate constant, s ⁻¹	References
Ethylene flame soot	1.2×10^{14}	$1,2 \times 10^{-6}$	<i>Buthlet and Crossley, 1981</i>
Wood smoke particles	$\approx 1 \times 10^{13}$	5.2×10^{-5}	<i>Kamens et al., 1985</i>
	1.3×10^{13}	6.3×10^{-6}	
Graphite particles	8×10^{13}	6.2×10^{-3}	<i>Esteve et al., 2004</i>
Diesel soot	8×10^{13}	3.2×10^{-3}	<i>Esteve et al., 2006</i>
Kerosene flame soot (under dark conditions)	$1 \times 10^{14} - 5 \times 10^{14}$	$<5 \times 10^{-5}$	<i>Nguen et al., 2009</i>
Silicagel	1.5×10^{12}	1.4×10^{-3}	<i>Perraudin et al., 2005</i>
	1.25×10^{12}	$7.3 \times 10^{-4*}$	<i>Cazaunau et al., 2010</i>

* - calculated value

The pseudo-first-order rate constants for reaction between nitrogen dioxide and B[a]P adsorbed on silicagel were obtained different authors using NO₂ concentrations close to those in the atmosphere. However, the results also differ more than by an order of magnitude (16 times).

Fig. 9 presents the dependences of pseudo-first order rate constant on nitrogen dioxide concentration for heterogenic reaction with B[a]P adsorbed on particles with various chemical composition.

These dependences manifest that rate constants for reaction between nitrogen dioxide and B[a]P in the case when the latter is adsorbed on silicagel in comparison with B[a]P sorbed on graphite particles.

Measurement results on concentrations of various B[a]P nitro-derivatives in the atmosphere are in good agreement with the results by [Cazaunau et al., 2010], where the kinetics of formation of various B[a]P nitro-derivatives due to the reaction with nitrogen dioxide is examined (see Table 8). The results obtained in this research allow justify theoretically the predominance of 6-Nitrobenzo[a]pyrene over two other compounds.

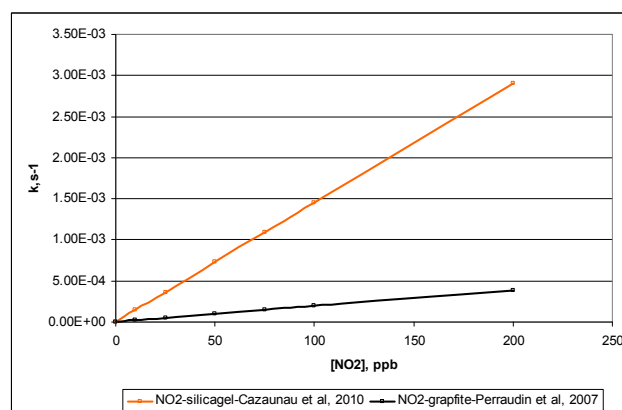


Fig. 9. The comparison of the dependencies of pseudo-first order reaction rates on nitrogen dioxide concentrations for particles-carriers of different composition.

Table 8. Second-order rate constants for reactions with NO₂ and B[a]P adsorbed on silicagel according to [Cazaunau et al., 2010].

B[a]P nitroderivatives	Second order rate constants, cm ³ /molecule s
1-Nitrobenzo[a]pyrene	$(2.2 \pm 0.6) \times 10^{-17}$
3-Nitrobenzo[a]pyrene	$(5.3 \pm 1.3) \times 10^{-17}$
6-Nitrobenzo[a]pyrene	$(3.7 \pm 0.9) \times 10^{-16}$

Concluding remarks

- The above literature analysis shows that B[a]P sorbed on atmospheric aerosol actively interacts with gaseous atmospheric reactants (ozone and nitrogen dioxide). The rate constants of heterogenic reactions between these compounds strongly depend on particle chemical composition.
- Degradation products (nitro- and oxy-derivatives of B[a]P) are also dangerous for human health and the environment. Measurements show the presence of these products in the atmosphere in Europe and Asia.
- In the investigations of B[a]P oxidation essential attention was paid to the influence of aerosol organic compounds. At present there are no similar investigations for reactions between particle-bound B[a]P and gaseous nitrogen compounds in the atmosphere.
- The presence of organic film on the surface of mineral aerosol particles and its properties (liquid or solid state) essentially affects rate constants of reactions between B[a]P and ozone. Solid film on the particle surface oxidation process essentially slows down B[a]P oxidation [Zhou *et al.*, 2011].
- The investigations of the kinetics of heterogenic reactions under simulated levels of gaseous compounds were performed for a single gaseous compound – ozone or nitrogen dioxide. The reaction rate constants obtained for these compounds are comparable in values, which leads to the conclusion that oxidation and nitration processes are concurrent under real conditions with all gaseous reactants simultaneously present in the atmosphere. However, measurements of concentrations of B[a]P oxy- and nitro-derivatives show that the latter ones exist in the atmosphere at lower concentrations, which means that above two processes differ in rates, nitration being slower than oxidation. Taking in mind second-order rate constants for B[a]P adsorbed on carbon-containing particles with nitrogen dioxide obtained by [Calvert *et al.*, 2002 and Guo and Kamens, 1991], one can conclude that the B[a]P degradation due to nitration is negligible compared with that due to oxidation.
- In [Kwamena *et al.*, 2004] the importance of the atmospheric humidity for determining reaction rate of the interaction between B[a]P and ozone. Water vapour in the atmosphere can also play the role of reagent in particular in formation of nitrating agents – nitric and nitrous acids.
- The values of reaction rate constants obtained by different authors under similar in temperature and humidity conditions differ by several orders of magnitude even for particles close in composition.
- For usage in model parameterization the values of second-order rate constants for reactions between B[a]P and ozone/nitrogen dioxide obtained in [Perraudin *et al.*, 2007 и Cazaunau *et al.*, 2010] can be proposed. However, in such a parameterization the composition of atmospheric aerosol will be taken into account in a rough manner since it uses only silicagel (as a surrogate for mineral compound) and graphite (as a surrogate for elemental carbon) or their combination. The degradation of B[a]P adsorbed on particles containing mixture of organic and non-organic compounds cannot at present be accurately parameterized due to poor knowledge on quantity and composition of organic compounds in aerosol and on reaction rate constants in organic films covering mineral particles and/or in particles with entirely organic composition. The information on temperature dependence of B[a]P degradation rates for heterogenic reactions is not found yet in literature.
- For modelling of atmospheric degradation of particle-bound B[a]P the information on chemical composition of organic aerosol fraction is necessary.

II.1.2. Chemical composition of atmospheric aerosol

Since B[a]P mostly is present in the atmosphere in particulate form, the processes of degradation of particulate phase of B[a]P may strongly affect the contamination levels. These processes are governed by two factors: atmospheric concentrations of the reactants involved in chemical and photochemical reactions with B[a]P and chemical composition of the atmospheric aerosol.

There are two processes that go differently for PAHs adsorbed at atmospheric aerosol of different chemical nature. First, this is the process of gas/particle partitioning, which determines PAH fraction existing in the atmosphere in particle-bound form. Second, chemical nature of particles-carriers (mineral aerosol, organic carbon and elemental carbon) strongly affects various atmospheric processes such as light absorption and reactions with various gaseous atmospheric reactants. It should be mentioned that rate constants of these reactions may depend on solar radiation flux which in turn is dependent on the atmospheric aerosol content, particularly on elemental carbon.

The atmospheric content of aerosol matter and its chemical composition is being investigated at the EMEP monitoring network [Yttri *et al.*, 2011; Hjellbrekke and Fjærøaa, 2011a].

In consideration of chemical composition of atmospheric aerosol the following classes of compounds are distinguished: inorganic matter (mineral matter, sulphates, nitrates, ammonium salts), organic matter and elemental carbon.

Measurements show that mineral compounds are constituents of both rough and fine particles. They are formed mainly due to soil and rock erosion and its composition is similar to that of the earth's crust consisting mainly of silicon dioxide.

According to [Yttri *et al.*, 2011], average fraction of mineral matter in the atmospheric aerosol within the period from 1996 to 2007 lie in wide range. In PM₁₀ mineral compound amounts to about 15% in southern Europe and 4% in northern and western Europe. In PM_{2,5} mineral compound constitutes from 5% in central and north-western Europe to 11% in southern Europe. However, at some locations mineral part may be predominant (Fig. 10). For particles from PM₁ mineral fraction presents at about 4%.

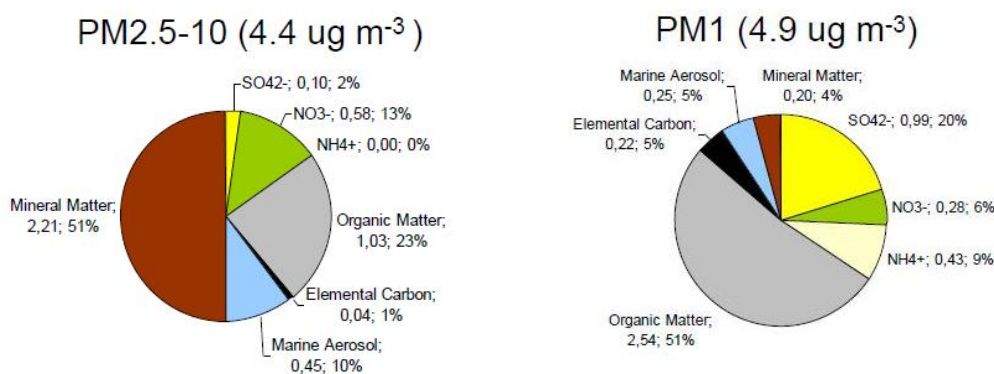


Fig. 10. Annual average composition of PM_{2,5-10} and PM₁ at regional background of Montseny (NE, Spain)

Besides mineral component atmospheric aerosol include also elemental carbon / black carbon (EC or BC) as well as various organic compounds (organic matter OM or organic carbon OC depending on determination method).

As follows from the data presented in Fig. 10, the content of elemental carbon increases with the decrease of particle size. The content of EC in the fine aerosol fraction is increased in comparison with more rough particles and amounts to 5%. Emissions of EC, predominantly to the atmosphere, are conditioned by combustion sources only.

The same takes place with organic matter. The content of organic matter in particles from PM_{2.5}–10 amounts to 23%, whereas for PM₁ organic matter content is about 50%. Here by organic matter we mean first of all organic substances of various classes. The amount of carbon in organic matter is often referred as organic carbon (OC).

The estimated OM/OC ratios span a range of 1.1–2.2, mostly between 1.2 and 1.6 for all samples considered. Average values fall slightly below 1.4, indicating that there is a predominance of unsaturated alkene and aromatic (including polycyclic) structures, and photochemical oxidation of hydrocarbons did not occur to a great extent during atmospheric transport for the bulk of organic matter [Gelencsér, 2004]. However, in [El-Zahan et al., 2009] is stated that, based on experimental results, for urban or rural areas heavily impacted by many emission sources the ratio OM/OC is close to 2.

Concentration levels of organic carbon in atmospheric aerosol

Investigation of levels of aerosol organic fraction is carried out in various countries, in particular, in the EMEP region. The results obtained in the course of various programs and campaigns are summarized in Annex B.

The Interagency Monitoring of Protected Visual Environments (IMPROVE) program provides the results for the longest period with widest spatial coverage. The program is managed by the IMPROVE steering committee that consists of representatives from the U.S. EPA; the four federal land managers (FLMs)—the National Park Service, U.S. Forest Service, Fish and Wildlife Service, and Bureau of Land Management; the National Oceanic and Atmospheric Administration; four organizations representing state air quality organizations—the State and Territorial Air Pollution Program Administrators/Association of Local Air Pollution Control Officials (STAPA/ALAPCO), Western Regional Air Partnership (WRAP), Northeast States for Coordinated Air Use Management (NESCAUM), and Mid-Atlantic Regional Air Management Association (MARAMA); and an associate member, the State of Arizona Department of Environmental Quality. The IMPROVE network initially consisted of 30 monitoring sites in Class I areas, 20 of which began operation in 1987 with the others starting in the early 1990s. An additional approximately 40 sites, most in remote areas, that used the same instrumentation and monitoring and analysis protocols (called IMPROVE protocol sites) began operation prior to 2000 and were operated individually by federal or state organizations [IMPROVE, Report IV, 2006].

General results of the program are shown in Fig. 11.

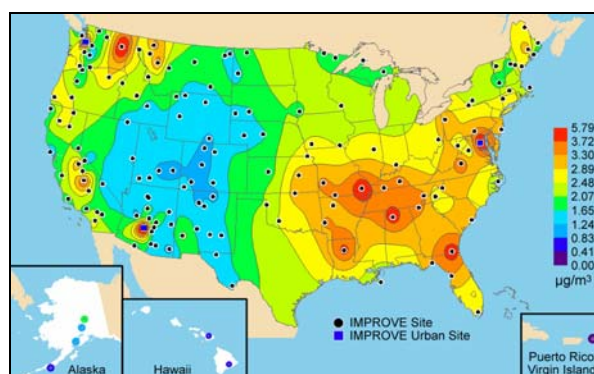


Fig. 11. *Isopleth maps of annual organic carbon concentrations include all sites from the IMPROVE network that met the prescribed completeness criteria including the urban sites for 2000–2004 [IMPROVE, Report IV, [2006].*

Based on the measurement results of OC in the US, it should be stated that typical range of OC concentrations for main part of the country area is from 1 to 3 $\mu\text{g}/\text{m}^3$. Maximum OC concentration levels do not exceed 6 $\mu\text{g}/\text{m}^3$.

The campaign on examination of EC, OC and total carbon (TC) content in PM_{10} aerosol fraction at 14 monitoring sites in 2002 – 2003 was organized by EMEP [Yttri *et al.*, 2007]. Twelve of these sites were located in rural background, and the rest are urban background sites. The results of these measurements available in the CCC database are presented in Fig. 12. These results show slightly higher concentration levels in comparison with the USA data. The range of measured concentrations in Europe is from 1 to 5 $\mu\text{g}/\text{m}^3$. Maximum values were obtained at Italian sites Ispra (IT04, rural background) and San Pietro Capofiume (IT08, urban background). In particular, at IT04 concentration levels in 2003 exceeded 8 $\mu\text{g}/\text{m}^3$.

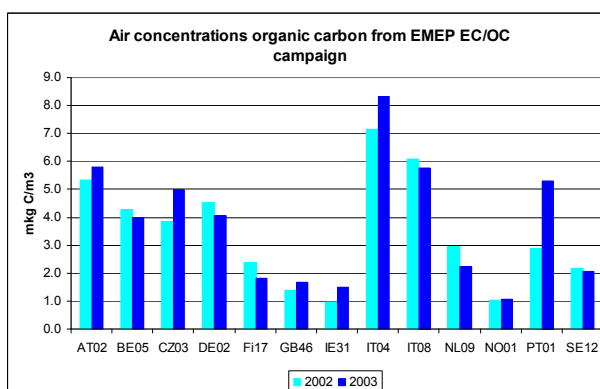


Fig. 12. OC air concentrations measured at EMEP sites (taken from the EMEP database).

Maximum value of the OC concentrations obtained in the course of the EU Project “A Study of the Present and Retrospective State of the Organic versus Inorganic Aerosol over Europe (CARBOSOL)” [Gelencsér *et al.*, 2007, Pio *et al.*, 2007 and Legrand and Puxbaum, 2007] was detected at Hungarian site K-Puszta was high enough (8.9 $\mu\text{g}/\text{m}^3$), see Annex B.

As was shown further, the concentrations of OC in aerosol fraction PM_{10} remained to be the highest among all EMEP sites amounting to 15.5 $\mu\text{g}/\text{m}^3$ in 2007. The concentrations at this site were growing from 2002 to 2007 (with exception of 2006) whereas at the Norwegian site Birkenes (NO01) the concentrations were approximately stable within this period amounting to about 1 $\mu\text{g}/\text{m}^3$.

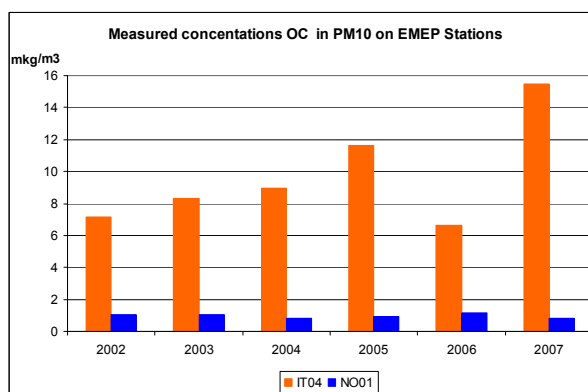


Fig. 13. The comparison of OC air concentrations measured at two EMEP sites (taken from the EMEP database).

High levels of OC concentrations are characteristic of a lot of Chinese regions. Here the concentrations vary from one to several tens of $\mu\text{g}/\text{m}^3$. For example, winter OC concentrations in cities Changchun and Xi’an, China amounted to 39.2 and 102.3 $\mu\text{g}/\text{m}^3$, respectively [Cao *et al.*, 2007]. The lowest OC concentrations were detected in background regions located far from urban and industrial centers and over the ocean. The table in Annex B demonstrated the very large spatial variability of OC mass concentrations in the atmosphere. The work [Gelencser, 2004] shows that, apart from urban sites, the mass concentration of OC is not as variable as other aerosol properties. The concentration values at rural and clean marine sites vary mostly within an order of magnitude.

The composition of submicron aerosols (PM_{10}) sampled in free troposphere (FT) and in marine boundary layer on Tenerife from [Putaud *et al.*, 2000] is shown in Fig. 14.

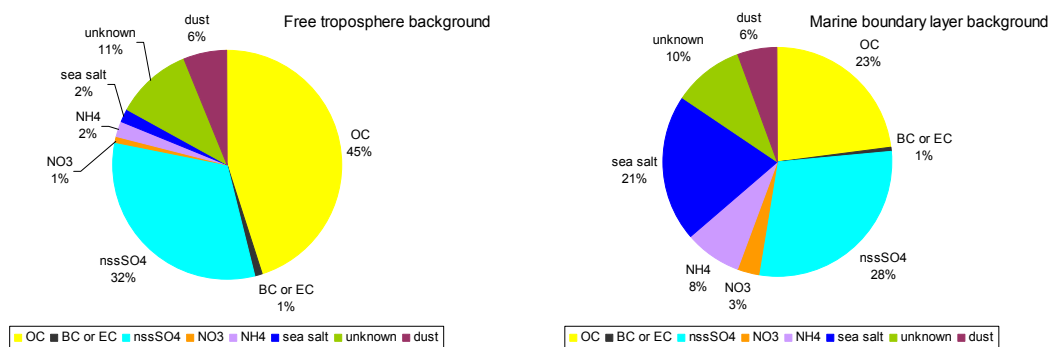


Fig. 14. Mean composition of the submicron aerosol in the FT and in marine boundary layer in background conditions.

Here nssSO₄ stands for non-sea salt sulfates. Secondary marine aerosol consists predominantly of nss-sulfate and condensable organic vapors with the sulfur cycle being the more studied and better quantified of the two. Sulfate aerosol can be formed via nucleation and growth processes; however, it is thought that the majority of nss-sulfate is formed through heterogeneous processes either on sea-salt and dust aerosol in cloud free conditions or within clouds where they would become associated with the cloud condensation nuclei upon evaporation [Bates *et al.*, 2006].

Figure 14 clearly demonstrates essential increase of the contribution of sea salts in aerosol composition over sea surface in comparison with island areas where organic compounds (OC) are predominant.

Depending on their origin, organic aerosol components can be classified as primary or secondary. Primary organic aerosol (POA) components are directly emitted in the condensed phase (liquid or solid particles) or as semivolatile vapors, which are condensable under atmospheric conditions. The main sources of POA particles and components are natural and anthropogenic biomass burning (forest fires, slashing and burning, domestic heating), fossil-fuel combustion (domestic, industrial, traffic), and wind-driven or traffic-related suspension of soil and road dust, biological materials (plant and animal debris, microorganisms, pollen, spores, etc.), sea spray, and spray from other surface waters with dissolved organic compounds [Pöschl, 2005]. Primary biogenic aerosol consists of pollen, bacteria, fungal and fern spores, viruses, and fragments of animals and plants. Several studies have show that fungal spores account for major fraction of primary biogenic aerosol particles [Monks *et al.*, 2009].

Secondary organic aerosol (**SOA**) components are formed by chemical reaction and gas-to-particle conversion of volatile organic compounds (VOCs) in the atmosphere, which may proceed through different pathways:

- new particle formation: formation of semivolatile organic compounds (SVOCs) by gas-phase reactions and participation of the SVOCs in the nucleation and growth of new aerosol particles;
- gas-particle partitioning: formation of SVOCs by gas-phase reactions and uptake (adsorption or absorption) by preexisting aerosol or cloud particles;
- heterogeneous or multiphase reactions: formation of low-volatility or non-volatile organic compounds (LVOCs, NVOCs) by chemical reaction of VOCs or SVOCs at the surface or in the bulk of aerosol or cloud particles [Pöschl, 2005].

SOA can be of both anthropogenic and biogenic nature; on a global scale, biogenic hydrocarbons are estimated to be the predominant source [Pandis *et al.*, 1991].

Secondary organic aerosol can be formed in marine boundary layer (MBL) through a number of different processes. Biogenic volatile organic compounds (BVOC), emitted by the sea surface, or their oxidation products, can be involved in new particle formation events via nucleation of stable clusters of 0.5-1 nm in size. BVOCs and related oxidation products can also condense on preexisting particles and droplets, contributing to the particulate mass. The best known SOA component in marine aerosol is methanesulfonic acid, resulting from the atmospheric oxidation of dimethylsulphide [Rinaldi et al., 2010].

The major biogenic compounds involved in aerosol formation are considered to be monoterpenes, which constitute more than 80% of VOC emission from conifers [Alves and Pio, 2005]. This explains higher OC content in samples from Sequoia National Park, California, USA in comparison with other forest reserves [Chung and Seinfeld, 2002], see Annex B.

On a global scale, formation of SOA appears to be dominated by oxidation of biogenic VOCs (mostly by ozonolysis of terpenes) amounting to at least 50% of POA anthropogenic emissions [Kanakidou et al., 2005, Tsigaridis and Kanakidou, 2003]. In the atmosphere, POA and SOA components are mixed with each other, with BC/EC, and with inorganic aerosol components (externally and internally mixed aerosols). Moreover, both POA and SOA components can be efficiently transformed upon interaction with reactive trace gases and solar radiation.

SOA formation occurs as a result of a number of chemical reactions most of which are poorly understood. Very recently, laboratory evidence has been presented on acid catalyzed carbonyl chemistry on aerosol particles. This chemistry includes various acid-catalyzed reactions, such as hydration, hemiacetal and acetal formation, aldol condensation, and polymerization in the aerosol phase [Jang et al., 2002]. According to Alves and Pio, while aromatic hydrocarbons and biogenic terpenes are undoubtedly major contributors to SOA in the atmosphere, these two compound classes are not solely responsible for SOA formation [Alves and Pio, 2005]. In [Gelencsér, 2004] humic-like substances are considered as major SOA components which are formed by heterogeneous or multiphase reactions. The formation of SOA represents one of the removal processes of VOC.

Investigations carried out in various countries show the presence of seasonal variations of OC concentrations. Such variations measured in two cities in California, USA (Los Angeles and Long Beach), are presented in Fig. 15. Seasonal variations in these cities are not pronounced but winter concentrations exceed summer ones. This allows concluding that there exist contributions from fuel combustion in “cold” periods though winter temperatures in California are positive (average range of temperatures in Los Angeles in January is 15 – 23 °C and in August – 26 – 32 °C) [http://en.wikipedia.org/wiki/Los_Angeles].

The investigation of seasonal variations of OC concentrations was one of the tasks of European project CARBOSOL. The data obtained are presented by the diagram in Fig. 16. For three sites from six winter concentrations exceed summer ones but for other three the opposite picture takes place.

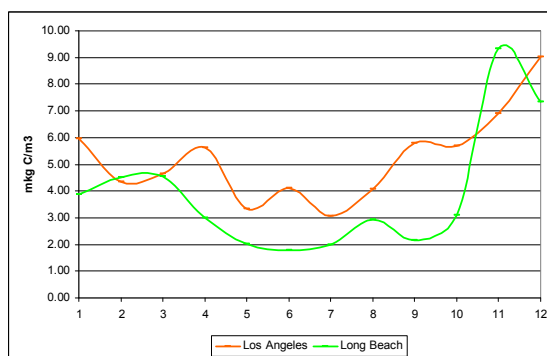


Fig. 15. Seasonal variations of OC concentrations in 1993 according to [Hannigan et al., 1996].

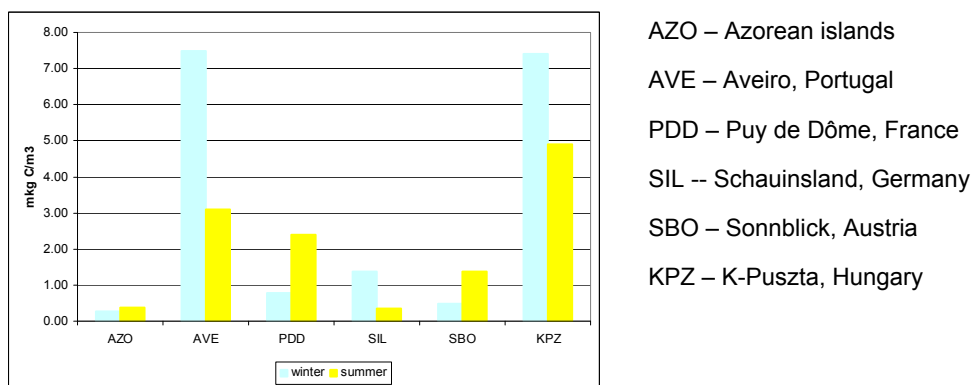


Fig. 16. The comparison of winter and summer of OC concentrations according to [Pio et al., 2007].

For two sites (K-Pusztá, Hungary and Schauinsland, Germany) the exceedance of winter concentrations over summer ones could be explained by the influence of fuel combustion sources in winter period. However, at Aveiro, Portugal the exceedance of winter concentrations takes place. Climatic conditions at this site (average temperature in January is 15.2 °C and in August – 24.4 °C) are not comparable with climatic conditions in Central Europe though are close to those in California. The detailed examination of OC sources performed by [Gelencsér et al., 2007, Legrand and Puxbaum, 2007] showed that high winter concentrations at this site is conditioned by

- formation of POA by biomass burning (52% – 69%) and fossil fuel combustion (0.6% – 7.8%);
- primary biogenic organic carbon emanated from vegetation 0.7% – 2.3%);
- formation of SOA from fossil fuel combustion (1.7% – 20%) and non-fossil fuel combustion (1.8% – 23%).

In summer period relative contributions of sources are changed. So, the share of biomass burning decreases up to 11%. The shares of the following sources slightly increase:

- POA from fossil fuel combustion (4.6% – 14%);
- primary biogenic organic carbon from vegetation (0.8% – 2.9%);

At that the share of SOA from non-fossil fuel combustion increases to 60% – 80% and becomes prevailing whereas the share of SOA from fossil fuel combustion slightly decreases.

The analysis of OC sources has shown that the OC concentration levels are formed in summer mainly due to SOA formation by non-fossil fuel combustion. It leads to the conclusion that the processes of atmospheric transformation with participation of different compounds are of extreme importance for formation of OC aerosol.

Thus the investigations in the framework of CARBOSOL project showed experimentally that the concentrations of organic compounds in atmospheric aerosol are conditioned by the formation of POA and SOA depending on ambient temperature and the presence of volatile organic compounds.

Chemical composition of organic carbon fraction

Chemical composition of aerosol organic fraction is intensively investigated during last decades. Analyzing the organic fraction of ambient PM can be challenging due to the large number and variety of compounds present. Many hundreds of organic compounds have been identified. These include *n*-alkanes, alkanals, alkanolic acids, mono- and di-carboxylic acids, ketones, alcohols, amides, amines, hopanes, polycyclic aromatic hydrocarbons, sugar derivatives, and more [Williams *et al.*, 2006].

Traditionally, chemical characterization of particulate OC has been performed using single or multiple solvent extractions of samples followed by GC/MS. Identified organic compounds in aerosol typically account less than 10% of total OC measured by thermal analysis, although this percentage could reach values above 60%, when more complex extraction methodologies and detection techniques are used [Alves, 2008].

For determination of OC content in aerosol samples collected at Tenerife island from Canary archipelago [Putaud *et al.*, 2000] the thermal method was used. It is based on transformation of carbonaceous material to CO₂ over CeO₂/CuO catalyst. The sample was exposed by stepped heating: from 80 to 120 °C – peak labeled as OC1.1, from 120 to 220 °C – peak OC1.2, from 220 to 340 °C – peak OC1.3 and from 340 to 650 °C – peak OC2. Organic compounds included to the composition of obtained fractions summarized in Table 9.

Table 9. Composition of OC fractions obtained by the analysis of organic aerosol compounds according to [Putaud *et al.*, 2000].

Fraction	Substances identified
OC1.1	HCHO, limonene
OC1.2	Anthracene vapor, benzoic acid
OC1.3	Coronene
OC2	Pinic acid, methane sulfonic acid, organic salts (acetate, oxalate), CaCO ₃

The data on the composition of organic fraction in aerosol matter with its seasonal variations in Chinese cities are shown in Fig. 17. Using the extraction by organic solvents, the authors selected major classes of organic substances: *n*-alkanes, fatty acid, sugars (saccharides), and phthalates. Minor compound classes were fatty alcohols, polyols and polyacids, lignin and resin products and sterols. Within each class particular substances were identified. So, in the group of fatty acids a homologous series from C9 to C30 were identified.

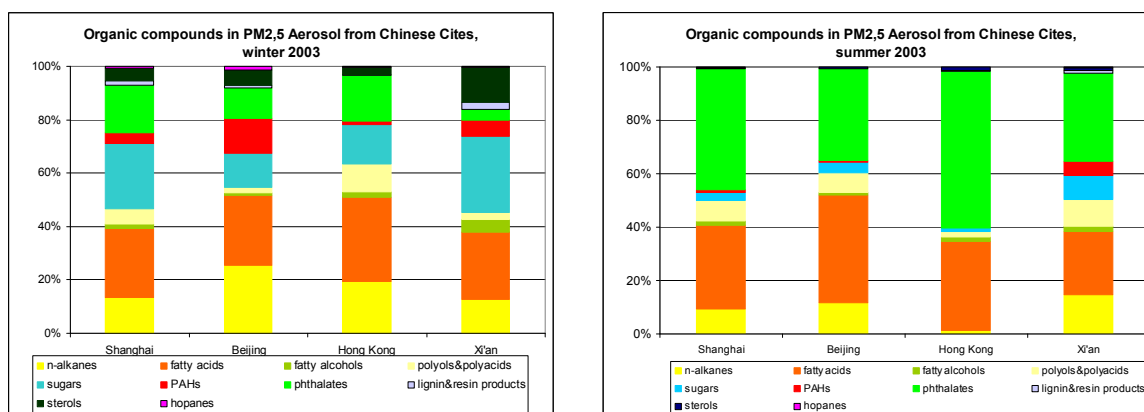


Fig. 17. Relative contributions of various classes of organic compounds identified in aerosol fraction PM_{2.5} in Chinese cities depending on season.

Fatty acids and phthalates are main contributors to organic aerosol fraction in Chinese cities. The emission of fatty acids to the atmosphere takes place both from biogenic sources such as vascular plants, microbes and marine phytoplankton (major source of lower molecular weight fatty acids), terrestrial higher plant waxes (source of higher molecular weight fatty acids), and from anthropogenic sources.

Fatty acids constitutes one of chief groups of solvent-extractable compounds presented in aerosol samples. They are majorly represented by *n*-alkanoic, *n*-alkenoic, dicarboxylic and oxo-carboxylic acids. The distribution patterns of the *n*-alkanoic acids range usually from *n*-C₇ to *n*-C₃₅. A pattern where the *n*-C₂₂-*n*-C₂₈ mode is predominant is characteristic of contributions from higher plant waxes. The homologues < *n*-C₂₀ are probably derived from microbial sources, although these acids are ubiquitous in biota [Abas and Simoneit 1996, Alves, 2008].

Other sources are cooking, grilling and food preparation, where these compounds are directly volatilized into the fumes [Rogge *et al.*, 1991].

While acid content in samples collected at Chinese cities show weak seasonal variation, the phthalate content in summer time considerably exceed that in winter time. Phthalates are released into the air from the matrix by evaporation because they are not chemically bonded to the polymer and, hence, are of anthropogenic nature.

Another important group is sugars, among which levoglucosan, arabitol, fructose, glucose, mannitol, inositol, sucrose and trehalose were detected. From them about 90% in mass is contributed by levoglucosan, which is a product of the breakdown of cellulose is a unique tracer for wood combustion [Simoneit *et al.*, 1999]. This explains large contribution of this substance group in winter period compared with summer one.

Besides, other substances-tracers that point at this or that source of emissions are determined, see Table 10.

Table 10. Specific tracers for organic components in atmospheric aerosol by [Alves, 2008].

Emission process	Major source	Specific tracers (markers)
Combustion	biomass and cellulose	Levogluconan
		Galactosan
		Mannosan
	biomass with legnin	Methoxyphenols
	biomass/coal	<i>n</i> -Alkanes, C ₁₅ -C ₃₇
	coal	<i>n</i> -Alkanones, C ₁₅ -C ₃₅ ; <i>n</i> -Alkanonals, C ₁₅ -C ₃₅ ; Alkylpicones/Alkylchrys
	direct, higher plant	Phytosterols, Triterpenoids, Diterpenoids (resin acids), <i>n</i> -Alkanoic acids, C ₂₀ -C ₃₆
biomass, vegetation	Triterpenyl alkanooates	
biomass, plant waxes	<i>n</i> -alkanes (C ₂₀ -C ₃₇), wax esters,	
Auto exhaust (vehicle exhaust)	vehicles	<i>n</i> -Alkanes, C ₁₅ -C ₃₇
	urban aerosol	Alkylcyclohexanes, C ₁₆ -C ₂₉
	petroleum	Hopanes/steranes
	ubiquitous/not in gasoline and diesel fuels	Triterpenoid hydrocarbon (steranes and diasteranes), C ₂₇ -C ₃₅
Cooking	direct, meat/algae	Cholesterol, mono- and diglycerides
	flora, fauna	Triacylglycerides
Volatilized (directly) during open burning	plastics	<i>n</i> -Alkanes, C ₁₆ -C ₄₀₊ (even predominant)
Volatilized by steam stripping during open burning	plastics	Plasticisers/Antioxidants
Sea slick re-suspension	marine biomass	<i>n</i> -Alkanoic acids, C ₆ -C ₂₈
Direct/re-suspension	microbial	<i>n</i> -Alkanes, C ₁₅ -C ₂₀ <i>n</i> -Alkanoic acids, C ₁₅ -C ₃₇
Direct	biomass	<i>n</i> -Alkanonals, C ₁₄ -C ₃₆
Photooxidation / combustion	various	<i>n</i> -Alkanedioic acids, C ₆ -C ₂₈

Concluding remarks

- The data on organic compounds in the atmospheric aerosol are of major importance for model description of POP gas/particle partitioning and degradation. Chemical composition of organic aerosol strongly influences atmospheric behaviour of POPs since heterogenic reactions with atmospheric reactants go with different rates for substances adsorbed at aerosol particles of different nature.
- Environmental levels and chemical composition of atmospheric aerosol are intensively investigated. It is found that organic aerosol fraction is a complex composition of substance groups, which depends both on various environmental factors and source types. The relations between substances of different groups are subject to strong spatial and temporal variability.
- At present the problem of determination of spatial distribution of organic carbon composition in aerosols is not completely solved [Fuzzi *et al.*, 2006, Kanakidou *et al.*, 2005]. Identified organic compounds in aerosol typically account less than 10% of total OC measured by thermal analysis, although this percentage could reach values above 60%, when more complex extraction methodologies and detection techniques are used.
- Large uncertainties in modeling of the levels of organic compounds in the atmosphere are connected with secondary organic aerosol [Simpson *et al.*, 2007].

So, for more accurate description of chemical composition of organic atmospheric aerosol and for the refinement of model description of POP environmental fate further investigations are needed.

Chapter II.2.

ADJUSTMENT OF EMISSION DATA FOR MODELLING

II.2.1. Temporal variability of POP emissions

One of the characteristic features of POPs is that they are often subject to temporal variability. This variability can be conditioned by both environmental factors and temporal variability of emissions.

First of all, physical-chemical properties of the most POPs are strongly temperature-dependent. This leads to seasonal variability of such important processes as gas-particle partitioning, dry and wet deposition and degradation of POPs. This variability is already taken into account in MSCE-POP model by usage temperature-dependent air-water and octanol-water partitioning coefficients and degradation rates where available. Further, usage temporally resolved data for atmospheric reactants (OH radicals, organic carbon in the atmospheric aerosol, etc.) allows describing temporal variability of the above listed processes more accurately. Finally, to refine the description of seasonal variations for B[a]P the process of photodegradation of particle-bound form of the pollutant was involved to the model.

However, in addition to temporal variability caused by environmental factors there exists temporal variability of contamination levels due to that of emissions. Such variability is particularly important for the pollutants which are emitted to the atmosphere by burning processes. As it will be shown below, this variability can essentially affect annual averages of air concentrations. Most typical examples of such pollutants are PCDD/Fs and PAHs. Taking into account that the latter group of pollutants is much more investigated (from the viewpoint of data on environmental levels and physical-chemical properties) one of the representatives of this group – B[a]P – was chosen to the analysis of temporal variability of POPs at this stage of investigations.

To construct temporal variability of emissions one should take into account that this variability depends on the type of emission source (emission source category). So, prior to modeling this variability, the contributions of various emission source categories to the overall B[a]P emissions should be assessed. According to the official emission data for 2010 complemented by the data from TNO emission inventory when necessary, the main contribution to the emissions is made by residential heating (about 50%), following by road transport (30%), industrial processes (11%) and waste incineration (3%). All the rest sources contribute to about 5% of emission altogether. Main source categories of B[a]P emissions is shown in Fig. 18.

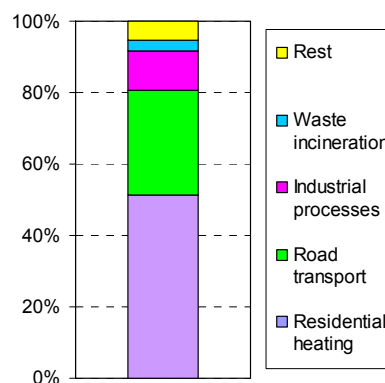


Fig. 18. Main source categories of B[a]P emissions

Temporal variability of emissions from residential heating

First the consideration of temporal variability of emissions from residential heating will be considered. For this source category model parameterization of emission temporal variations follows the approach introduced in [Aulinger et al., 2010].

This approach was worked out on the basis of the data on power supply dynamics during 2005 – 2006 in Hamburg, Germany. In [Beecken, 2007] it was shown that the quantity of heat that is supplied to consumers linearly decreases with the increase of the ambient temperature up to 18° C where the supplied heat reaches a minimum and remains constant for higher temperatures. Under the assumption that B[a]P emissions are directly proportional to the supplied heat, it could be concluded that B[a]P emissions drop linearly with the temperature up to 18° C and remain constant at higher temperatures.

Starting from temperature dependence of power supply dynamics, temperature-dependent scaling coefficients for emissions $SC(T)$ were calculated. To do this, power supply temperature dependence was normalized with respect to its minimal value reached at temperatures exceeding 18° Celsius:

$$SC(T) = \begin{cases} -0.2805 \cdot T + 6.0445, & T \leq 18 \\ 1, & T > 18 \end{cases} \quad (1)$$

The result of calculating $SC(T)$ for the range of temperatures from -30° C to +30° C is presented in Fig. 19. Under the above assumptions, B[a]P emissions from residential heating at one and the same location should be proportional to the obtained values of scaling coefficients.

So, in each particular grid cell temperature-dependent emissions E_i in the day i should be given by the relation

$$E_i = N \cdot E_{ann} \cdot SC(T_i),$$

where T_i is the average temperature in the day i , E_{ann} is annual emissions in the considered grid cell, N is the normalizing coefficient, which is chosen in such a way that total annual emissions in the grid cell equals E_{ann} , that is

$$N = \frac{1}{\sum_{i=1}^{365} SC(T_i)}. \quad (3)$$

Normalizing coefficient N is calculated for each grid cell prior to simulations on the basis of meteorology data of the corresponding year.

Up to now factors 1.2 for fall and winter months and 0.8 for summer and spring months (proposed by [Baart et al., 1995]) were applied in the MSCE-POP model to take into account seasonal variation of emissions. The example of emission temporal variations at some location in the Central Europe calculated with new approach is given in Fig. 20 in comparison with earlier used emissions.

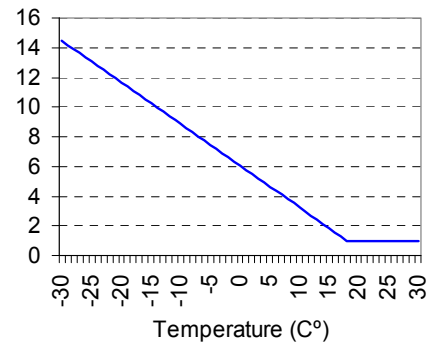


Fig. 19. Scaling coefficients for temperature dependence of B[a]P emissions on temperature.

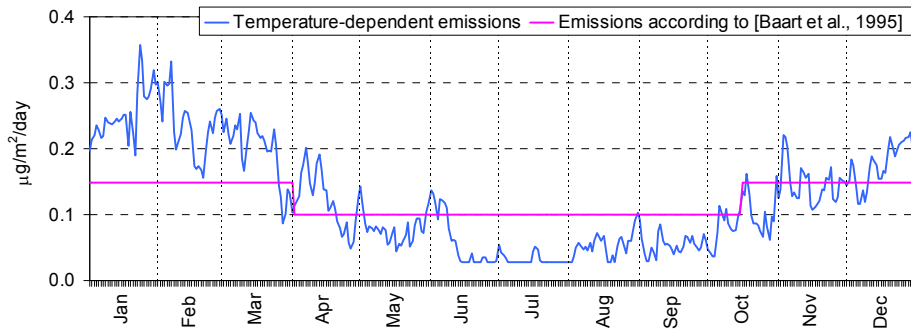


Fig. 20. Temporal variations of B[a]P emissions at a particular location in the Central Europe.

It is seen that usage of temperature dependent scheme of emission seasonal variations leads to essentially higher emissions (by 44% on the average) in cold season (from December to March) and lower emissions (by 51% on the average) in warm seasons (from June to September). In April, May and October temperature-dependent emissions are oscillating around values predicted by [Baart et al., 1995] approach.

It should be stressed that the dependence of emissions from residential heating on the temperature given by formula (1) can be different in different countries and regions. The investigation of the influence of the coefficients used on the results of evaluation of temporal emission variations was presented in the above cited paper [Aulinger et al., 2010]. At present one and the same dependence for all locations in Europe was used due to the lack of country-specific information on temporal variations of emissions from residential heating.

Temporal variability of emissions from sources of other categories

Similar to [Aulinger et al., 2010], temporal variations of emissions from road transport and industrial processes are performed in accordance to the coefficients used in LOTOS/EUROS model [Schaap et al., 2005]. Seasonal variations of emissions from road transport are illustrated in Fig. 21a, where fractions of annual emissions for each month are shown. Besides, variations of emission from road transport within a week are taken into account (Fig. 21b).

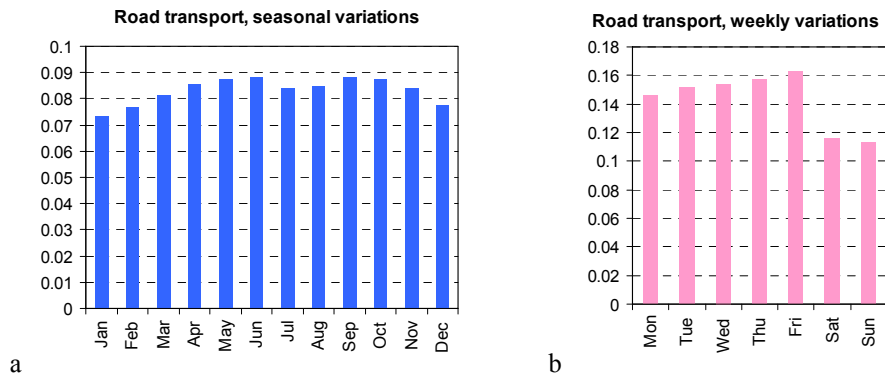


Fig. 21. Monthly fractions of annual emissions (a) and daily fractions of weekly emissions (b) for emissions from road transport.

Similar diagrams for emissions from industrial processes are presented in Fig. 22.

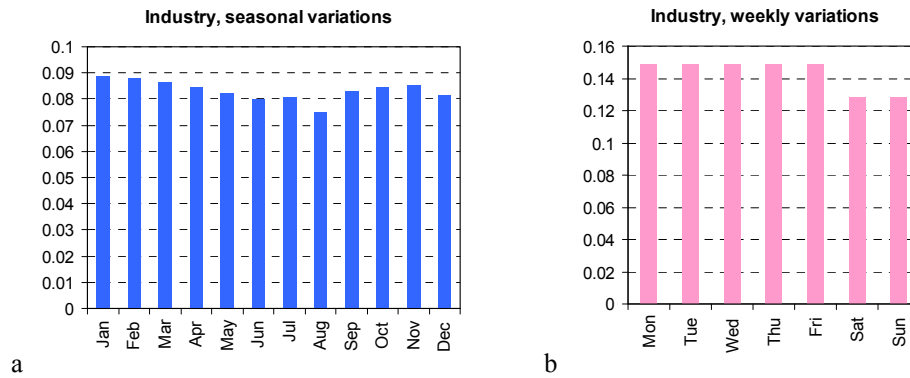


Fig. 22. Monthly fractions of annual emissions (a) and daily fractions of weekly emissions (b) for emissions from industrial sources.

The diagrams show that both seasonal and weekly variations of emissions from industry sources and road transport are low enough in comparison with those used for emissions from residential heating. Emissions of all other source categories are supposed to be constant over the year.

Comparison with measurements

This section is aimed at the comparison of measurement data for 2010 at the EMEP monitoring network with model predictions made with the use of the above described scheme of emission temporal variations.

Calculated B[a]P contamination levels are shown in Fig.23 together with values measured at the sites from EMEP monitoring network. The comparison between calculated and measured values of B[a]P air concentrations is presented in Fig. 24.

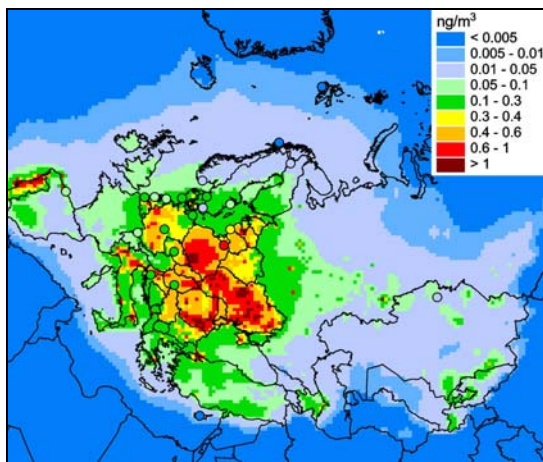


Fig. 23. Calculated annual means of B[a]P concentrations in the ground air in 2010 together with measurements at the EMEP monitoring network.

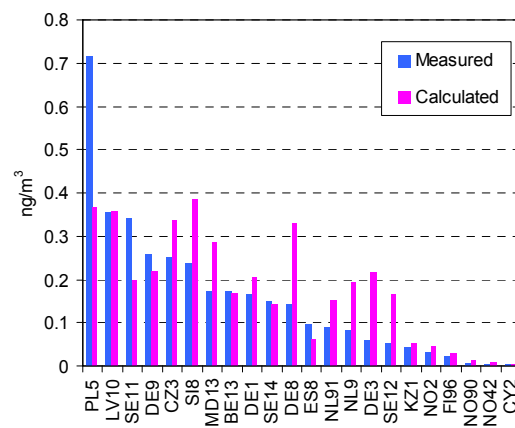


Fig. 24. Comparison between calculation results and measurement data at EMEP monitoring sites (annual averages), ng/m³.

The comparison shows that about 70% of measurements agree with calculations within a factor of 2, and correlation coefficient between measurements and modelling at the EMEP monitoring sites is 0.73. Normalized mean bias is -0.14 , which meets the threshold ± 0.2 used for the evaluation of agreement between measurements and model predictions. So, it can be concluded that measurement data and calculations are in reasonable agreement with each other showing close estimates of contamination levels.

The model shows essential amplitude of seasonal variations of B[a]P pollution. This can be demonstrated by the comparison of annual averages of B[a]P concentrations with the concentrations averaged over February – the month with low temperature (see Fig. 26).

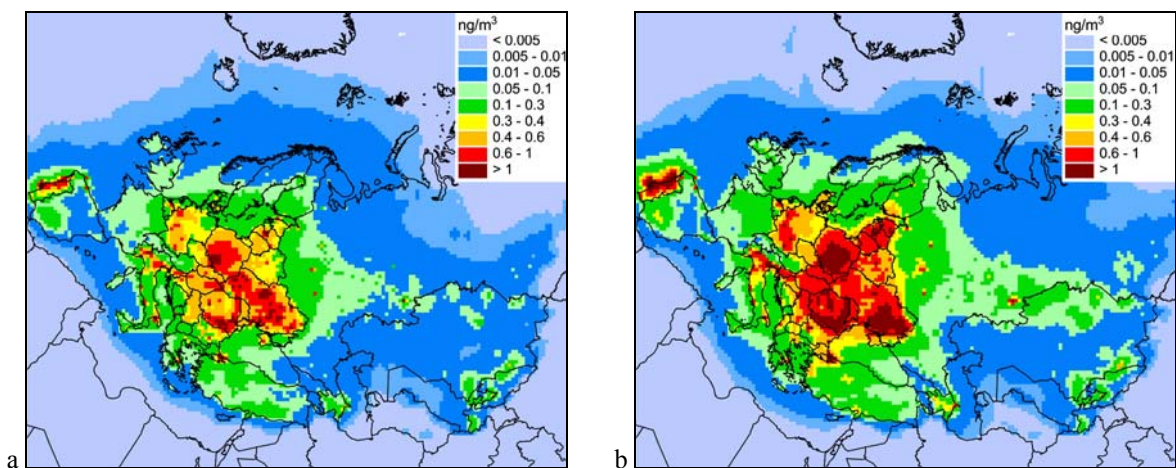


Fig. 25. Calculated B[a]P concentrations in the surface air for 2010:

a – annual means, *b* – means over February.

It is worth mentioning that annual averages of B[a]P air concentrations essentially depend on emission seasonal variations. As an example, the difference between annual averages of air concentrations calculated with previous and modified emission seasonal variations (SVs) is shown in Fig. 27.

The reason of these differences is that degradation rates of B[a]P in the atmosphere are much higher in warm month than in the cold ones. So, if emission seasonal variations are such that most of B[a]P is emitted in winter, less amount of the pollutant is degraded and, hence, annual averages are higher. According to the model estimates, differences in calculations of **annual means** of air concentrations due to **emission seasonal variations** may reach 40% and more. These differences can be essential in regions of Eastern Europe where exceedances of EU target value takes place. This shows that the information on emission seasonal variations is required for reliable assessment of exceedances of target values in Europe.

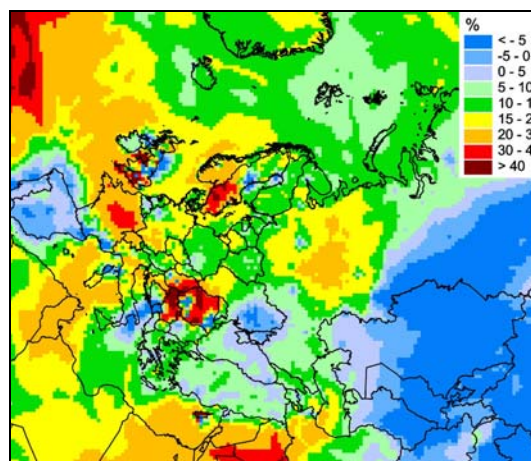


Fig. 27. Difference between calculations with previous and modified SVs.

The comparison of seasonal variations of measured and calculated B[a]P air concentrations at some EMEP monitoring sites is given in Fig. 28.

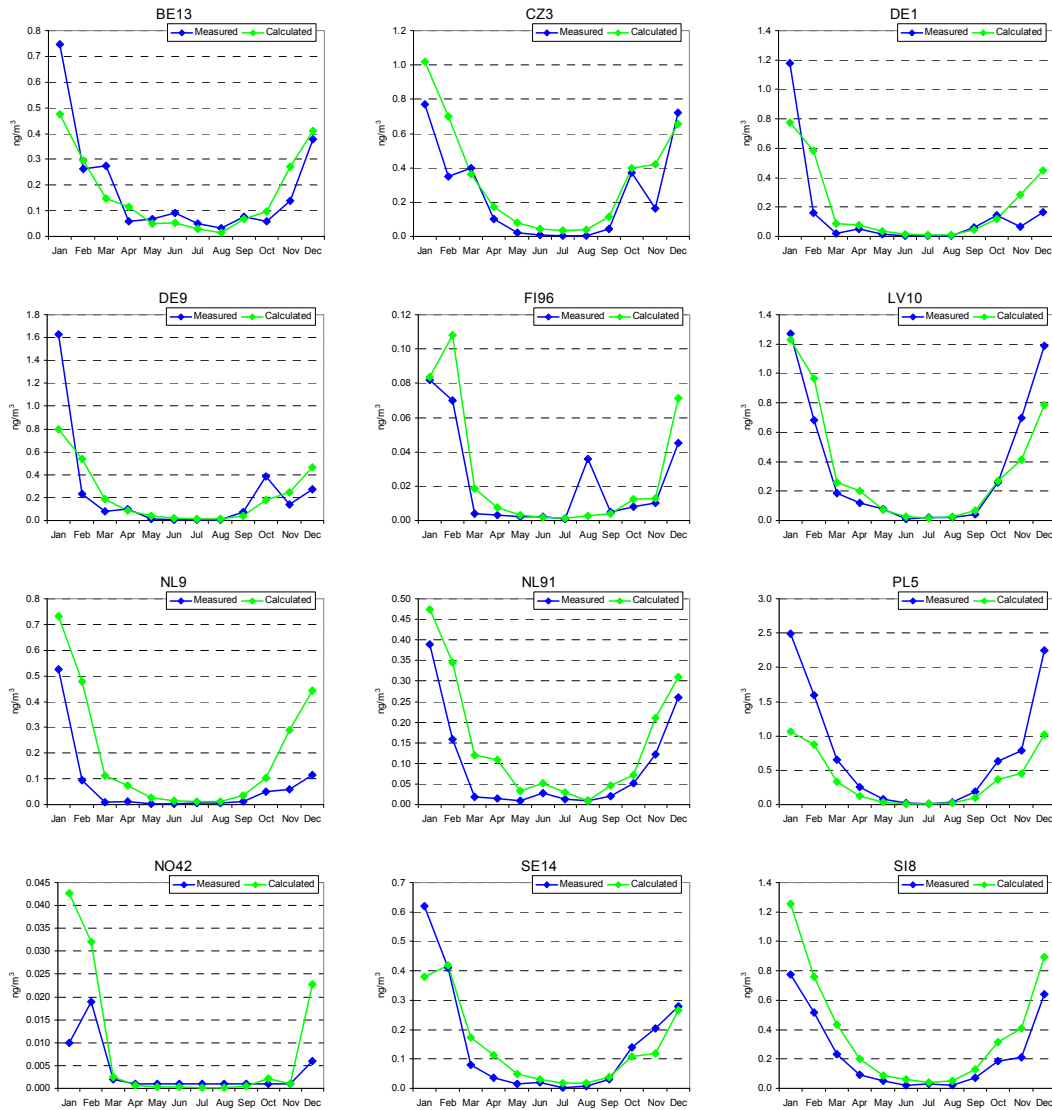


Fig. 28. The comparison of measured and calculated seasonal variations of B[a]P air concentrations at a number of EMEP monitoring sites.

The comparison shows that monthly averages of measured and calculated air concentrations generally well agree with each other. At the same time seasonal variations at Polish site PL5 are strongly underestimated. On the opposite, model overestimates seasonal variations of B[a]P pollution at NL9, NL91 and NO42. Thus, the comparison manifests that for better agreement between measurements and model predictions emission seasonal variations should be evaluated on the country-specific basis.

Let us consider in more detail the comparison of measured and calculated air concentrations at site PL5. The comparison of raw measurements with ambient temperature at this site is displayed in Fig. 29. It is seen that underestimation of B[a]P air concentrations by the model takes place mainly in cold months (from January to March and from November to December).

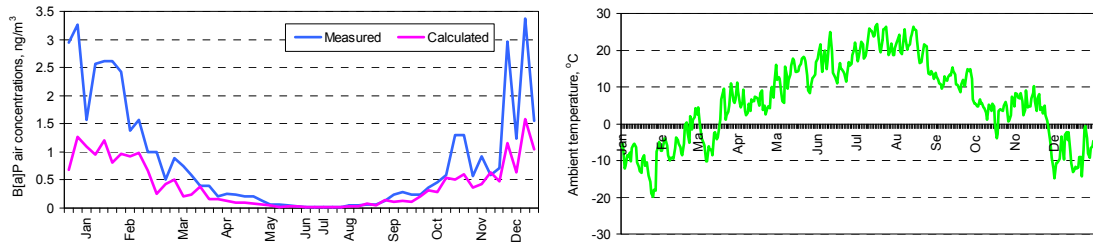


Fig. 29. Calculated and measured B[a]P concentrations in the ground air at PL5, in comparison with ambient temperature.

For additional information measurements from three sites from EEA AirBase are included into consideration. They are: Cherniawa (rural), Zielonka (rural background) and Legionowo (suburban background). Locations of these sites together with calculated values of B[a]P in Poland is shown in Fig. 30.

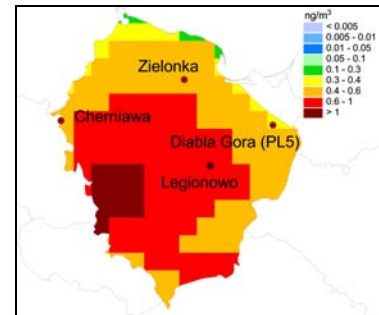


Fig. 30. Calculated values of B[a]P concentrations in Poland and locations of additional measurement sites.

At the sites Cherniawa and Zielonka situation similar to that at PL5 take place (see Fig. 31). Concentration levels found at these two sites are close to those obtained at PL5. Annual average at the site Cherniawa (0.65 ng/m^3) is underestimated since measurements for November and December are not available. At these sites the agreement of calculated and measured values of air concentrations is out of factor 2 in January and February at Cherniawa and for October, November and December at Zielonka. Similar to PL5, the underestimation of air concentrations by the model takes place in cold months.

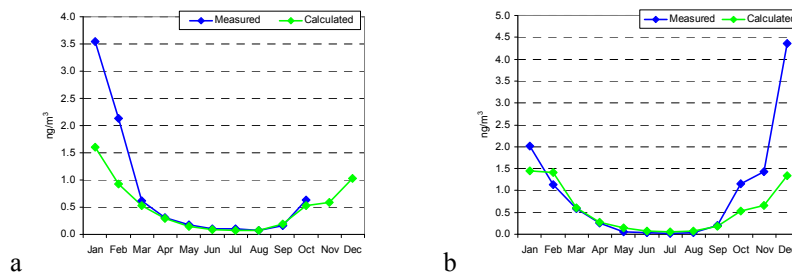


Fig. 31. Calculated and measured monthly means of B[a]P concentrations in the surface air at Cherniawa (a) and Zielonka (b). Annual averages of measured values are shown by red lines.

Suburban background site Legionowo (Fig. 32) is characterized by essentially higher levels of contamination (up to 17 ng/m^3 in January with annual average 5.2 ng/m^3) in comparison with the above considered three sites. The model shows essentially lower values of concentrations comparable with those obtained at three above sites (with annual average 0.72 ng/m^3 , see Fig. 29). At the same time the agreement between measured and calculated seasonal variations is good (the correlation between measurements and calculations is 0.95). The reason of underestimation of absolute values at this site can be underestimation of spatial variations of B[a]P concentration levels by the model with $50 \times 50 \text{ km}$ cells which leads to smoothing of concentrations. Modelling with higher spatial resolution inside a country complemented by the analysis with the help of inverse modelling can give more correct description of pollution levels.

Concluding remarks

The above investigation shows that:

- Modification of model description of emission seasonal variations refines the agreement between measured and calculated values of B[a]P air concentrations.
- Temporal variability of B[a]P emissions can considerably (up to 40% and higher) affect annual means of air concentrations. This variability strongly depends on emission composition from the viewpoint of source categories.
- Information on temporal variations for various emission source categories is desirable for correct assessment of B[a]P contamination levels.

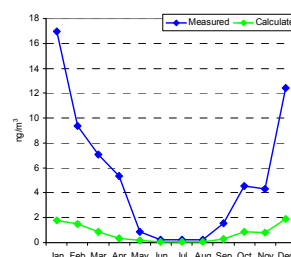


Fig. 32. Calculated and measured monthly means of B[a]P concentrations in surface air at Legionowo (suburban background)

II.2.2. Congener composition of emissions

The problem of environmental contamination by PCDD/Fs is recently in the focus of a lot of national and international organizations and programs (the Stockholm Convention, HELCOM, SEPA and others). A number of studies on PCDD/F environmental levels by means of measurements and modelling are performed in different regions. The overview of measurement activities is given below. Among modelling activities we mention a study by Zhang et al (2009) where total atmospheric concentrations of PCDD/Fs over the North American continent were calculated by means of modified version of the CMAQ model. The factor of agreement ranged from 1 to about 12. Over- and underestimations were attributed to uncertainty in the official emission estimates used as model input.

Within environmental protection activities both environmental levels of PCDD/Fs and emissions of these pollutants are often characterized by 2,3,7,8-TCDD toxicity equivalents (TEQs) of PCDD/F mixture calculated using toxic equivalency factors (TEFs). Below international toxicity equivalency factors I-TEFs adopted by NATO/CCMS (1988) are used. Similarly, the results of measurements of PCDD/Fs are mostly reported in the literature in the form of toxic equivalents (I-TEQ or WHO-TEQ). However, for model evaluation of total toxicity of PCDD/F mixture it is reasonable to simulate the transport of 17 toxic (2,3,7,8 - substituted) PCDD/F congeners separately to take into account differences in their physical-chemical properties leading to the corresponding differences in their fate in the environment. Total toxicity of PCDD/Fs is determined as a sum of those of 17 toxic congeners. To perform such simulations the data on congener composition of PCDD/F emissions (that is, shares of all toxic congeners) is needed.

However, official emission data on PCDD/Fs received by Centre on Emission Inventories and Projections (CEIP) as well as other emission inventories used in preparation of emission data for modelling present the information on total toxicity of PCDD/F mixture only. The only emission inventory dealing with emission congener composition was worked out under POPCYCLING-Baltic project refers to 1995 at latest and hence needs corrections when used for subsequent years.

An objective of this study is to identify uncertainties in the PCDD/F emission inventories by analyzing the degree of disagreement between model calculations and monitoring data and to construct

adjusted emission scenarios for each of 17 toxic PCDD/F congeners to optimize the calculation-to-measurement agreement.

Methods

In the present Section the method of construction of adjusted emission scenarios from the viewpoint of total toxicity and emission congener composition is described. As mentioned above, this construction is based on the analysis of disagreement between model predictions and available monitoring data. The input data on emissions and measurements used in the analysis are also described.

Measurement data. Since measurements of PCDD/Fs are not included in the regular EMEP measurement program, MSC-E has performed literature search of available measurement data from national and international projects and campaigns. More than 750 measurements made in various years and at various locations within the Northern Hemisphere have been found. The summary of these measurements is given in Table 11.

Table 11. Measurement data on PCDD/Fs found in literature.

Country	Years	Station type	Number of measurements	Including congener profile	Value range (fg I-TEQ/m ³)
Italy	1990 – 2005	Contaminated	14	10	13 – 480
		Clean	9	9	1.48 – 54
Greece	1999 – 2006	Contaminated	12	1	4 – 482
		Clean	2	1	2 – 178
Portugal	1999 – 2004	Contaminated	10	–	2 – 816
		Clean	5	–	1.7 – 59.6
Spain	1994 – 2008	Contaminated	57	23	5 – 1196
		Clean	3	1	5 – 45
Austria	1992 – 2000	Contaminated	24	–	1.3 – 587
		Clean	1	–	10.8 – 110
Belgium	1992	Contaminated	4	–	59 – 296
		Clean	4	–	53 – 197
Germany	1990 – 1996	Contaminated	56	–	3 – 1600
		Clean	3	–	3.3 – 88
Luxembourg	1992 – 1994	Contaminated	2	–	54 – 77
		Clean	2	–	30 – 64
Netherlands	1989 – 1993	Contaminated	4	–	10 – 150
		Clean	2	–	9 – 63
Slovakia	1996 – 1997	Contaminated	1	–	50 – 130
		Clean	1	–	40 – 70
Sweden	1986 – 2009	Contaminated	12	–	0.16 – 29
		Clean	10	8	0.08 – 55
Poland	1995 – 2002	Contaminated	14	9	39 – 12000
		Clean	3	3	71 – 3200
France	2005 – 2008	Clean	20	20	2 – 135
Denmark	2002 – 2005	Contaminated	22	–	3 – 57

		Clean	56	–	3 – 180
United Kingdom	1997 – 2009	Contaminated	75	75	2 – 168
		Clean	127	91	0.1 – 320
China	1997 – 2010	Contaminated	148	64	17 – 3030
		Clean	7	–	3 – 247
Japan	1992 – 2007	Contaminated	30	–	4 – 1700
USA	1987 – 2007	Contaminated	8	–	15 – 2200
		Clean	15	8	2 – 60

About 65% of available measurements are made in contaminated regions, and the rest 35% – in relatively clean regions. Here rural and background regions are viewed as clean, and regions from urban and industrial to suburban – as contaminated. Essential amount of measurements made in clean regions (over 100 individual measurements) are reported together with congener composition of total PCDD/F mixture. In particular, such data (not reported to EMEP) are available at two EMEP sites (SE12 and SE14) for particular periods.

These measurements characterize environmental levels of PCDD/Fs for different locations from background ones (up to 15 – 20 fg I-TEQ/m³) to urban/industrial regions (about several hundreds of fg I-TEQ/m³). Extremely high contamination levels of PCDD/Fs (more than 1000 fg I-TEQ/m³) were obtained at some urban/industrial locations in China, Korea and Poland.

Since the model used has spatial resolution 50×50 km it cannot reproduce local levels of contamination in immediate proximity of large sources (cities, industrial enterprises, waste incinerators, roads with heavy traffic, etc). For this reason mainly measurements in background/rural regions were selected for the emission adjustment. Further, we have restricted ourselves by the consideration of those sites where congener composition of air concentrations was reported.

Thus, the selected data are: measurements in France (Thau lagoon) for 2005 and 2007; measurements at Swedish sites SE12 and SE14 for 2009, measurements in Spain (Arenys de Mar) made in November 2008, measurements in Italy (Ispra IT04 JRC EMEP site) made in March 2005 and measurements at the UK sites (London, Manchester, Middlesbrough, Stoke Ferry and Hazelrigg) for the period from 2004 to 2008 (see Fig. 21). The site High Muffles was not considered due to large number of measurements being below the detection limit. In addition, measurements at Great Lakes (sites Eagle Harbor, Sleeping Bear Dunes, Sturgeon Point and Chicago) for the period from 2004 to 2007 were also used for the comparison.

It is difficult to quantify the uncertainty in the POP measurements since it depends on several factors (methodology, sample handling and preparation etc) and the component in question. In addition, measurements at a given site could be not representative for characterization of background contamination levels due to site location (the influence of local sources can be strong enough). An impression on the influence of site location can be obtained by the consideration of measurements at two locations near Thau lagoon (France) for four days in November 2005 (see Fig. 33). The measurement sites are located at a distance of about 5 km at South and North shore of Thau lagoon within one and the same model grid cell. It is seen that the measured values of atmospheric PCDD/F toxicity can differ about 2 times at these two locations. It manifests that the contamination of the atmosphere by PCDD/F can to a considerable extent be conditioned by local sources.

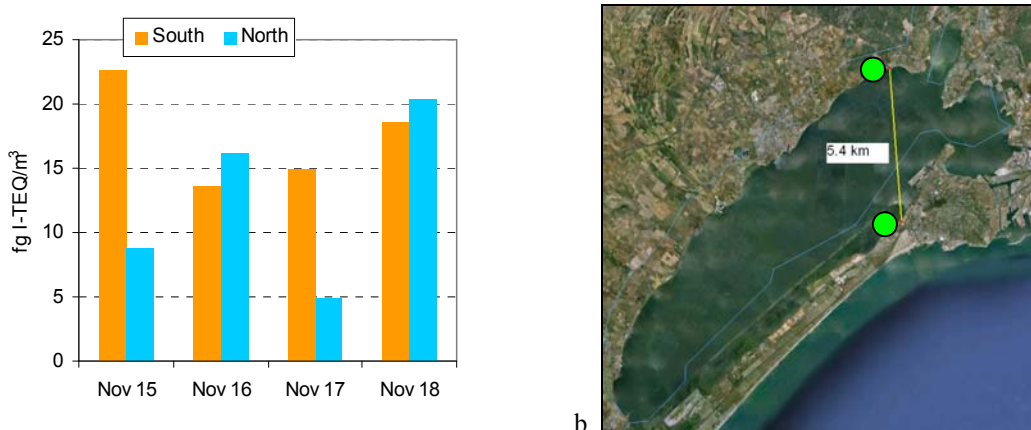


Fig. 33. PCDD/F toxicity (fg/m^3) measured at two sites near Thau lagoon in four days in November 2005 (a) and site locations (b)

So, uncertainties in measurement data can be roughly estimated as a factor of 2.

Emission inventories. Preparation of emission data for modelling can be split into two stages: compiling the data on total toxicity of PCDD/F mixture, and evaluation of its congener composition.

Initial emission data on total toxicity for the regional modelling was prepared on the basis of official information submitted by CEIP complemented by unofficial data of emission inventories [Denier van der Gon et al., 2005; Pulles et al., 2006] when necessary. The latest available information on PCDD/F emission in the USA was taken from the dioxin and furan inventories prepared by [UNEP, 1999] for 1995. The emissions of PCDD/F in the Central Asian countries and the Asian part of Russia was constructed on the basis of the non-Party inventory of PCDD/F emissions in the Central Asian countries made in the framework of the global International POPs Elimination Project (IPEP) [Hodjamberdiev, 2006] and the data on population density [Li, 1996]. PCDD/F emissions in China are taken from the inventory of potential PCDD and PCDF emission sources in the mainland of China [Jin et al., 2004]. PCDD/F emissions of Japan are derived from national dioxins emission inventory [Government of Japan, 2009].

Initial evaluation of emissions of individual congeners was performed on the basis of total toxicity of the mixture of 17 toxic PCDD/F congeners and congener composition of PCDD/F emissions according to the estimates of POPCYCLING-Baltic project [Pacyna et al., 2003]. In this study congener-specific emissions for 1995 were reported separately for all European countries. Spatial distribution of dioxin-to-furan ratio (D/F ratio, that is the ratio of toxicities of dioxins to that of furans in total toxicity) according to these data together with location of selected measurement sites are shown in Fig. 34. The ratio varies from 0.09 to 0.43, manifesting that the share of dioxins in emission toxicity is less than the half according to the above data.

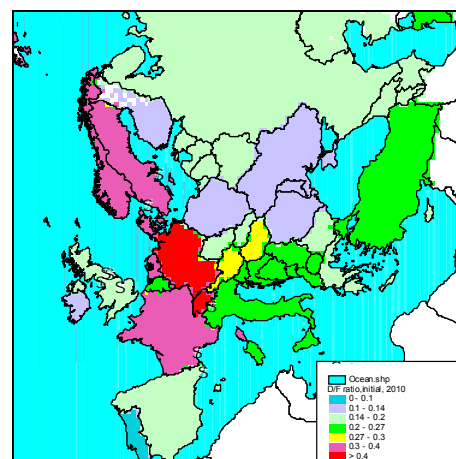


Fig. 34. Spatial distribution of D/F ratio according to [Pacyna et al., 2003] and location of measurements used

On the basis of the comparison between calculation results obtained with initially generated emission data with measurements adjusted emission scenarios are worked out. The description of the adjusting method is given below.

The uncertainties in PCDD/F emissions reported by seven European countries (Croatia, Cyprus, Denmark, Finland, France, Sweden and the UK) vary from 50% (Finland) to 700% (Denmark). The following reasons can possible cause the underestimation of observed air concentrations and deposition fluxes by the model.

1. General underestimation of PCDD/F emission in particular European countries can be conditioned by the fact that data for some regions and sectors are missing. The reported contributions of main emission sectors to national total emissions of PCDD/Fs for some countries are presented in Table 12.

Table 12. The contribution of main emission sectors to emissions of some European countries as reported to UN ECE

	Contributions (%)								
	DK	EE	FI	DE	LV	LT	NO	PL	SE
Combustion in Power Plants and Industry	8	47	36	8	42	13	13	10	72
Transport	1	2	19	4		2	14		2
Commercial Residential and Other Stationary Combustion	67	50	8	28	47	85	39	45	8
Industrial Processes	25		35	57	2		17	3	16
Agriculture					8		7		
Waste incineration		2	1				9	41	3

DK – Denmark, EE – Estonia, FI – Finland, DE – Germany, LV – Latvia, NO – Norway, PL – Poland, SE – Sweden, RF – the Russian Federation.

It is, for example, clear that the contributions of transport to the emissions of PCDD/Fs in Latvia and Poland are not taken into account. The industrial processes contribute to the PCDD/F emissions in rather different extent. Waste incineration in Poland is rather large whereas in other countries the contribution of this sector is minimal or absent.

2. One more reason for the disagreement between measurement and calculations are the discrepancies in evaluation of congener profile in emissions. To illustrate the uncertainties arising in evaluation of emission congener composition, measured congener profiles of air concentrations at Aspvreten are compared with congener profiles in emission used in modelling. In addition, profiles obtained from measurements at three sites near Great Lakes [Venier *et al.*, 2009] are also considered (see Table 13).

Table 13. Comparison of measured fractions of some PCDD/F congeners in total toxicity in the atmosphere with that used in the above mentioned emission inventory.

Congener	Aspvreten	Eagle Harbor	Sleeping Bear Dunes	Sturgeon Point	Emission inventory
2,3,4,7,8-PeCDF	32%	21.5%	22.5%	20.1%	39.7%
1,2,3,7,8,9-HxCDD	4.5%	6.9%	7.4%	8.1%	1.6%
OCDD	1.4%	3.8%	3.8%	4.2%	0.23%
OCDF	0.3%	0.25%	0.26%	0.21%	0.05%

It can be seen that the fraction of congener 2,3,4,7,8-PeCDF in emission used in calculations approximately corresponds to its fraction in air concentrations. On the opposite, for the rest three congeners their fractions in emission inventory are essentially lower than in the atmosphere. The difference is about 4 times for 1,2,3,7,8,9-HxCDD, about 10 – 20 times for OCDD, and about 5 – 6 times for OCDF.

3. Variability of emission factors between particular types of sources can serve as an additional source of emission uncertainties vary in a very wide range (see Table 14).

Table 14. Contributions of selected congeners to emissions for various types of emission sources (%).

	Combustion					Road Transport	Metallurgy
	natural wood, flay ash [1]	trae [2]	wood - working industry [3]	coal-fired utility/industrial power plants [3]	municipal waste [3]	diesel engine [5]	Standard steel production using ferrous scrap [4]
23478 PeCDF	6.3%	26.5%	31.2%	47.4%	37.82%	22.2%	46.4%
123789 HxCDD	2.9%	0.7%	7.3%	0.5%	3.07%	8.5%	3.28%
OCDD	1.3%	0.02%	0.2%	0.7%	0.66%	2.6%	0.49%
OCDF	0.2%	0.006%	0.03%	0.2%	0.08%	0.2%	0.34%

1 – [Oehme et al., 1995]; 2 – [Delrapport 5, 2006]; 3 – [EPA inventory, 2006]; 4 – [Öberg T., 2007]; 5 – [EPA Health assessment, 2002]

From these data it is clear that for reasonable evaluation of contamination levels of particular PCDD/F congeners further refinement of congener profile in emissions is required.

4. Further, missing sectors, underestimation of uncontrolled emissions, emissions from natural sources can be additional sources of emission data uncertainties. For example, dioxins in the environment may arise as by-products or contaminants during the processes concerned, or through the chemical transformation or degradation of other compounds, produced intentionally or unintentionally. In fact, heavy dioxin congeners (particularly OCDD) are contained in wood treated by PCP (see [SEPA report, 2009]). The contributions of particular congeners in total PCDD/F toxicity in PCP-containing preparations taken from the cited report are shown in Fig. 35.

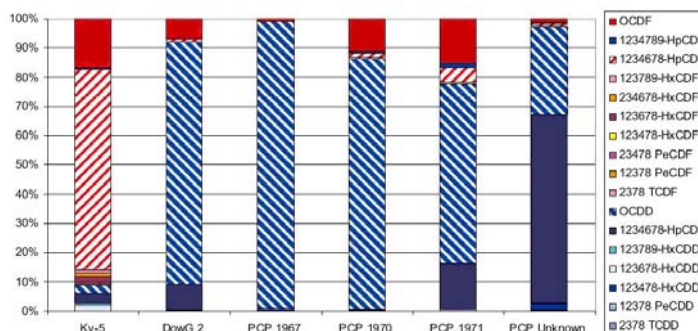


Fig. 35. Contributions of particular congeners in total PCDD/F

From the diagram it is seen that the contribution of OCDD is very high in most of PCP-containing preparations. Moreover, Baker and Hites [Baker and Hites, 2000] suggest that “the photochemical synthesis of OCDD from pentachlorophenol (PCP) in atmospheric condensed water is the most.

From the diagram it is seen that the contribution of OCDD is very high in most of PCP-containing preparations. Moreover, Baker and Hites [Baker and Hites, 2000] suggest that “the photochemical synthesis of OCDD from pentachlorophenol (PCP) in atmospheric condensed water is the most.

Models. For calculation of environmental levels of individual PCDD/F congeners corresponding to the given emission data two versions of MSCE-POP model are used. For calculations of PCDD/F environmental levels regional version of MSCE-POP model [Gusev et al., 2005] is used. This is a

three-dimensional Eulerian multi-compartment model operating on the EMEP grid with a spatial resolution of $50 \times 50 \text{ km}^2$ including main environmental compartments (the atmosphere, surface soil, seawater and vegetation). Main processes defining PCDD/F environmental fate (emissions, long-range atmospheric transport, deposition flux, degradation and gaseous exchange between the atmosphere and the underlying surfaces) are parameterized in the model.

To evaluate the contributions from distant sources located outside the EMEP domain, boundary and initial conditions for the above regional simulations are generated by hemispheric version of MSCE-POP model operating with spatial resolution $2.5^\circ \times 2.5^\circ$. Calculations by this model were made over sufficiently long period (from 1970 to 2010) to take into account the contributions from long-term accumulation in the environmental media.

The data on physical-chemical properties and degradation half-lives of 17 toxic PCDD/F congeners are compiled in Annex A of EMEP/MSC-E Technical Report 5/2005 [Gusev *et al.*, 2005]. For the analysis of the disagreement between model predictions and monitoring data the influence of possible uncertainties in physical-chemical data was performed.

The most important source of uncertainties in model calculations is the description of the processes of removal from the atmosphere. These are atmospheric degradation of POPs and deposition processes both for gaseous and particulate forms. To evaluate possible uncertainties in calculating PCDD/F toxicity both two processes are analysed.

First, validation of the model with respect to deposition processes can be done with the help of simultaneous measurements of air concentrations and deposition flux at one and the same location. Such measurements are available at sites SE12 and SE14 for four months in 2009. To exclude the influence of uncertainties in emission data measured-to-calculated ratios (M/C ratios) for air concentrations and for depositions are compared instead of the direct comparison of air concentrations and deposition fluxes. It is clear that closeness of M/C ratios for concentrations and deposition fluxes manifests correct description of deposition processes. On the opposite, if M/C ratios for air concentrations essentially differ from those for deposition flux, it can be concluded that there are essential uncertainties in the model description of deposition process.

The comparison of average M/C ratios for air concentrations and depositions for all 17 toxic PCDD/F congeners at sites SE12 and SE14 are displayed in Fig. 36.

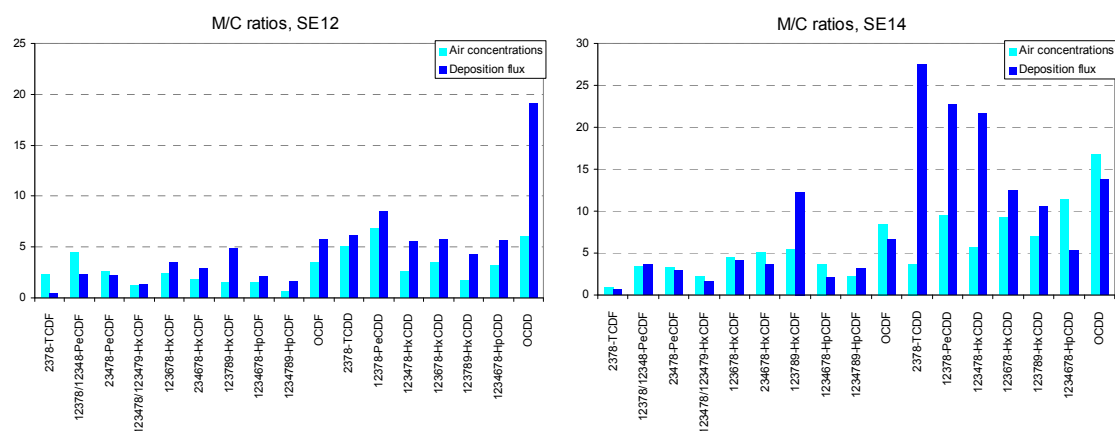


Fig. 36. Comparison of measured-to-calculated ratios for air concentrations and deposition flux on the basis of the data from measurements at SE12 and SE14 sites.

It can be seen that for half of measurements M/C ratios for air concentrations and deposition flux differ less than by 50%. Essential differences (out of factor of 2) between M/C ratios for air concentrations

and deposition fluxes obtained at both of the considered measurement sites takes place for 1,2,3,7,8,9-HxCDF and 1,2,3,4,7,8-HxCDD. For these two congeners the difference between the two considered M/C ratios is about 3 times. For all other congeners the agreement between these ratios is within a factor of 2 at least at one site. So, the uncertainties in the model description of deposition processes can be evaluated as a factor of 2 – 3 at maximum.

To estimate possible influence of the uncertainties in the description of deposition processes to the values of air concentrations sensitivity analysis of air concentrations with respect to deposition processes was undertaken. Namely, possible changes in air concentrations due to 3-fold enlarging and diminishing of deposition processes intensity were calculated. For these calculations the approach described in Chapter 3 of [Gusev *et al.*, 2005] was applied. For brevity, only two congeners were included into the sensitivity analysis: 2,3,4,7,8-PeCDF and 1,2,3,4,7,8-HxCDD.

We recall that according to the above mentioned approach for evaluation of sensitivity one-dimensional model of pollutant transport from a point source taking into account atmospheric transport and deposition and degradation processes is used. Wind velocity is assumed to be constant; calculations were made with values of wind velocity equal to 4 m/s and 7 m/s to reveal the influence of wind velocity change. Parameters needed for the model calculations (deposition velocities over various land-use types and degradation rate) are taken as the average parameters obtained during model runs of MSCE-POP model. The model was used with these parameters, with deposition velocities enlarged 3 times and deposition velocities diminished 3 times.

It was found that for 2,3,4,7,8-PeCDF enlarging deposition velocities 3 times leads to 80% diminishing of air concentrations, and diminishing deposition velocities 3 times gives enlarging air concentrations by 70% from the base value independently of the chosen value of wind speed. Moreover, maximum diminishing of air concentrations is reached at such distance from the source where air concentrations drop essentially (10000 km and more). The plot of changes in air concentrations together with their absolute values for various distances from the emission source is presented in Fig 37. For 1,2,3,4,7,8-HxCDD possible enlargement of air concentrations due to 3-fold diminishing of deposition velocity is estimated as 58%.

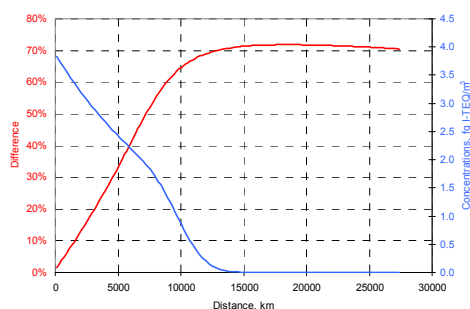


Fig. 37. Changes in air concentrations due to 3-fold diminishing of deposition velocities together with their absolute values for various distances from the emission source for 2,3,4,7,8-PeCDF

The same approach was applied for the evaluation of sensitivity of air concentrations with respect to degradation process. It was found that the increase of air concentrations due to diminishing deposition rate 10 times equals about 10% for 2,3,4,7,8-PeCDF and only 2% for 1,2,3,4,7,8-HxCDD.

So, it can be concluded that the uncertainty of calculations of air concentrations due to model parameterization can be evaluated as 80% at maximum.

Adjustment procedure. Since Parties to the Convention report the emission data on total toxicity of PCDD/Fs only, to assess environmental pollution by PCDD/Fs the congener composition of emissions should be evaluated. To perform this task, the following approach is used.

At the first stage initial model simulations for each of 17 toxic congeners based on the available emission data are performed. For these calculations congener-specific emissions are generated on the basis of official emission data on total toxicity of PCDD/F mixture provided by CEIP. To split the

data on total toxicity to emissions of particular congeners the expert estimates from POPCYCLING-Baltic project [Pacyna *et al.*, 2003] are used as described in Section 1.2 above. To take into account remote emission sources (located outside the EMEP domain) and the influence of long-term accumulation of PCDD/F congeners in the environmental media other than the atmosphere, hemispheric simulations for the period from 1970 to 2010 are carried out. Then calculations of environmental levels of each of 17 toxic congeners are done on the regional level for 2009 and 2010 with initial and boundary conditions generated on the basis of hemispheric calculations.

At the second stage the results of initial simulations are compared with available measurement data on atmospheric concentrations of PCDD/F congeners. This task is complicated by the fact that regular measurements of PCDD/Fs at the EMEP measurement sites are currently performed. To obtain monitoring data for the comparison MSC-E performed literature search of congener-specific PCDD/F measurements obtained by national and international monitoring campaigns. These data reported for different years and time periods are compared with calculation results obtained for corresponding periods. The comparison shows essential underestimation of total toxicity of PCDD/F mixture (about 4 – 5 times) and disagreement between measured and calculated congener composition.

According to the above estimates, the above disagreement between measurements and model predictions cannot be determined solely by model uncertainty and is within the range of the uncertainty of emission data. So, at the third stage correction of emissions of individual congeners is done on the basis of minimization of Root Mean Square Error (RMSE) for each of the considered 17 toxic congeners under the assumptions of a small observation noise and neglecting uncertainties in atmospheric transport model. This correction (being in line with estimates of emission uncertainties) leads to the refinement of the agreement between both measured and calculated total toxicity of PCDD/F mixture and between fractions of individual congeners in total toxicity in modelling results and observations.

The use of one and the same correction coefficients for emissions from all EMEP countries is rather rough procedure. Application of such procedure is conditioned by deficiency of congener-specific measurement data on PCDD/F air concentrations. In particular, large areas in Central and Eastern Europe are not covered by measurements. As will be seen below, agreement between measurements and calculations based on the advanced emission scenario strongly depend on geographical location of measurement sites. To refine further the agreement collection of additional measurement data from national measurement sites and campaigns is required. With measurement data with better covering of the EMEP domain spatially resolved correction of emission data is possible. However, even in the present situation some conclusions on evaluating approximate magnitude to which European emission estimates are in error with respect both to total toxicity and congener composition.

Results and discussions

As indicated above, initially calculations of contamination levels for each of 17 toxic PCDD/F congeners were performed on the basis of official emission data on total toxicity together with emission congener composition from POPCYCLING-Baltic project. The results of these calculations were compared with available congener-specific measurement data obtained at clean locations.

Comparison of initial calculations with measurements. The comparison between the results of initial model calculations and measurement data was performed for all measurements described in Section 1.1. As an example, the comparison at sites SE14 in September 2009 and Hazelrigg in third quarter of 2004 is presented in Fig. 38. Measurement data for illustration are chosen in such a way that measurements for all PCDD/F congeners are higher than detection limit.

At both considered sites the model underestimates the values of air concentrations. It can also be seen that the concentrations of PCDDs are underestimated in higher extent that those of PCDFs. So, it can be concluded that there exists underestimation of total toxicity of PCDD/F mixture in line with uncertainties in model description of congener composition.

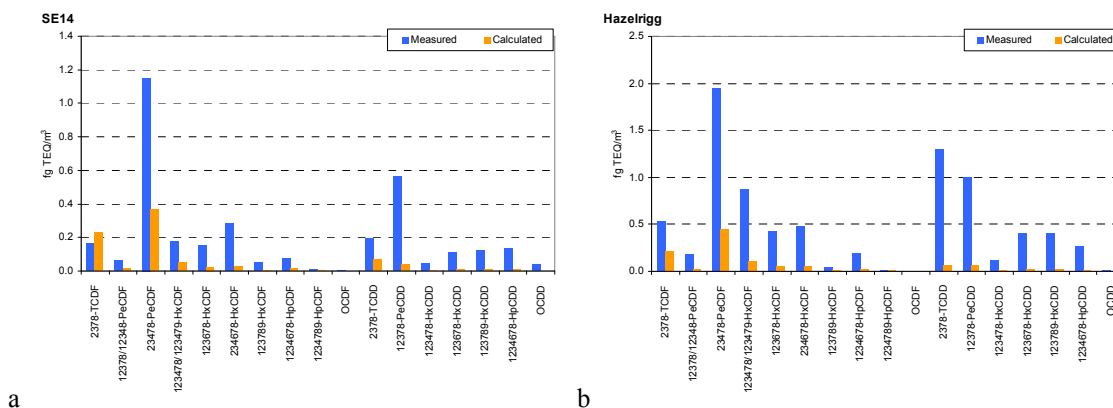


Fig. 38. Comparison of measured air concentrations with that obtained by initial calculations at SE14 in September 2009 (a) and at Hazelrigg in third quarter of 2004 (b).

This situation is even more pronounced for measurements in the UK (Great Lake district. For example, calculated and measured PCDD/F congener profiles at Eagle Harbor (background site) and Chicago (urban site) are shown by the plots in Fig. 39. It can be noticed that high measured values of D/F ratio are characteristic of western countries (locations) whereas lower value of the ratio were measured at the locations situated in the Eastern/Southern Europe (Italy and Poland). It is interesting to note that measurements for China show rather low fraction of dioxins (measured value of D/F ratio in Beijing, February 2006, is 0.12).

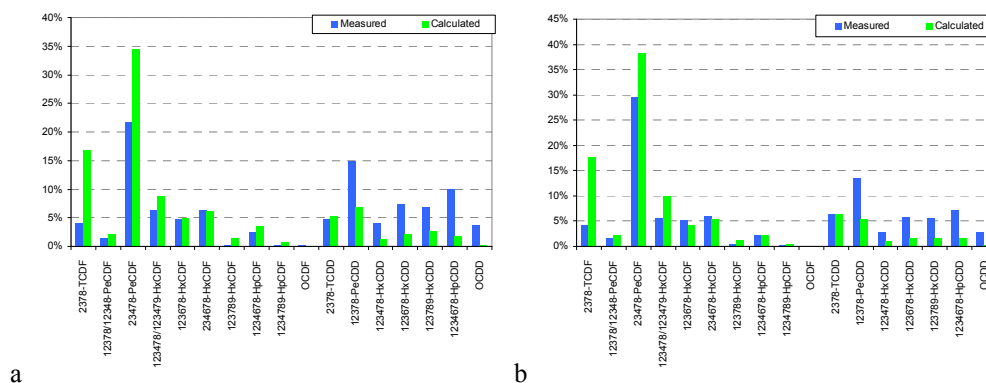


Fig. 39. Comparison of calculated and measured congener composition at Eagle Harbor (a) and Chicago (b) in 2004 – 2007.

For Eagle Harbor measured D/F ratio is 1.08 whereas calculated ratio is 0.26. Similar, D/F ratios for Chicago are: measured – 0.79, and calculated – 0.22. So, from this comparison it is clear that the model overestimates furan contribution to total toxicity in the Great Lakes district similar to the situation in the western part of Europe.

The cumulative distribution of measurement-to-calculation factor for total toxicity is presented in Fig. 40. In compilation of statistical parameters to characterize the agreement between measurements and modelled values of total toxicity only those measurements for which no congener concentrations occur to be under the detection limit are used. It is seen that the median value of measurement-to-calculation factor equals 5.3, which means that the model underestimates PCDD/F toxicity approximately 5 times. The agreement within a factor of three is achieved by initial calculations for 20% of the considered measurements only.

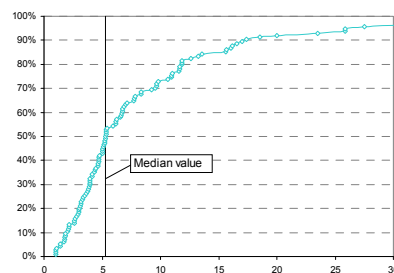


Fig. 40. Cumulative distribution of measurement-to-calculation factor for total toxicity

In addition, the comparison of measured and calculated values of PCDD/F total toxicity at the USA/Canada sites located in the Great Lakes district was carried out. The comparison between model predictions and measurement data at four Great Lakes sites is shown in Fig. 41.

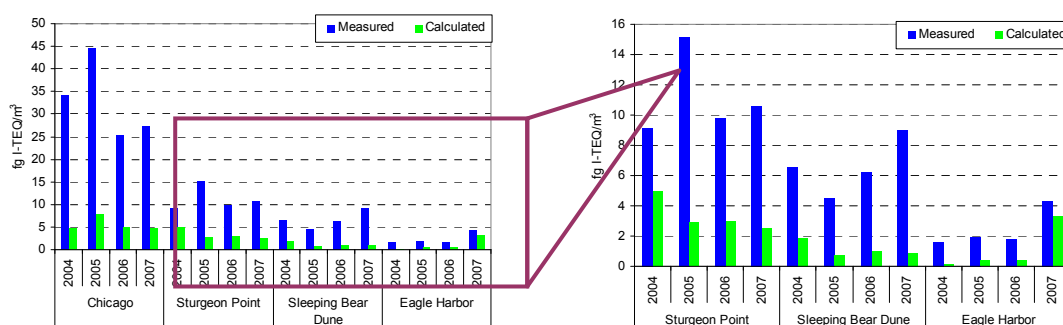


Fig. 41. Comparison of total PCDD/F toxicity calculated and measured at four Great Lakes sites for 2004 – 2007, fg I-TEQ/m³.

It is seen that the model approximately reflects temporal and spatial variations of PCDD/F toxicity at the considered four sites (from the lowest levels at Eagle Harbor to the highest values at Chicago site) but essentially underestimate absolute values of total PCDD/F toxicity. The underestimation is as much as 5 times on the average with the range from 1.3 to 7 times for various sites and years. This is in line with the results obtained by the comparison at European sites.

It was found that measured-to-calculation ratio is essentially different for different PCDD/F congeners. For the illustration, the comparison of calculated and measured concentrations of the “indicator” congener 2,3,4,7,8-PeCDF is shown in Fig. 42. We recall that this congener contributes to the total toxicity in maximum extent (30% – 40%).

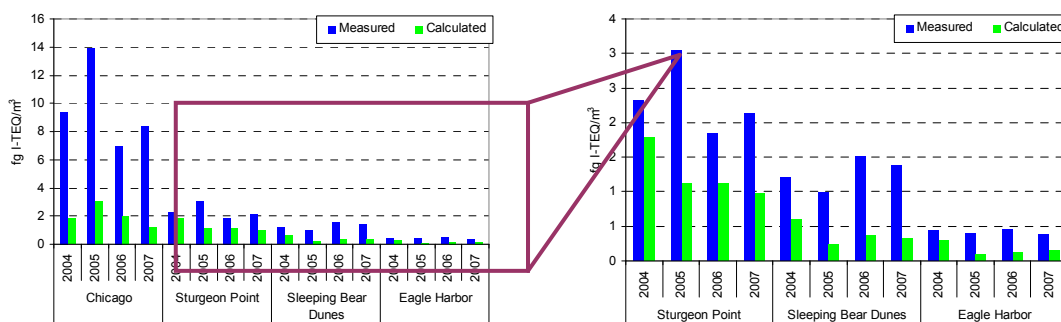


Fig. 42. Comparison of 2,3,4,7,8-PeCDF toxicity calculated and measured at four Great Lakes sites for 2004 – 2007, fg I-TEQ/m³.

Here the underestimation of air concentrations by the model is lower than for total toxicity. In fact, the underestimation is about 3.4 times on the average with the range mainly from 1.3 to 5.2 times. The difference of the comparison results obtained for total toxicity and for the “indicator” congener indicates that the congener composition calculated by the model is subject to essential uncertainties.

To provide statistical characterization of PCDD/F congener composition in the atmosphere dioxin-to-furan ratio (D/F ratio) is used. The latter is one of the characteristics of PCDD/F congener composition, which is often used in the literature. It is defined as the ratio of contribution of dioxins to total toxicity to that of furans. Measured and calculated D/F ratios for some locations and time periods in Europe are given in Table 15. The table contains both background and urban measurements. The latter can be used for direct evaluation of PCDD/F congener composition in the corresponding region since measurement locations are for these sites close to sources and congener composition in the atmosphere is not subject to modifications during to long-range transport due to differences in physical-chemical properties of particular congeners.

Table 15. Measured and calculated values of D/F ratio for some locations in Europe

Period and location	D/F ratio	
	Measured	Calculated
Hazelrigg (the UK), 2004 – 2008	1.02	0.22
Thau lagoon (France), 2005	0.97	0.27
London (the UK), 2004 – 2008	0.75	0.22
Stoke Ferry (the UK), 2004 – 2007	0.71	0.22
Arenis de Mare (Spain), November 2008	0.67	0.21
SE14 (Sweden), 2009	0.57	0.38
Middlesbrough (the UK), 2004 – 2008	0.55	0.22
Thau lagoon (France), 2007	0.48	0.21
Manchester (the UK), 2004 – 2008	0.48	0.22
SE12 (Sweden), 2009	0.43	0.40
Ispra, IT04 (Italy), March 22 – 30, 2005	0.23	0.20
Krakow (Poland), June and December 2002	0.12	0.22

It can be noticed that high measured values of D/F ratio are characteristic of western countries (locations) whereas lower value of the ratio were measured at the locations situated in the Eastern/Southern Europe (Italy and Poland). It is interesting to note that measurements for China show rather low fraction of dioxins (measured value of D/F ratio in Beijing, February 2006, is only 0.12).

The differences in congener composition of PCDD/F toxicity in emissions are conditioned by the differences of congener composition in emissions from different emission sectors and by the differences in the distributions of country emissions by sectors. Average values of D/F ratios for some emission sectors are presented in Table 16.

Table 16. Average D/F ratios for some emission sectors

	D/F ratio		
	Average	Median	SqD
Marine transport	0.99	0.73	0.45
Road transport	0.92	0.48	1.20
Fuel burning	0.79	0.51	0.99
Waste incinerators	0.47	0.27	0.58
Cement kilns	0.44	0.33	0.23
Metallurgy	0.26	0.18	0.20

It can be seen that high values of D/F ratios (that is, predominance of dioxins in emissions) is characteristic of sectors connected with fuel burning such as marine transport, road transport, etc. On the opposite, emissions from waste incinerators and industry seem to be characterized by lower value of D/F ratio. Unfortunately, gaps in the information on the distribution of country emissions by sectors and uncertainties in emission factors for individual congeners hamper the construction of correct country-specific congener composition of emissions.

The above comparison leads to the conclusion that

- total PCDD/F toxicity is underestimated by the model approximately by a factor of 5;
- there are essential uncertainties in congener composition of PCDD/F mixture in the atmosphere.

The estimates of uncertainties due to measurements, model design and emissions show that uncertainties in measurement data and model design alone cannot explain the disagreement between measurements and calculation results in full extent. So, to obtain more reasonable description of PCDD/F contamination levels it is reasonable to consider certain adjustment of emission from the viewpoint both total toxicity and congener composition (emission scenarios). The approach to emission adjustment was described above in Section 1.4. The results of calculations of PCDD/F contamination levels with adjusted emissions are presented in the next section.

Calculation results based on adjusted emission data. The result of the adjustment procedure is as follows. First, enlargement coefficient for total toxicity in emissions was found to be 5.4, which is in accordance to underestimation of air concentrations by initial calculations obtained in the previous section. The difference between congener profile used in preliminary calculations and refined congener profile is shown in Fig. 43.

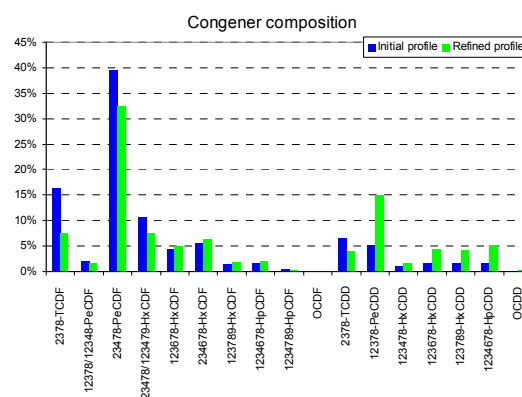


Fig. 43. Change in congener profile in emissions obtained in the optimization procedure based on European measurement data.

To give the impression of the change in spatial distribution of PCDD/F congener composition D/F ratio is used. The comparison of D/F ratios used in initial calculations with those according to adjusted emission scenario is presented in Fig. 44.

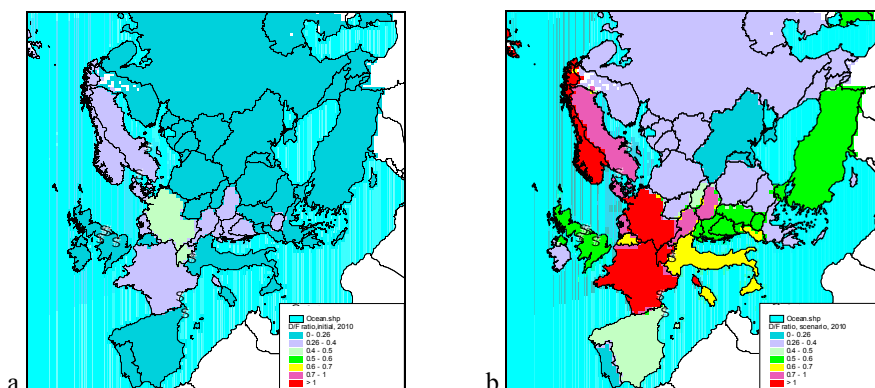


Fig. 44. Comparison of spatial distributions of D/F ratio in emissions used in initial calculations (a)

It is seen that while D/F ratio in emissions used for initial calculations does not exceed 0.4 for all European countries, it becomes higher according to the adjusted scenario lying in the range from 0.26 to 1 and higher. As a result, calculated D/F ratio for atmospheric concentrations is also enlarged. Spatial distribution of D/F ratio in air is shown in Fig. 45.

It is seen that D/F ratio in the atmospheric air occur to be somewhat lower than that in emissions. The reason of this difference is the change of PCDD/F congener composition during the atmospheric transport. The range of calculated D/F ratios is from 0.27 to 1 which corresponds to measured values of this ratio presented in Table 15.

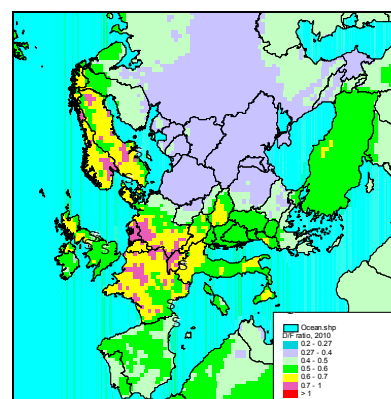


Fig. 45. Calculated D/F ratio

The comparison of measured values of total toxicity of PCDD/F mixture with those calculated using the adjusted emission scenario was performed for the same set of measurements as for initial scenario calculations (see Fig. 39 and corresponding discussion). The cumulative distribution of measurement-to-calculation factor for total toxicity is presented in Fig. 46. It occurs that:

- median value of measurement-to-calculation factor is 1.75;
- more than 80% of measurements agree with calculations within a factor of three;
- among them about 60% of measurements agree with calculation results within a factor of 2.

This shows that from the viewpoint of total toxicity calculations based on the adjusted emission scenario reasonably agree with measurements.

The refinement of the agreement between measurements and calculations due to usage of adjusted scenario is illustrated by the comparison of measured and calculated values of toxicities of individual PCDD/F congeners at two locations: site SE14 (Råö, Sweden) and Hazelrigg (the UK), see Fig. 47. It can be

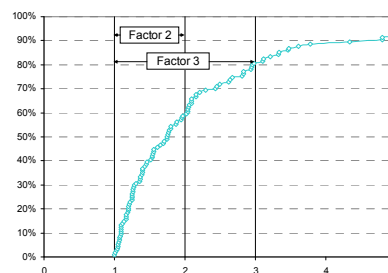


Fig. 46. Cumulative distribution of measurement-to-calculation factor for total toxicity calculated with adjusted emission scenario

seen that the consideration of adjusted emission scenario essentially improves the agreement between measurements and model predictions at these two sites.

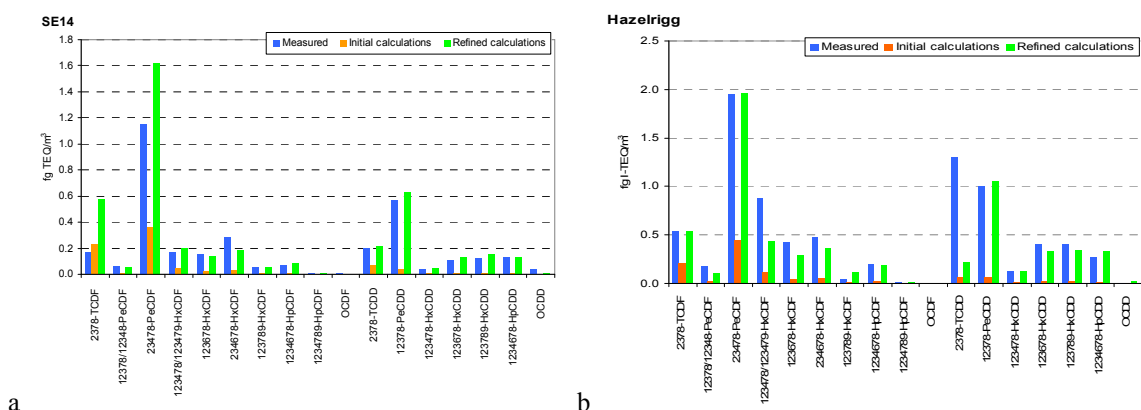


Fig. 47. Comparison of measured air concentrations with that obtained by calculations based on the adjusted scenario at SE14 in September 2009 (a) and at Hazelrigg in third quarter of 2004 (b).

Additional information for the validation of the adjusted scenario can be obtained with the use of measurements at site SE12 (Aspvreten) for some days in 2006 – 2007. These data is supplied by compass sectors from which prevailing transport takes place (E – east, NNE – north-north-east, NNW – north-north-west, NW – north-west, etc.). These sectors together with D/F ratios in emissions of the EMEP countries are shown in Fig. 48.

The values of D/F ratio measured at SE12 for the considered compass sectors are given in Table 17.

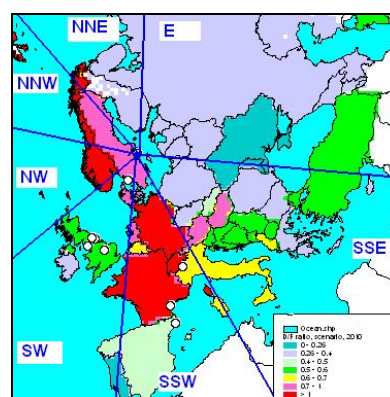


Fig. 48. Compass sectors used for measurement data at SE12 together with values of D/F ratio

Table 17. Values of D/F ratio measured for various compass sectors in Aspvreten site in 2006 – 2007

Compass sector	D/F ratio
South-West (SW)	0.92
South-South-West (SSW)	0.49
South-South-East (SSE)	0.26
East (E)	0.33
North-North-East	0.44
North-North-West	1.13
North-West	1.10

It can be seen that the measured values of D/F ratio in considered compass sectors approximately correspond to the values of D/F ratio in emissions of countries contained in these sectors. In the comparison it should be taken into account that closer sources imply higher influence at D/F ratio at measurement location and that D/F ratio have the tendency to decrease during air transport. For example, D/F ratio in SW, NW and NNW sectors is mainly determined by emissions of Norway, Sweden and Denmark and therefore is close to 1. For SSW sector D/F ratio is lower due to the

distance from main sources to measurement location. For NNE sector D/F ratio is determined partly by emissions of Finland and the RF (D/F ratio from 0.26 to 0.4), and partly by emissions of Sweden and Norway (D/F ratio close to 1). As a result D/F ratio in this sector is slightly less than in SSW sector (0.44). Finally, D/F ratio for countries in sectors SSE and E is from 0.26 to 0.4, which correspond to measured values of D/F ratio for this sector.

So, usage of the adjusted emission scenario can essentially improve the agreement between measurements and model calculations both from the viewpoint of total toxicity and congener composition. It should be noted that usage of one and the same set of correction coefficients is rather rough assumption, and for further refinement of evaluation of PCDD/F contamination levels country-specific adjustment should be refined. This is possible provided that more measurements of PCDD/F with congener composition reported are included into the comparison.

Concluding remarks

1. Existing emission inventory based on official emission data complemented with expert estimates when necessary seems to underestimate total toxicity of PCDD/F mixture in emissions about 5 times.
2. The reason of underestimation can be both underestimation of emission factors for source categories taken into account in the inventory and missing emission sectors.
3. The adjustment scenario constructed on the basis of the comparison of measurement data with calculation results allows refine the agreement between measurements and calculations so that more than 60% of measurements agree with calculations within a factor of 2.
4. Country-specific adjustment procedure can further refine the agreement. However, such a procedure requires more congener-specific measurement data from various locations within the EMEP domain.

REFERENCES

- Abas M.R.B. and Simoneit B.R.T. [1996] Composition of extractable organic matter of air particles from Malaysia: initial study. *Atmos. Environ.* vol.30, No.15, pp. 2779–2793.
- Aggarwal S. , Aggarwal S.G., Okuzawa K., K. Kawamura [2010] Size distributions of dicarboxylic acids, ketoacids, -dicarbonyls, sugars, WSOC, OC, EC and inorganic ions in atmosphere particles over Northern Japan: implication for long-range transport of Siberian biomass burning and East Asian polluted aerosols, *Atmos.Chem.Phys.*, vol.10, pp. 5839-5858.
- Aggarwal S. G. and K. Kawamura [2009] Carbonaceous and inorganic composition in long-range transported aerosols over northern Japan: Implication for aging of water – soluble organic fraction, *Atmos. Environ.*, vol.43, pp. 2532-2540.
- Albinet A. , Leoz-Garziandia E., Budzinski H., Villenave E. [2007] Polycyclic Aromatic Hydrocarbons (PAHs), nitrated PAHs and oxygenated PAHs in ambient air of the Marseilles area (South of France). Concentrations and sources, *Science of the Total Environ*, vol.384 (104), pp. 280-292.
- Albinet A. , Leoz-Garziandia E., Budzinski H., Villenave E., Jaffrezou J.L.. [2008] Nitrated and oxygenated polycyclic aromatic hydrocarbons in the ambient air of two French alpine valleys. Part 1: concentrations, sources and gas/particle partitioning, *Atmos. Environ.*, vol.42, Issue 1, pp. 43-53.
- Alebić-Juretić A., Cvitaš T., Klasinc L. [2000] Kinetic of heterogeneous ozone reactions, *Chemosphere*, vol.41, pp. 667-670.
- Alebić-Juretić, A., Cvitaš, T., Klasinc, L. [1990] Heterogeneous polycyclic aromatic hydrocarbon degradation with ozone on silica gel carrier. *Environ. Sci. Technol.* vol.24, No.1, pp.62-66..
- Alfaro S.C. and L. Gomes [2001] Modeling mineral aerosol production by wind erosion: Emission intensities and aerosol size distributions in source areas. *Journal of Geophysical Research*, vol. 106, No. D16, pp.18,075 – 18,084.
- Allen J.O. [1997] Atmospheric Partitioning of Polycyclic Aromatic Hydrocarbons (PAH) and Oxygenated PAH, Thesis Doctor of Science, 346 p.
- Alves C., Oliveira T., Pio C., Silvestre A. J.D., Fialho P., Barata F., Legrand M. [2007] Characterisation of carbonaceous aerosols from the Azorean Island of Terceira, *Atmos.Environ.*, vol.41, pp. 1359-1373.
- Alves C.A. and C.A.Pio [2005] Secondary Organic Compounds in Atmosphere Aerosols: Speciation and Formation Mechanisms, *J. Braz. Chem. Soc.*, vol.16, No.5, pp. 1017-1029.
- Alves C.A. [2008] Characterisation of solvent extractable organic constituents in atmospheric particulate matter: an overview, *Annals of the Brazilian Academy of Sciences*, vol.80 (1), pp. 21-82.
- Araki Y., Tang N., Ohno M., Kameda T., Toriba A., Hayakawa K. [2009] Analysis of atmospheric Polycyclic Aromatic Hydrocarbons and Nitropolycyclic Aromatic Hydrocarbons in Gas/Particle Phases Separately Collected by a High-volume Air Sampler Equipped with a Column Packed with XAD-4 Resin, *Journal of health Science*, vol.55(1), pp.77-85.
- Atkinson R. [1991] Kinetics and mechanisms of the gas-phase reactions of the NO₃ radical with organic compounds, *J.Phys.Chem. Refe. Data*, vol.20,No.3, pp. 459-507.
- Aulinger A., V. Matthias and M. Quante [2010]. An Approach to Temporally Disaggregate Benzo(a)pyrene Emissions and Their Application to a 3D Eulerian Atmospheric Chemistry Transport Model, *Water, Air, & Soil Pollution*, vol. 216, No. 1-4, pp. 643-655.
- Baart A., Berdowski J., van Jaarsveld J. and K. Wulfraat [1995] Calculation of atmospheric deposition of contaminants on the North Sea. TNO-MEP-R 95/138, Delft, The Netherlands..
- Bae M.-S., Schauer J.J., DeMinter J.T., Turner J.R. [2004] Hourly and daily patterns of particle –phase organic and elemental carbon concentrations in the urban atmosphere, *J.Air&Waste Manage.*, vol.54, pp.823-833.
- Baker and Hites [2000] Is Combustion the Major Source of Polychlorinated Dibenzo-p-dioxins and Dibenzofurans to the Environment? A Mass Balance Investigation. *Environ. Sci. and Techn.*, vol 34, No 14, pp 2879 – 2886.
- Baklanov A., A. Aloyan, A. Mahura, V. Arutyunyan, P. Luzan [2011] Evaluation of source–receptor relationship for atmospheric pollutants using approaches of trajectory modelling, cluster, probability fields analyses and adjoint equations. *Atmospheric Pollution Research*, 2, 400 – 408.
- Bamford H.A., Bezabeh D.Z., Schantz M.M., Wise S.A., Baker J.E. [2003] Determination and comparison of nitrated-polycyclic aromatic hydrocarbons measured in air and diesel particulate materials, *Chemosphere*, vol.50, pp. 575-587.

- Bates T.S., Anderson T.L., Baynard T., Bond T., Boucher O., Carmichael G., Clarke A., Erlick C., Guo H., Horowitz L., Howell S., Kulkarni S., Maring H., McComiskey A., Middlebrook A., Noone K., O'Dowd C.D., Ogren J., Penner J., Quinn P.K., Ravichankara A.R., Savoie D.L., Schwartz S.E., Shinozuka Y., Tang Y., Weber R.J., Wu Y. [2006] Aerosol direct radiative effects over the northwest Atlantic, northwest Pacific, and North Indian Oceans; estimated based on in-situ chemical and optical measurements and chemical transport modelling, *Atmos.Chem.Phys.*, vol.6, pp. 175-362.
- Bates T.S., T.L. Anderson, T. Baynard, T. Bond, O. Boucher, G. Carmichael, A. Clarke, C. Erlick, H. Guo, L. Horowitz, S. Howell, S. Kulkarni, H. Maring, A. McComiskey, A. Middlebrook, K. Noone, C.D. O'Dowd, J. Ogren, J. Penner, P.K. Quinn, A.R. Ravishankara, D.L. Savoie, S.E. Schwartz, Y. Shinozuka, Y. Tang, R.J. Weber, and Y. Wu [2006] Aerosol direct radiative effects over the northwest Atlantic, northwest Pacific, and North Indian Oceans: Estimates based on in-situ chemical and optical measurements and chemical transport modeling, *Atmos. Chem. Phys.*, vol.6, pp.1657–1732.
- Bedjanian Y. and Mai Lan Nguyen [2010] Kinetics of the reactions of soot surface-bound polycyclic aromatic hydrocarbons with O₃, *Chemosphere*, vol.79, pp. 387-393.
- Beecken J. [2007] Pilotprojekt KWK-Optimierung, Teilbericht des Netzes des Forschungsprojektes KWK-Optimierung. Tech. rep., Vattenfall Hamburg.
- Bessagnet B., Menut L., Aymoz G., Chepfer H., and Vautard R. [2008]. Modeling dust emissions and transport within Europe: The Ukraine March 2007 event. *JOURNAL OF GEOPHYSICAL RESEARCH*, VOL. 113, D15202, 13 PP., 2008 oi:10.1029/2007JD009541.
- Birmili W., Schepanski K., Ansmann A., Spindler G., Tegen I., Wehner B., Nowak A., Reimer E., Mattis I., Müller K., Brüggemann E., Gnauk T., Herrmann H., Wiedensohler A., Althausen D., Schladitz A., Tuch T., and Löschau G. [2008]. A case of extreme particulate matter concentrations over Central Europe caused by dust emitted over the southern Ukraine. *Atmos. Chem. Phys.*, 8, 997–1016, 2008.
- Brulfert G., Chemel. G., Chaxel E., Chollet J.-P. [2005] Modelling photochemistry in alpine valleys, *Atmos. Chem. Phys.*, vol.5, pp. 2341-2355 .
- Burkhard E., Johnson P., Graham J., Praveen A., Cooper C., Skelton E., Lowell D., van Atten C., Berwick A. [2008] Assessment of carbonaceous PM_{2,5} for New York and the region, Final Report, vol.II, NYSERDA 8642, 383 p.
- Calvert J.G., Atkinson R., Becker K.H., Kamens R.M., Seinfeld J.H., Wallington T.S., Yarwood G. [2002] The mechanism of atmospheric oxidation of aromatic hydrocarbons, Oxford. University Press, 464 p.
- Cao J.J., Lee S.C., Chow J.C., Watson J.G., Ho K.F., Zhang R.J., Jin Z.D., Shen Z.X., Chen G.C., Kang Y.M., Zou S.C., Zhang L.Z., Qi S.H., Dai M.H., Cheng Y., Hu K. [2007] Spatial and seasonal distributions of carbonaceous aerosols over China, *Journal of Geophysical Research*, vol.112, D22S11.
- Cao J.-J., Xu B.-Q., He J.-Q., Liu X.-Q., Han Y.-M., Wang G.h., Zhu C.-S. [2009] Concentrations, seasonal variations, and transport of carbonaceous aerosols at remote Mountainous region in western China, *Atmospheric Environment*, vol.43, pp. 4444-4452.
- Cazaunau M., Le Ménach K., Budzinski H., and E. Villenave [2010] Atmospheric Heterogeneous Reactions of Benzo(a)pyrene, *Zeitschrift für Physikalische Chemie: Vol. 224, No. 7-8*, pp. 1151-1170.
- Chen G., Ziemba L. D., Chu D. A., Thornhill K. L., Schuster G. L., Winstead E. L., Diskin G. S., Ferrare R. A., Burton S. P., Ismail S., Kooi S. A., Omar A. H., Slusher D. L., Kleb M. M., Reid J. S., Twohy C. H., Zhang H., and Anderson B. E. [2011]. Observations of Saharan dust microphysical and optical properties from the Eastern Atlantic during NAMMA airborne field campaign. *Atmos. Chem. Phys.*, 11, 723–740.
- Chesselet, R., M. Fontugne, P. Buat-Ménard, U. Ezat, and C.E. Lambert [1981] The origin of particulate organic carbon in the marine atmosphere as indicated by its stable carbon isotopic composition, *Geophys. Res. Lett.*, vol. 8 (4), pp. 345–348.
- Chung S.H. and Seinfeld J.H. [2002] Global distribution and climate forcing of carbonaceous aerosols, *Journal of Geophysical Research*, vol.107, No.D19, 4407.
- Cicinato A., Balducci C., Nervegna G., Pareti S., Tagliacozzo G., Brachetti A. [2008] Year time modulation of n-alkanes, PAH, Nitro-PAH and organic acids at Montelibretti Rome , Italy, *Polycyclic Aromatic Compounds*, vol.28, pp. 500-517.
- Delrapport 5 [2006] Emissionskortlægning for decentral kraftvarme 2007 – energinet.dk miljøprojekt NR 07/1882.
- Denier van der Gon H.A.C., van het Bolscher M., Visschedijk A.J.H. and P.Y.J.Zandveld [2005]. Study to the effectiveness of the UNECE Persistent Organic Pollutants Protocol and costs of possible additional measures. Phase I: Estimation of emission reduction resulting from the implementation of the POP Protocol. TNO-report B&O-A R 2005/194.

- Duan J., Tan J., Cheng D., Bi X., Deng W., Sheng G., Fu J., Wong M.N. [2007] Sources and characteristics of carbonaceous aerosol in two largest cities in Pearl River Delta Region, China, *Atmos. Environ.*, vol.41, pp. 2895-2903.
- El-Zahan H. S., Zielinska B., Mazzoleni L.R. [2009] Analytical Determination of the Aerosol Organic Mass-to-Organic Carbon Ratio, *Journal of the Air & Waste Management Association*, vol.59, pp. 58-69.
- EMEP particulate matter data: <http://www.nilu.no/projects/ccc/emepdata.html>.
- Environmental Health Criteria 229, Nitrogenated Polycyclic Aromatic Hydrocarbons [2003] Part I and Part II: http://www.who.int/ipcs/publications/ehc/ehc_229/en/index.html.
- EPA Health Assessment Document for Diesel Engine Exhaust, EPA/600/8-90/057F May 2002.
- EPA/600/P-03/002F An Inventory of Sources and Environmental Releases of Dioxin-like Compounds in the United States for Years 1987, 1995, and 2000.
- Esteve W., Budzinski H., Villenave E. [2004] Relative rate constants for the heterogeneous reactions of OH, NO₂ and NO radicals with polycyclic aromatic hydrocarbons adsorbed on carbonaceous particles. Part 1: PAH adsorbed on 1-2 µm calibrated graphite particles, *Atmospheric Environment*, vol.38, pp. 6063-6072.
- Esteve W., Budzinski H., Villenave E. [2006] Relative rate constants for the heterogeneous reactions of NO₂ and OH radicals with polycyclic aromatic hydrocarbons adsorbed on carbonaceous particles. Part 2: PAH adsorbed on diesel particulate exhaust SRM 1650a. *Atmos. Environ.*, vol.40, pp.201-211.
- Fécan F., Marticorena B. and G.Bergametti [1999] Parameterization of the increase of the aeolian erosion threshold wind friction velocity due to soil moisture for arid and semi-arid areas. *Annales Geophysicae*, vol. 17, pp. 149 – 157.
- Feng Y., Chen Y., Guo H., Zhi G., Xiong S., Li J., Sheng G., Fu J. [2009] Characteristics of organic and elemental carbon in PM_{2.5} samples in Shanghai, China, *Atmospheric Research*, vol.92, pp. 434-442.
- Finlayson-Pitts B.J. and J.N. Pitts [2000] *Chemistry of the upper and lower atmosphere. Theory, Experiments, and Applications*, Academic Press, San Diego, 969 p.
- Finlayson-Pitts B.J. and J.N. Pitts [1997] *Tropospheric air pollution: Ozone, Airborne Toxics, Polycyclic Aromatic Hydrocarbons, and Particles*, *Science*, vol.276, pp. 1045-1052.
- Finlayson-Pitts B.J., Wingen L.M., Summer A.L., Syomin D., Ramazan K.A. [2003] The heterogeneous hydrolysis of NO₂ in laboratory systems and outdoor and indoor atmosphere: an integrated mechanism. *Physical Chemistry Chemical Physics*, vol.5, pp.223-242.
- Friedman C.L. and N.E. Selin [2012] Long-range transport of polycyclic aromatic hydrocarbons: A global 3-D model analysis including evaluation of Arctic sources, *Environ. Sci. Technol.* 2012, in press.
- Fu P.Q., Kawamura K., Pavuluri C.M., Swaminathan T., Chen J. [2010] Molecular characterization of urban organic aerosol in tropical India: contributions of primary emissions and secondary photooxidation, *Atmos.Chem.Phys.*, vol.10, pp. 2663-2689.
- Fuzzi J., M.O. Andreae, B.J. Huebert, M. Kulmala, T.C. Bond, M. Boy, S.J.Doherty, A. Guenther, M. Kanakidou, K. Kawamura, V.-M. Kerminen, U. Lohmann, L.M., Russel, U.Poschl [2006] Critical assessment of the current state of scientific knowledge, terminology, and research needs concerning the role of organic aerosols in atmosphere, climate, and global change, *Atmos. Chem. Phys.*, vol.6, pp. 2017-2038.
- Gelencsér A. [2004] *Carbonaceous Aerosol*, Atmospheric and Oceanographic Sciences Library, vol.30, Springer, Dordrecht, The Netherlands, 352 p.
- Gelencsér A., May B., Simpson D., Sanchez-Ochoa A., Kasper-Giebl A., Puxbaum H., Caseiro A., Pio C., Legrand M. [2007] Source apportionment of PM_{2.5} organic aerosol over Europe: Primary/secondary, natural/anthropogenic, and fossil/biogenic origin, *Journal of Geophysical Research*, vol.112, D23S04.
- Gomes L., Rajot J.L., Alfaro S.C. and A. Gaudichet [2003] Validation of a dust production model from measurements performed in semi-arid agricultural areas of Spain and Niger. *Catena*, vol. 52, pp. 257 – 271.
- Government of Japan [2009] *Dioxins*, p.5.
- Guerreiro C., J.Horálek, F. de Leeuw, C. Hak, C. Nagl, P. Kurfürst, J. Ostatnická [2010] Status and trends of NO₂ ambient concentrations in Europe, ETC/ACC Technical paper 2010/19: The European Topic Centre on Air and Climate Change (ETC/ACC) is a consortium of European institutes under contract of the European Environmental Agency PBL UBA, 69 p.- http://acm.eionet.europa.eu/reports/docs/ETCACC_TP_2010_19_NO2trends.pdf.
- Guo Z. and Kamens R.M. [1991] An experimental technique for studying heterogeneous reactions of polyaromatic hydrocarbons on particle surfaces, *J. of Atmospheric Chemistry*, vol.12, pp. 137-151.

- Gusev A., E.Mantseva, V.Shatalov, B.Strukov [2005] Regional Multicompartment Model MSCE-POP EMEP/MSCE- Technical Report 5/2005.
- Gusev A., I. Ilyin, L.Mantseva, O.Rozovskaya, V. Shatalov, B. Strukov, N. Vulyh [2006a]. Persistent Organic Pollutants in the Environment. EMEP Status Report 3/2006.
- Gusev A., Ilyin I., Mantseva L., Rozovskaya O., Shatalov V. and Travnikov O. [2006b]. Progress in further development in MSCE-HM and MSCE-POP models (implementation of the model review recommendations). EMEP/MSCE- Technical report 4/2006. 114 p.
- Hakami A., D. K. Henze, J. H. Seinfeld, T. Chai, Y. Tang, G. R. Carmichael, A. Sandu [2005] *JOURNAL OF GEOPHYSICAL RESEARCH*, VOL. 110, D14301, doi:10.1029/2004JD005671.
- Hannigan M. P., Salmon L.G., Christoforou S., Gharib S.S., Butcher C.H., Cass G.R., Chow J.C., Frazier C.A. [1996] Determination of Fine Particle Concentration and Chemical Composition in the South Coast Air Basin, 1993, Final Report to the South Coast Air Quality Management District, Reno, NV 89506, 72 p.
- Harvey R.G. [1991] Polycyclic aromatic hydrocarbons: chemistry and carcinogenicity, Cambridge Monographs on Cancer Research, Cambridge University Press, 396 p.
- He Z., Kim Y.J., Ogunjobi K.O., Kim J.E., Ryu S.Y. [2004] Carbonaceous aerosol characteristics of PM_{2.5} particles in Northeastern Asia in summer 2002, *Atmos. Environ.*, vol.38, pp. 1795-1800.
- Heald C.L., A. H. Goldstein, J. D. Allan, A. C. Aiken, E. Apel, E. L. Atlas, A. K. Baker, T. S. Bates, A. J. Beyersdorf, D. R. Blake, T. Campos, H. Coe, J. D. Crouse, P. F. DeCarlo, J. A. de Gouw, E. J. Dunlea, F. M. Flocke, A. Fried, P. Goldan, R. J. Griffin, S. C. Herndon, J. S. Holloway, R. Holzinger, J. L. Jimenez, W. Junkermann, W. C. Kuster, A. C. Lewis, S. Meinardi, D. B. Millet, T. Onasch, A. Polidori, P. K. Quinn, D. D. Riemer, J. M. Roberts, D. Salcedo, B. Sive, A. L. Swanson, R. Talbot, C. Warneke, R. J. Weber, P. Weibring, P. O. Wennberg, D. R. Worsnop, A. E. Wittig, R. Zhang, J. Zheng, and W. Zheng [2008] Total observed organic carbon (TOOC) in the atmosphere: a synthesis of North American observation, *Atmos. Chem. Phys.*, vol.8, pp.2007-2025.
- Hjellbrekke A.-G. and A.-M. Fjæraa [2011] Acidifying and eutrophying compounds and particulate matter. Data Report 2009, EMEP/CCC-Report 1/2011, 139 p.
- Hjellbrekke A.-G. and Ann Mari Fjæraa [2009] Ozone measurements, EMEP/CCC-Report 2/2011, 100 p. - <http://www.nilu.no/projects/ccc/reports/cccr2-2011.pdf>.
- Ho K.F., Lee S.C., Yu J.C., Zou S.C., Fung K. [2002] Carbonaceous characteristics of atmosphere particulate matter in Hong Kong, *The Science of the Total Environment*, vol.300, p.59-67.
- Hodjamberdiev I. [2006] Determination of dioxins, furans, PCB sources and anti-POPs campaign in Central Asia. <http://www.ecoaccord.org/pop/ipep/hodjamberdiev.htm>.
- Ilyin I., A. Gusev, O. Rozovskaya, V. Shatalov, V. Sokovykh, O. Travnikov [2010] Modelling of heavy metals and persistent organic pollutants: New developments. EMEP/MSCE- Technical report 1/2010 DRAFT.
- Ilyin I., Rozovskaya O., Travnikov O., and Aas W. [2007]. Heavy metals: transboundary pollution of the environment. EMEP Status Report 2/2007. 54 pp.
- Ilyin I., Rozovskaya O., Travnikov O., Varygina M., Aas W. and Uggerud H.T. [2011]. Heavy metals: Transboundary pollution of the environment. EMEP status report 2/2011, 78p.
- IMPROVE, Report IV [2006] Spatial and Seasonal Patterns and Temporal Variability of Haze and its Constituents in the United States, /Authors: DeBell L.J., Gebhart K.A., Hand J.L., Malm W.C., Pitchford M.L., Schichtel B.A., White W.H, Cooperative Institute for Research in the Atmosphere (CIRA), Colorado State University, National Park Service, National Oceanic and Atmospheric Administration, Desert Research Institute, Crocker Nuclear Laboratory University of California, 251 p.
- Ishii S., Hisamata Y., Inazu K., Kobayashi T., Aika K. [2000] Mutagenic nitrated benzo[a]pyrene derivatives in the reaction product of benzo[a]pyrene in NO₂ – air in the presence of O₃ or under photoirradiation, *Chemosphere*, vol. 41, pp. 1809-1819.
- Jang M.S., N.M. Czoschke, S. Lee, and R.M. Kamens [2002] Heterogeneous atmospheric aerosol production by acid-catalyzed particle-phase reactions, *Science*, vol. 298 (5594), pp. 814–817.
- Joseph A.E., Unnikrishnan S., Kumar R., 2012, Chemical Characterization and Mass Closure of Fine Aerosol for Different Land Use Patterns in Mumbai City, *Aerosol and Air Quality Research*, vol.12, pp. 61-72.
- Kahan T.F., Kwamena N.-O.A., Donaldson D.J. [2006] Heterogeneous ozonation kinetics of polycyclic aromatic hydrocarbons on organic film, *Atmos. Environ.*, vol. 40, pp. 3448-3459.
- Kamens R.M. , Guo J., Guo Z., McDow S. [1990] Polynuclear aromatic hydrocarbon degradation by heterogeneous reactions with N₂O₅ on atmospheric particles, *Atmos. Environ.*, vol.24A, No.5, pp. 1161-1173.

- Kamens R.M., Guo Z., Fulcher J.N., Bell D.A. [1988] The influence of humidity and temperature on the daytime decay of polyaromatic hydrocarbons on atmospheric soot particles, *Environ. Sci. Technol.*, vol.22, No.1, pp. 103-108.
- Kamens R.M., Perry J.M., Saucy D.A., Bell D.A., Newton D.L., Brand B. [1985] Factors Which Influence PAH Decomposition on Airborne Wood Smoke Particles, *Environ. Internat.*, 11, 131-136.
- Kanakidou, M. and Seinfeld, J. H. and Pandis, S. N. and Barnes, I. and Dentener, F. J. and Facchini, M. C. and Van Dingenen, R. and Ervens, B. and Nenes, A. and Nielsen, C. J. and Swietlicki, E. and Putaud, J. P. and Balkanski, Y. and Fuzzi, S. and Horth, J. and Moortgat, G. K. and Winterhalter, R. and Myhre, C. E. L. and Tsigaridis, K. and Vignati, E. and Stephanou, E. G. and Wilson, J. [2005] Organic aerosol and global climate modelling: a review. *Atmospheric Chemistry and Physics*, 5 (4). pp. 1053-1123.
- Kim B.M., Teffera S., Zeldin M.D. [2000] Characterization of PM_{2.5} and PM₁₀ in the South Coast Air Basin of Southern California: Part 1-Spatial Variations, *Air & Waste Manage. Assoc.*, vol.50, pp. 2034-2044.
- Kim Y. S., Iwasaka Y., Shi G.-Y., Nagatani T., Shibata T., Trochkin D., Matsuki A., Yamada M., Chen B., Zhang D., Nagatani M. and H. Nakata [2004]. Dust particles in the free atmosphere over desert areas on the Asian continent: Measurements from summer 2001 to summer 2002 with balloon-borne optical particle counter and lidar, Dunhuang, China. *JOURNAL OF GEOPHYSICAL RESEARCH*, VOL. 109, D19S26, doi:10.1029/2002JD003269.
- Koerber R., Bayona J.M., Niessner R. [1999] Determination of Benzo[a]pyrene Diones in Air Particulate Matter with Liquid Chromatography Mass Spectrometry, *Environ. Sci. Technol.*, vol.33, pp. 1552-1558
- Kok J. F. [2011a]. Does the size distribution of mineral dust aerosols depend on the wind speed at emission? *Atmos. Chem. Phys.*, 11, pp. 10149 – 10156.
- Kok J. F. [2011b]. A scaling theory for the size distribution of emitted dust aerosols suggests climate models underestimate the size of the global dust cycle. *Proc. Natl. Acad. Sci., UAS*, 108, pp. 1016 – 1021.
- Kwamena N.-O.A., Thornton J.A., Abbatt J.P.D. [2004] Kinetics of surface-bound benzo[a]pyrene and ozone on solid organic and salt aerosols, *J. Phys. Chem. A*, vol.108, pp.11626-11634.
- Lazzati Z [2009] Speciation of particulate matter organic fraction and its mechanism of action on human health, Phd Tesis: [http://boaboa.unimib.it/phd_unimib_R00789_\(1-7\).pdf](http://boaboa.unimib.it/phd_unimib_R00789_(1-7).pdf).
- Legrand M. and Puxbaum H. [2007] Summary of the CARBOSOL project: Present and retrospective state of organic versus inorganic aerosol over Europe, *Journal of Geophysical Research*, vol.112, D23S01.
- Li Y.-F. [1996] Global Population Distribution Database, A Report to the United Nations Environment Programme, under UNEP Sub-Project FP/1205-95-12, March 1996.
- Lim H.-J., Turpin B.J., Russel L.M., T.S.Bates [2003] Organic and elemental carbon measurements during ACE-Asia suggest a longer atmospheric lifetime for elemental carbon, *Environ.Sci. & Technol.*, vol.37, No.14, pp. 3055-3060.
- Marchuk, G. I. [1986] Mathematical models in environmental problems. *Studies In Mathematics and Its Applications*, Vol. 16. Springer, Berlin.
- Martcorena B., Chatenet B., Rajot J. L., Traore S., Coulibaly M., Diallo A., Kone I., Maman A., NDiaye T., and Zakou A. [2010]. Temporal variability of mineral dust concentrations over West Africa: analyses of a pluriannual monitoring from the AMMA Sahelian Dust Transect. *Atmos. Chem. Phys.*, 10, 8899–8915.
- Martcorena B., Kardous M., Bergametti G., Callot Y., Chazette P., Khatteli H., Le Hégarat-Masclé S., Maillé M., Rajot J.-L., Vidal-Madjar D., Zribi M. [2006] Surface and aerodynamic roughness in arid and semiarid areas and their relation to radar backscatter coefficient. *Journal of Geophysical Research*, vol. 111, F03017.
- Matsushita H. and Iida Y. [1986] Application of capillary gas chromatography to environmental analysis. *J. High Resol. Chromatogr.*, vol.9, pp. 708–711.
- Matthias, V., Aulinger, A., Quante, M. [2009] CMAQ simulations of the benzo(a)pyrene distribution over Europe for 2000 and 2001, *Atmos. Environ.* 43, 4078-4086.
- McKendry I.G., Strawbridge K.B., O'Neill N.T., Macdonald A. M., Liu P.S.K., Leitch W.R., Kurt K.G., Jaegle L., Fairlie T.D and Westphal D.L. [2007] Trans-Pacific transport of Saharan dust to western North America: A case study. *JOURNAL OF GEOPHYSICAL RESEARCH*, VOL. 112, D01103, doi:10.1029/2006JD007129.
- Milukaitė A., Kviatkus K., Rimšelytė I., 2007, Organic and elemental carbon in coastal aerosol of the Baltic Sea, *Lithuanian Journal of Physics*, vol.47, No.2, pp. 202-210.
- Monks P.S., Granier C., Fuzzi S., Stohl A., Williams M.L., Akimoto H., Amann M., Baklanov A., Baltenspreger U., Bey I., Blake N., Blake R.S., Carslaw K., Cooper O.R., Dentener F., Fowler D., Fradkou E., Frost G.J., Generoso S., Ginoux P., Grewe V., Guenther A., Hansson H.C., Henne S., Hjorth J., Hofzumahaus A., Huntrieser H., Isaksen I.S.A., Jenkin M.E., Kaiser J., Kanakidou M., Klimont Z., Kulmala M., Laj P., Lawrence M.G., Lee J., Liousse C.,

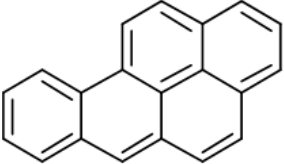
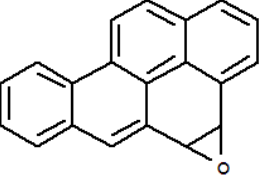
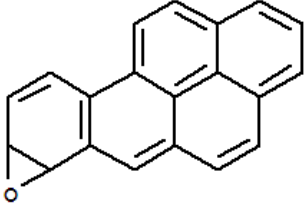
- Maione M., McFiggans G., Metzger A., Mieville A., Moussiopoulos N., Orlando J.J., O'Dowd C.D., Palmer P.I., Parrish D.D., Petzold A., Platt U., Pöschl U., Prévôt A.S.H., Reeves C.E., Reiman S., Rudich Y., Sellegri K., Steinbrecher R., Simpson D., ten Brink H., Theloke J., van der Werf G.R., Vautard R., Vestreng V., Vlachokostas Ch., von Glasow R. [2009] Atmospheric composition change – global and regional quality, *Atmos. Environ.*, vol.43, pp. 5268-5350.
- Na K., Sawant A.A., Song C., D.R.Cocker III [2004] Primary and secondary carbonaceous species in the atmosphere of Western Riverside County, California, *Atmos. Environ.*, vol.38, pp. 1345-1355.
- Nguyen Mai Lan, Bedjanian Y., Guillebeau A. [2009] Kinetics of the reaction of soot surface-bound polycyclic aromatic hydrocarbons, *J. Atmos. Chem.*, vol.62, pp. 139-150.
- Novakov T., C.E. Corrigan, J.E. Penner, C.C. Chuang, O. Rosario, O.L. Mayol Bracero [1997] Organic aerosols in the Caribbean trade winds: A natural source?, *J. of Geophysical Research*, vol. 102, No. D17, pp. 21,307-21, 313.
- Novakov, T., T.S. Bates, and P.K. Quinn [2000] Shipboard measurements of concentrations and properties of carbonaceous aerosols during ACE-2, *Tellus B*, vol.52 (2), pp.228–238.
- Öberg T. [2007] Low-temperature formation and degradation of chlorinated benzenes, PCDD and PCDF in dust from steel production, *Science of the Total Environment*, 382, pp. 153-158.
- Oehme M. and Mueller M.D. [1995] Levels and congener patterns of polychlorinated dibenzo-p-dioxins and dibenzofurans in solid residues from wood-fired boilers/ Influence of combustion conditions and fuel type, *Chemosphere*, 30, 8, pp. 1527-1539.
- Organic chemistry of the atmosphere [1991] Hansen Lee D. and Eatough Delbert J., Editors, CRC Press (Boca Raton), 343 p.
- Pacyna J.M., K. Breivik, J. Münch, J. Fudala [2003]. European atmospheric emissions of selected persistent organic pollutants, 1970-1995. *Atmos. Environ.*, vol. 37, pp.S119-S131.
- Pandis, S. N., S. E. Paulson, J. H. Seinfeld, and R. C. Flagan [1991] Aerosol formation in the photooxidation of isoprene and β -pinene, *Atmos. Environ.*, vol. 25A, pp. 997– 1008.
- Park S.S., Bae M.S., Kim Y.J. [2001a] Chemical Composition and source apportionment of PM_{2,5} Particles in the Sihwa Area, Korea, *J. Air & Waste Manage. Assoc.*, vol.51, pp. 393-405.
- Park S.S., Kim Y.J., Fung K. [2001] Characteristics of PM_{2,5} carbonaceous aerosol in the Sihwa industrial area, South Korea, *Atmos. Environ.*, vol.35, pp. 657-665.
- Perraudin E., Budzinski H., Villenave E., [2005] Kinetic study of the reactions of NO₂ with polycyclic aromatic hydrocarbons adsorbed on silica particles, *Atmos. Environ.*, vol.39, pp. 6557-6567
- Persson, C., Rodhe, H. and De Geer, L. E. [1987] The Chernobyl accident - A meteorological analysis of how radionuclides reached and were deposited in Sweden. *Ambio*, 16, pp. 20-31.
- Pio C.A., Castro L.M., Cequeira M.A., Santos I.M., Belchior F., Salgueiro M.L. [1996] Source assessment of particulate air pollutants measured at the southwest European coast, *Atmos. Environ.*, vol.30, No.19, pp.3309-3320.
- Pio C.A., M. Legrand, T. Oliveira, J. Afonso, C.Sanytos, A. Caseiro, P. Fialho, F.Barata, H. Puxbaum, A. Sanchez-Ochoa, A.Kasper-Giebl, A. Gelencsér, S. Preunkert, M. Schock [2007] Climatology of aerosol composition (organic versus inorganic) at nonurban sites on a west-east transect across Europe, *Journal of Geophysical Research*, vol.112, D23S02.
- Pio C.A., M. Legrand, C.A. Alves, T. Oliveira, J. Afonso, A. Caseiro, H. Puxbaum, A. Sanchez-Ochoa, A. Gelencsér [2008] Chemical composition of atmospheric aerosols during the 2003 summer intense forest fire period, *Atmos. Environ.*, vol.42, pp. 7530-7543.
- Pitts, J. N. , Paur H-R., Zielinska B, Arey J., Winer A. M., Ramdahl T. Mejia V. [1986] Factors influencing the reactivity of polycyclic aromatic hydrocarbons adsorbed on filters and ambient POM with ozone, *Chemosphere*, 15, 675-685.
- PORG [1997] Ozone in the United Kingdom 1997. Fourth Report of the United Kingdom, Photochemical Oxidants Review Group. Department of the Environment, London.
- Pöschl U. [2005] Atmospheric Aerosols: Composition, Transformation, Climate and Health Effects, *Angewandte Chemie*, vol.44, pp. 7520 – 7540.
- Pöschl U., Letzel T., Schauer C., Niessner R. [2001] Interaction of ozone and water vapor with spark discharge soot aerosol particles coated with benzo[a]pyrene: O₃ and H₂O adsorption, benzo[a]pyrene degradation and atmospheric implications, *J. Phys. Chem. A*, vol.105, pp. 4029-4041.
- Pulles T., Kok H. and U.Quass [2006] Application of the emission inventory model TEAM: uncertainties in dioxin emission estimates for central Europe. *Atmos. Environ.*, vol.40, pp.2321-2332.

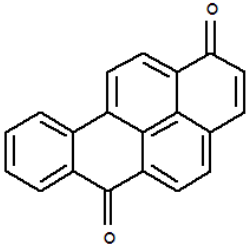
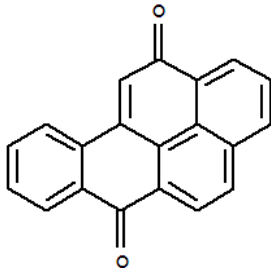
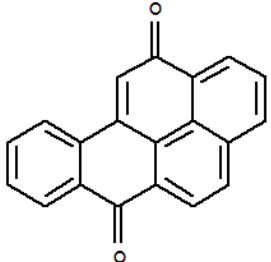
- Putaud J.-P., van Dingenen R., Mangoni M., Virkkula A., Raes F., Maring H., Prospero J.M., Sweitlicki E., Berg O.H., Hillamo R., Mäkelä T. [2000] Chemical mass closure and assessment of the origin of the submicron aerosol in the marine boundary layer and the free troposphere at Tenerife during ACE-2, *Tellus*, vol.52B, pp. 141-168.
- Reisen F. and Arey J. [2005] Atmospheric Reactions Influence Seasonal PAH and Nitro-PAH Concentrations in the Los Angeles Basin, *Environ. Sci. Technol.*, vol. 39 (1), pp 64–73.
- Rinaldi M., Decesari S., Finessi E., Giulianelli L., Carbone C., Fuzzi S., O'Dowd C.D., Ceburnis D., Facchini M.C. [2010] Primary and secondary organic marine aerosol and oceanic biological activity: Recent results and new perspectives for future studies, *Advances in meteorology*, article ID 310682, pp.1-10.
- Robertson [2004] Extended back-trajectories by means of adjoint equations. Swedish Meteorological and Hydrological Institute, RMK 105, August 2004.
- Rogge W.F., Hildemann L.M., Mazurek M.A., Cass M.A., Simoneit B.R.T. [1991] Sources of fine organic aerosol. 1.Charbroilers and meat cooking operations. *Environ. Sci. Technol.*, vol.25, pp. 1112–1125.
- Schaap M., M. Roemer, F. Sauter, G. Boersen, R. Timmermans, and P. G. H. Bultjes [2005] LOTOS-EUROS: documentation, TNO report B&O-A R 2005/297.
- SEPA [2009] The role of pentachlorophenol treated wood for emissions of dioxins into the environment, Report 5935, 2009.
- Sera N., Kai M., Horikawa K., Fukuhara K., Miyata N. and Tokiwa H. [1991] Detection of 3,6-dinitrobenzo(a)pyrene in airborne particulates. Mutation Research/ Fundamental and Molecular Mechanisms of Mutagenesis or Genetic Toxicology and Environmental Mutagenesis, vol. 263, pp. 27–32.
- Shao Y. and Yang Y. [2005] A scheme for drag partition over rough surfaces. *Atmospheric Environment*, vol. 39, pp.7351-7361.
- Shao Y., Ishizuka M., Mikami M. and Leys J.F. [2011]. Parameterization of size-resolved dust emission and validation with measurements. *JOURNAL OF GEOPHYSICAL RESEARCH*, Vol 116, D08203, doi:10.1029/2010JD014527.
- Shimizu A., Sugimoto N., Matsui I., Arai K., Uno I., Murayama T., Kagawa N., Aoki K., Uchiyama A. and Yamazaki A. [2004]. Continuous observations of Asian dust and other aerosols by polarization lidars in China and Japan during ACE-Asia. *JOURNAL OF GEOPHYSICAL RESEARCH*, VOL. 109, D19S17, doi:10.1029/2002JD003253.
- Shiraiwa M., Sosedova Y., Rouviere A., Yang H., Zhang Y., Abbatt J.P.D., Ammann M., Pöschl U. [2011] The role of long-lived reactive oxygen intermediates in the reaction of ozone with aerosol particles, *Nature Chemistry*, vol.3, pp.291-295 (88 -92?).
- Simoneit, B.R.T., J.J. Schauer, C.G. Nolte, D.R. Oros, V.O. Elias, M.P. Fraser, W.F. Rogge, and G.R. Cass [1999] Levoglucosan, a tracer for cellulose in biomass burning and atmospheric particles, *Atmos. Environ.*, vol.33, No.2, pp.173–182.
- Simoneit B.R.T., Kobayashi M., Mochida M., Kawamura K., Lee M., Lim H.-J., Turpin B.J., Komazaki Y. [2004] Composition and major sources of organic compounds of aerosol particulate matter sampled during the ACE-Asia campaign, *Journal of Geophysical Research*, vol.109, D19S10.
- Simpson D., K. E. Yttri, Z. Klimont, K. Kupiainen, A. Caseiro, A. Gelencsér, C. Pio, H. Puxbaum, M. Legrand [2007]. Modelling carbonaceous aerosol over Europe: Analysis of the CARBOSOL and EMEP EC/OC campaigns, *Journal of Geophysical Research*, vol. 112, D23S14, 26 pages.
- Sodemann H., Palmer A. S., Schwierz C., Schwikowski M., and Wernli H. [2006]. The transport history of two Saharan dust events archived in an Alpine ice core. *Atmos. Chem. Phys.*, 6, 667–688.
- Tang N., Araki Y., Tamura K., Dong L., Zhang X., Liu Q., Li R., Kameda T., Toriba A., Hayakawa K. [2009] Distribution and Source of Atmospheric Polycyclic Aromatic Hydrocarbons and Nitropolycyclic Aromatic Hydrocarbons in Tieling City, Liaoning Province, a Typical Local City in Northeast China, *Asian Journal of Atmospheric Environment*, vol.3-1, pp. 52-58.
- Toxicological Profile for polycyclic aromatic hydrocarbons [1995] U.S. Department of health and human services, Agency for Toxic Substances and Disease Registry (ASTDR), 487 p.
- Tsigaridis K., M. Kanakidou [2003] Global modelling of secondary organic aerosol in the troposphere: A sensitivity analysis, *Atmos. Chem. Phys.* 2003, vol.3, No.5, pp.1849-1869.
- Uliasz M. [1987] Application of influence functions in numerical modelling of air pollution dispersion. *Przegląd Geofizyczny*, Warsaw. Vol. 32, no. 1, pp. 3-19.
- UNEP [1999] Dioxin and Furan Inventories. National and Regional Emissions of PCDD/PCDF. Prepared by UNEP Chemicals. Geneva, Switzerland.

- Vega E., Ruiz H., Escalona S., Cervantes A., Lopez-Veneroni D., Gozalez-Avalos E., Sanchez-Reyna G. [2011] Chemical composition of fine particles in Mexico City during 2003-2004, *Atmospheric Pollution Research*, vol.2, pp. 477-483.
- Venier M., Ferrario J and Hites R.A. [2009] Polychlorinated dibenzo(p)dioxins and dibenzofurans in the atmosphere around Great Lakes, *Environ. Sci. Technol.*, vol. 43, pp. 1036 – 1041.
- Villani M. G., P. Bergamaschi, M. Krol, J. F. Meirink, and F. Dentener, 2010. Inverse modeling of European CH₄ emissions: sensitivity to the observational network, *Atmos. Chem. Phys.*, 10, 1249–1267.
- Wang G., Kawamura K., Lee S., Ho K., Cao J. [2006] Molecular, Seasonal, and Spatial Distributions of Organic Aerosols from Fourteen Chinese Cities, *Environ.Sci.Technol.*, vol.40, No.15, pp. 4619-4625.
- Wayne, R.P., Barnes, I., Biggs, P., Burrows, J.P., Canosa-Mas, C.E., Hjorth, J., Le Bras, G., Moortgat, G.K., Perner, D., Poulet, G., Restelli, G., Sidebottom, H. [1991] The nitrate radical: physics, chemistry and the atmosphere. *Atmos. Environ.*, 25A (1), 1-206.
- Williams B.J., Goldstein A.H., Kreisberg N.M., Hering S.V. [2006] An in -situ instrument for speciated organic composition of atmospheric aerosols: Thermal desorption aerosol GM/MS-FID (TAG), *Aerosol Science and Technol.*, vol.40, pp. 627-638.
- Wolf G.T., Ruthkosky M.S., Stroup D.P., Korsog P.E., Ferman M.A. [1986] *Atmos.Environ.*, vol.20, No.6, pp. 1229-1239.
- Wu C.H., I. Salmeen, H. Niki [1984] Fluorescent spectroscopic studies of reaction between gaseous ozone and surface-adsorbed polycyclic aromatic hydrocarbons, *Environ. Sci. Technol.*, vol.18, pp.1004-1006.
- Xu J., Bergin M.H., Greenwald R., Schauer J.J Shafer M.M., Jean L. Jaffrezo J.L., and Aymoz G. [2004]. Aerosol chemical, physical, and radiative characteristics near a desert source region of northwest China during ACE-Asia. *JOURNAL OF GEOPHYSICAL RESEARCH*, VOL. 109, D19S03, doi:10.1029/2003JD004239.
- Yttri et al. [2011] Transboundary particulate matter in Europe [2011] EMEP Status report 4/2011, Ed. by Karl Espen Yttri, Joint CCC, MSC-W, CEIP and CIAM, 129 p.
- Yttri K.E., Simpson D., Nøjgaard J.K., Kristensen K., Genberg J., Stenström K., Swietlicki E., Hillamo R., Aurela M., Bauer H., Offenberg J.H., Jaoui M., Dye C., Eckhardt S., Burkhardt J.F., Sthol A., Glasius M., [2011] Source apportionment of the summer time carbonaceous aerosol at Nordic rural background sites, *Atmos. Chem. Phys.*, vol.11, pp. 13339-13357.
- Yttri K.E., W.Aas, A.Bjerke, J.N. Cape, F. Cavalli, D.Ceburnis, C.Dye, L.Embllico, M.C.Facchini, C Foster, J.C.Hansson, S.G. Jennings, W. Maenhaut, J.P. Putaud, K. Tørseth [2007] Elemental and organic carbon in PM₁₀: a one year measurement campaign within the European Monitoring and Evaluation Programme EMEP, *Atmos.Chem. Phys.*, vol.7, pp. 5711-5725.
- Zhang BN, Meng F, Shi CN, Yang FQ, Wen DY, et al. [2009] Modeling the atmospheric transport and deposition of polychlorinated dibenzo-p-dioxins and dibenzofurans in North America. *Atmospheric Environment*, vol. 43, pp. 2204-2212.
- Zhou S., Lee A., McWhinney R., Abbatt J. [2011] Effect of Organic Coatings on the Heterogeneous Reactivity of Ozone with Particle Borne PAHs: http://presentations.copernicus.org/EGU2011-2557_presentation.pdf.
- Zhou S., Lee A.K., McWhinney R.D., Abbatt J.P.D. [2012] Burial Effect of organic coatings on the heterogeneous reactivity of particle-borne Benzo[a]pyrene (BaP) toward ozone, *J.Phys. Chem. A*, vol.116 (26), pp. 7050-7056.
- Ziemba L.D., Dibbs J.E., Griffin R.J., Anderson C.H., Whitlow S.I., Lefer B.L., Rappenglück B., Flynn J. [2010] Heterogeneous conversion of nitric acid to nitrous acid on the surface of primary organic aerosol in an urban atmosphere, *Atmos. Environ.*, vol.44, pp. 4081-4089.

Annex A. B[a]P degradation products

Table A. 1. Main characteristics of B[a]P and some its oxidation products

Substance IUPAC name and CAS number.	Chemical formula	Structure	Molecular mass	Hazard classification
Benzo[a]pyrene (Synonyms: 3,4-Benz[a]pyrene;3,4-Benzopyrene;3,4- Benzpyrene) CAS 50-32-8	C ₂₀ H ₁₂		252.32	Carcinogen of group 2A IARC Cancer Review: http://www.lookchem.com/Benzo-a-pyrene/
Benzo[a]pyrene-4,5-oxide Synonyms: 4,5-Dihydrobenzo[a]pyrene 4,5- oxide; Benzo[a]pyrene 4,5-epoxide; Benzo[a]pyrene4,5-oxide; Benzopyrene CAS 37574-47-3	C ₂₀ H ₁₂ O		268.32	Strong mutagen Californian Air Resources Board, 1994) http://www.mfe.govt.nz/publications/air/air-quality-tech-report-43/html/page10.html .
Benzo[a]pyrene 7,8-oxide Synonyms: Benzo[10,11]chryseno[1,2- b]oxirene, Benzo[a]pyrene 7,8-epoxide CAS 36504-65-1	C ₂₀ H ₁₂ O		268.32	Questionable carcinogen with experimental carcinogenic, neoplastigenic, and tumorigenic data. Mutation data reported. http://www.lookchem.com/cas-375/37574-47-3.html

Substance IUPAC name and CAS number.	Chemical formula	Structure	Molecular mass	Hazard classification
Benzo[a]pyrene-1,6-dione (Synonyms: 1,6-Dihydrobenzo[a]pyrene-1,6-dione; Benzo[a]pyrene-1,6-quinone) CAS 3067-13-8	$C_{20}H_{10}O_2$		282.30	Questionable carcinogen with experimental neoplastigenic data by skin contact. Mutation data reported. http://www.lookchem.com/benzo-a-pyrene-1-6-dione/
Benzo[a]pyrene-6,12-dione (Synonyms: benzo[a]pyrene-3,6-dione; Benzo[a]pyrene-3,6-quinone) CAS 3067-14-9	$C_{20}H_{10}O_2$		282.30	Questionable carcinogen with experimental neoplastigenic data by skin contact. Human mutation data reported. http://www.lookchem.com/benzo-a-pyrene-3-6-dione/
Benzo[a]pyrene-6,12-dione (Synonyms: 6,12-Dihydrobenzo[a]pyrene-6,12-dione; Benzo[a]pyrene-6,12-quinone) CAS 3067-12-7	$C_{20}H_{10}O_2$		282.30	Questionable carcinogen with experimental neoplastigenic data. Mutation data reported. http://www.lookchem.com/cas-306/3067-12-7.html

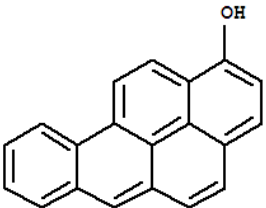
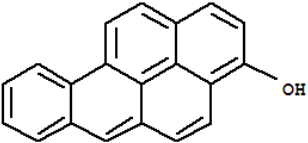
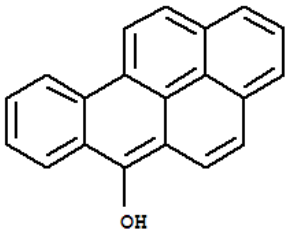
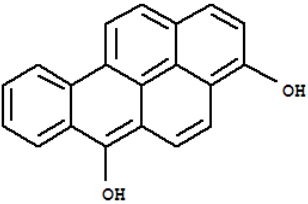
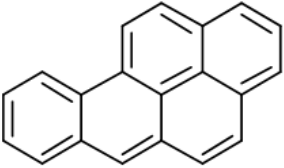
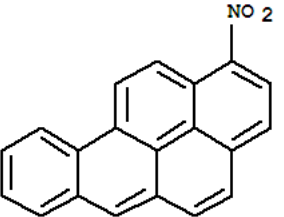
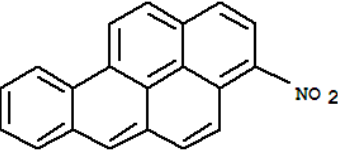
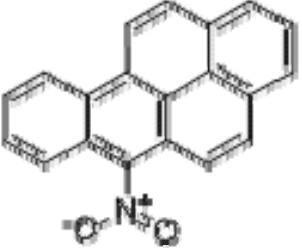
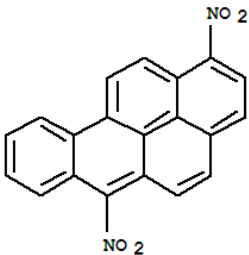
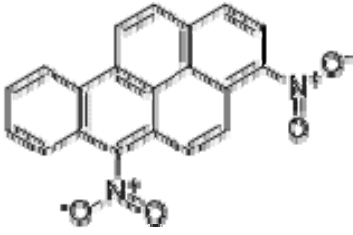
Substance IUPAC name and CAS number.	Chemical formula	Structure	Molecular mass	Hazard classification
1-Hydroxybenzo[a]pyrene or Benzo[a]pyren-1-ol CAS 13345-23-8	$C_{20}H_{12}O$		268.32	
Benzo[a]pyren-3-ol (Synonyms: 3-Hydroxy-3,4-benzo[a]pyrene; 3-Hydroxybenzo[a]pyrene; 3-Hydroxybenzopyrene) CAS 13345-21-6	$C_{20}H_{12}O$		268.32	Questionable carcinogen with experimental tumorigenic and neoplastigenic data by skin contact. Human mutation data reported. http://www.lookchem.com/Benzo-a-pyren-3-ol/
Benzo[a]pyren-6-ol (Synonyms: 5-Hydroxy-3,4-benzopyrene; 6-Hydroxybenzo[a]pyrene) CAS 33953-73-0	$C_{20}H_{12}O$		268.32	Questionable carcinogen with experimental neoplastigenic and tumorigenic data. Mutation data reported. http://www.lookchem.com/benzo-a-pyren-6-ol/
Benzo[a]pyrene-3,6-diol (Synonyms: 3,6-Dihydroxybenzo[a]pyrene; Benzo[a]pyrene-3,6-hydroquinone) CAS 63148-10-7	$C_{20}H_{12}O_2$		284.308	

Table A 2. Main characteristics of B[a]P and some its nitroderivatives

Substance IUPAC name and CAS number.	Chemical formula	Structure	Molecular mass	Hazard classification
Benzo[a]pyrene (Synonyms: 3,4-Benz[a]pyrene; 3,4-Benzopyrene;3,4-Benzpyrene) CAS 50-32-8	C ₂₀ H ₁₂		252.32	Carcinogen of group 2A IARC Cancer Review: http://www.lookchem.com/Benzo-a-pyrene/
1-Nitrobenzo(a)pyrene (Synonyms: Benzo[a]pyrene,1-nitro-) CAS 70021-99-7	C ₂₀ H ₁₁ NO ₂		297.32	Mutation data reported http://www.lookchem.com/cas-700/70021-99-7.html
3-Nitrobenzo(a)pyrene (Synonyms: Benzo[a]pyrene,3-nitro-) CAS 70021-98-6	C ₂₀ H ₁₁ NO ₂		297.32	Mutation data reported
6-Nitrobenzo(a)pyrene (Synonyms: Benzo[a]pyrene,6-nitro-) CAS 63041-90-7	C ₂₀ H ₁₁ NO ₂		297.32	Carcinogen of group 3 International Agency for Research on Cancer (IARC) - Summaries and Evaluations: http://www.inchem.org/documents/iarc/vol46/46-08.html Questionable carcinogen. Human mutation data reported. http://www.lookchem.com/6-NITROBENZ-a-PYRENE/

Substance IUPAC name and CAS number.	Chemical formula	Structure	Molecular mass	Hazard classification
1,6-dinitrobenzo[a]pyrene (Synonyms: Benzo(a)pyrene, 1,6-dinitro-) CAS 128714-75-0	$C_{20}H_{10}N_2O_4$		342.32	Mutagen http://www.chemcas.com/msds/cas/msds29/128714-75-0.asp
Benzo(a)pyrene, 3,6-dinitro- (Synonyms: Benzo(a)pyrene, 3,6-dinitro-) CAS 128714-76-1	$C_{20}H_{10}N_2O_4$		342.32	Mutagen http://www.chemcas.com/msds/cas/msds29/128714-76-1.asp

Annex B.

OBSERVED OC MASS CONCENTRATIONS

Location	Longitude	Latitude	Time period	OC concentration, $\mu\text{g C/m}^3$	Field campaigns, Project or Program	Reference
Background, marine remote						
Enewetak atoll, Marshall Island	162°E	11°N	Juli, 1979	0.44		<i>Chesselet et al., 1981</i>
Sargasso Sea	50°W	30°N	Apryl-May 1979	0.97		
Bermuda, Atlantic Ocean	64.5°W	32.2°N	January-February 1983	0.57		<i>Wolf et al., 1986</i>
Cape San Juan, Puerto Rico, Atlantic Ocean	66.1°W	18.5°N	February-May 1995	0.39		<i>Novakov et al., 1997</i>
San Nicolas Island, USA	119.3 W	33.15 N	January-December 1993	0.65	South Coast Air Quality Management District (SCAQMD)	<i>Hannigan et al., 1996</i>
San Nicolas Island, USA	119.3 W	33.15 N	January 1995-February 1996	1.49	South Coast Air Quality Management District (SCAQMD)	<i>Kim et al., 2000</i>
Arão, Portugal, northwestern coast	8°47'W	40°30'N	November 1993-August 1994	0.52 – pure maritime periods	EC Project - Background Maritime Contribution to Atmospheric Pollution in Europe (BMCAPE)	<i>Pio et al., 1996</i>
Tenerife, Atlantic Ocean	35-55°W	20-55°N	June – July 1997	0.17 – 0.20	Second Aerosol Characterization Experiment (ACE-2)	<i>Putaud et al., 2000</i>
Atlantic Ocean, coasts of Portugal and North Africa	7° – 15°W	29° – 41°N	June – July 1997	0.1 – 2.8	Second Aerosol Characterization Experiment (ACE-2)	<i>Novakov et al., 2000</i>
Punto del Hidalgo, Spain, Canary islands, Tenerife, Atlantic Ocean	16° 19' W	28° 34'N	June – July 1997	0.52	Second Aerosol Characterization Experiment (ACE-2)	<i>Novakov et al., 2000</i>
Sagres, Atlantic Ocean, Portugal	16° 19' W	28° 34'N	June – July 1997	0.75	Second Aerosol Characterization Experiment (ACE-2)	<i>Novakov et al., 2000</i>
North-western Atlantic Ocean			July-August 2002	4.5	New England Air Quality Study (NEAQS) on NOAA research vessels	<i>Bates et al., 2006</i>
North-western Atlantic Ocean			July-August 2004	2.9	International Consortium for Atmospheric Research on Transport and Transformation (ICARTT) or New England Air Quality Study (NEAQS-2004) on NOAA research vessels	<i>Bates et al., 2006</i>
Terceira Island in Azorean Islands, North-Eastern Atlantic Ocean, Portugal	27° 21' W	38° 41' N	July 2002–June 2004	0.33	Present and Retrospective State of Organic versus Inorganic Aerosol over Europe: Implications for Climate – EU Project CARBOSOL	<i>Alves et al., 2007</i>
			summer (September 2002 – September 2004)	0.38		<i>Pio et al., 2007 and Legrand and Puxbaum, 2007</i>
			winter (September 2002 – September 2004)	0.27		
Preila, Curonian Spit, coast of the Baltic Sea	21°.04'E	55° 21' N	19-18 June 2006	1,29	EMEP Station -LT15 and Global Earth Observation and Monitoring of the atmosphere (GEOMON)	<i>Milukaite et al., 2007</i>
Birkines, Norway	8°15'E	58°23'N	August-September 2009	0,84	EMEP station - NO ₂ ; Global Atmospheric Watch (GAW); Secondary Organic aerosol in the Nordic RurAL Environment study (SONORA)	<i>Yttri et al., 2011</i>
Hyytiala, Finland	24°17'E	61°51'N	August-September 2009	1,6	Station for Measuring Forest Ecosystem-	<i>Yttri et al., 2011</i>

Location	Longitude	Latitude	Time period	OC concentration, $\mu\text{g C/m}^3$	Field campaigns, Project or Program	Reference
Vavihill, Sweden	13°09'E	56°01'N	August-September 2009	1.1	Atmosphere Relations- SMEAR-II; Secondary Organic aerosol in the NOrdic RurAL Environment study (SONORA) EMEP station – SE11; European Supersites for Atmospheric Research – EUSAAR; Secondary Organic aerosol in the NOrdic RurAL Environment study (SONORA)	<i>Yttri et al., 2011</i>
Pacific Ocean, offshore Hawaii	178 °W	20-33°N	March 2001	0.21	Asian Aerosol Characterization Experiment (ACE-Asia)	<i>Lim et al., 2003</i>
Miyakejima, offshore of Hachijo Island, Japan	139° 32 'E	34° 04'N	March 2001	1.86	Asian Aerosol Characterization Experiment (ACE-Asia)	<i>Lim et al., 2003</i>
Sea of Japan	126°-133° E	32-38°N	April 2001	0.66-0.91	Asian Aerosol Characterization Experiment (ACE-Asia)	<i>Lim et al., 2003</i>
East China Sea	129° E	32° N	April 2001	0.6	Asian Aerosol Characterization Experiment (ACE-Asia)	<i>Lim et al., 2003</i>
Chichi-jima Island	142°11' E	27° 06 N	April 1990	1.4	Asian Aerosol Characterization Experiment (ACE-Asia)	<i>Simoneit et al., 2004</i>
			June 1990	0.28		
			September 1991	0.76		
Arabian Peninsula, North Indian Ocean	45-108°E	0-36° N	February-March 1999	0.49	Experiment in North Indian Ocean (NIO) during An International Field Experiment in the Indian Ocean (INDOEX)	<i>Bates et al., 2006</i>
Indian Subcontinent, North Indian Ocean				0.77		
Kaashido, ground station, Malé Atoll, Maldives	73.5°E	5 °N	February-March 1999	2.7		
Muztagh Ata Mountain, Tibet, China	75°02'E	38°17'N	December 2003-February 2005	0.48		<i>Cao et al, 2009</i>
Rural, semirural						
Long Beach, USA	118°9' W	33°49'N	January-December 1993	3.98	South Coast Air Quality Management District (SCAQMD)	<i>Hannigan et al., 1996</i>
Rubidoux, California, USA	117.44 ° W	34.0° N	January 1995-February 1996	1.09	South Coast Air Quality Management District (SCAQMD)	<i>Kim et al, 2000</i>
Acadia National Park, Maine, USA	68.26 ° W	44.37 ° N	March 1996-February 1999	1.47	Federal Government program – Interagency Monitoring of Protected Visual Environments (IMPROVE)	<i>Chung and Seinfeld, 2002</i>
Badlands National Park, South Dakota, USA	101.94 ° W	43.74 ° N	March 1996-February 1999	1.13	IMPROVE	<i>Chung and Seinfeld, 2002</i>
Bandelier National Monument, New Mexico, USA	106.27 ° W	35.78 ° N	March 1996-February 1999	1.14	IMPROVE	<i>Chung and Seinfeld, 2002</i>
Big Band National Park, Texas, USA	103.18 ° W	29.30 ° N	March 1996-February 1999	1.45	IMPROVE	<i>Chung and Seinfeld, 2002</i>
Boundary Waters Canoe Area, Minnesota, USA	101.94 ° W	43.74 ° N	March 1996-February 1999	1.47	IMPROVE	<i>Chung and Seinfeld, 2002</i>
Bryce Canyon National Park, Utha, USA	112.17 ° W	37.42 ° N	March 1996-February 1999	0.99	IMPROVE	<i>Chung and Seinfeld, 2002</i>
Bridger Wilderness, Wyoming, USA	109.76 ° W	42.98 ° N	March 1996-February 1999	0.94	IMPROVE	<i>Chung and Seinfeld, 2002</i>

Location	Longitude	Latitude	Time period	OC concentration, $\mu\text{g C}/\text{m}^3$	Field campaigns, Project or Program	Reference
Brigantine National Wildlife Refuge, New Jersey, USA	74.45 ° W	39.47 ° N	March 1996-February 1999	2.39	IMPROVE	<i>Chung and Seinfeld, 2002</i>
Canvonlands National Park, Utah, USA	109.82 ° W	38.46 ° N	March 1996-February 1999	0.82	IMPROVE	<i>Chung and Seinfeld, 2002</i>
Chassahowitzka National Wildlife, Florida, USA	82.55 ° W	28.75 ° N	March 1996-February 1999	2.78	IMPROVE	<i>Chung and Seinfeld, 2002</i>
Chiricahua National monument, Arizona, USA	109.39 ° W	32.01 ° N	March 1996-February 1999	0.92	IMPROVE	<i>Chung and Seinfeld, 2002</i>
Crater Lake National Park, Oregon, USA	122.14 ° W	42.90 ° N	March 1996-February 1999	1.10	IMPROVE	<i>Chung and Seinfeld, 2002</i>
Denali National Park, Alaska, USA	148.97 ° W	63.72 ° N	March 1996-February 1999	0.67	IMPROVE	<i>Chung and Seinfeld, 2002</i>
Dolly Sods/Otter Creek Wilderness, West Virginia, USA	79.43 ° W	39.11 ° N	March 1996-February 1999	2.44	IMPROVE	<i>Chung and Seinfeld, 2002</i>
Glacier National Park, Montana, USA	114.00 ° W	48.51 ° N	March 1996-February 1999	2.52	IMPROVE	<i>Chung and Seinfeld, 2002</i>
Great Basin National Park, Nevada, USA	114.22 ° W	39.01 ° N	March 1996-February 1999	1.03	IMPROVE	<i>Chung and Seinfeld, 2002</i>
Hopi Point (Grand Canyon), Arizona, USA	112.15 ° W	36.07 ° N	March 1996-February 1999	0.73	IMPROVE	<i>Chung and Seinfeld, 2002</i>
Great Sand Dunes National Monument, Colorado, USA	105.52 ° W	37.72 ° N	March 1996-February 1999	0.92	IMPROVE	<i>Chung and Seinfeld, 2002</i>
Great Smokey Mountains National Park, Tennessee, USA	83.94 ° W	35.63 ° N	March 1996-February 1999	2.91	IMPROVE	<i>Chung and Seinfeld, 2002</i>
Guadalupe Mountains National Park, Texas, USA	1041.81 ° W	31.83 ° N	March 1996-February 1999	1.01	IMPROVE	<i>Chung and Seinfeld, 2002</i>
Jarbridge Wilderness, Nevada, USA	115.43 ° W	41.89 ° N	March 1996-February 1999	1.07	IMPROVE	<i>Chung and Seinfeld, 2002</i>
Lassen Volcanic National Park, California, USA	121.58 ° W	40.44 ° N	March 1996-February 1999	1.38	IMPROVE	<i>Chung and Seinfeld, 2002</i>
Lone Peak Wilderness, Utah, USA	111.71 ° W	40.44 ° N	March 1996-February 1999	1.56	IMPROVE	<i>Chung and Seinfeld, 2002</i>
Lye Brook Wilderness, Vermont, USA	73.12 ° W	43.15 ° N	March 1996-February 1999	1.52	IMPROVE	<i>Chung and Seinfeld, 2002</i>
Mammoth Cave National Park, Kentucky, USA	86.15 ° W	37.13 ° N	March 1996-February 1999	2.83	IMPROVE	<i>Chung and Seinfeld, 2002</i>
Mesa Verde National Park, Colorado, USA	108.49 ° W	37.20 ° N	March 1996-February 1999	0.91	IMPROVE	<i>Chung and Seinfeld, 2002</i>
Moosehorn National Wildlife Refuge, Maine, USA	67.26 ° W	45.12 ° N	March 1996-February 1999	1.70	IMPROVE	<i>Chung and Seinfeld, 2002</i>
Mount Rainier National Park, Washington, USA	122.12 ° W	46.76 ° N	March 1996-February 1999	2.05	IMPROVE	<i>Chung and Seinfeld, 2002</i>
Mount Zirkel Wilderness, Colorado, USA	106.73 ° W	40.47 ° N	March 1996-February 1999	0.82	IMPROVE	<i>Chung and Seinfeld, 2002</i>
Okfenokee National Wildlife Refuge, Georgia, USA	82.13 ° W	30.74 ° N	March 1996-February 1999	2.99	IMPROVE	<i>Chung and Seinfeld, 2002</i>
Petrified Forest National Park, Arizona, USA	109.77 ° W	35.08 ° N	March 1996-February 1999	1.07	IMPROVE	<i>Chung and Seinfeld, 2002</i>
Pinnacles National Monument,	121.16 ° W	36.49 ° N	March 1996-February 1999	1.78	IMPROVE	<i>Chung and Seinfeld, 2002</i>

Location	Longitude	Latitude	Time period	OC concentration, $\mu\text{g C/m}^3$	Field campaigns, Project or Program	Reference
California, USA						
Point Reyes National Seashore, California, USA	122.90 ° W	38.12 ° N	March 1996-February 1999	1.23	IMPROVE	<i>Chung and Seinfeld, 2002</i>
Redwood National Park, California, USA	124.08 ° W	41.56 ° N	March 1996-February 1999	0.98	IMPROVE	<i>Chung and Seinfeld, 2002</i>
Cape Romain National Wildlife Refuge, South Carolina, USA	76.99 ° W	32.94 ° N	March 1996-February 1999	2.80	IMPROVE	<i>Chung and Seinfeld, 2002</i>
Rocky Mountain National Park, Colorado, USA	105.55 ° W	40.28 ° N	March 1996-February 1999	1.02	IMPROVE	<i>Chung and Seinfeld, 2002</i>
San Geronio Wilderness, California, USA	116.90 ° W	34.18 ° N	March 1996-February 1999	2.04	IMPROVE	<i>Chung and Seinfeld, 2002</i>
Sequoia National Park, California, USA	118.82 ° W	36.50 ° N	March 1996-February 1999	3.28	IMPROVE	<i>Chung and Seinfeld, 2002</i>
Shenandoah National Park, Virginia, USA	78.43 ° W	38.52 ° N	March 1996-February 1999	2.20	IMPROVE	<i>Chung and Seinfeld, 2002</i>
Shining Rock Wilderness, North Carolina, USA	82.77 ° W	35.39 ° N	March 1996-February 1999	1.79	IMPROVE	<i>Chung and Seinfeld, 2002</i>
Sipsy Wilderness, Alabama, USA	87.31 ° W	34.34 ° N	March 1996-February 1999	3.40	IMPROVE	<i>Chung and Seinfeld, 2002</i>
Snoqualamie Pass, Washington, USA	121.43 ° W	47.42 ° N	March 1996-February 1999	1.45	IMPROVE	<i>Chung and Seinfeld, 2002</i>
Three Sisters, Oregon, USA	122.04 ° W	44.29 ° N	March 1996-February 1999	1.49	IMPROVE	<i>Chung and Seinfeld, 2002</i>
Tonto National Monument, Arizona, USA	111.11 ° W	33.65 ° N	March 1996-February 1999	1.28	IMPROVE	<i>Chung and Seinfeld, 2002</i>
Upper Buffalo Wilderness, Arkansas, USA	93.20 ° W	35.83 ° N	March 1996-February 1999	2.35	IMPROVE	<i>Chung and Seinfeld, 2002</i>
Weminuche Wilderness, Colorado, USA	107.80 ° W	37.66 ° N	March 1996-February 1999	0.76	IMPROVE	<i>Chung and Seinfeld, 2002</i>
Yellowstone National Park, Wyoming, USA	110.40 ° W	44.57 ° N	March 1996-February 1999	1.32	IMPROVE	<i>Chung and Seinfeld, 2002</i>
Yosemite National Park, California, USA	119.70 ° W	37.71 ° N	March 1996-February 1999	2.28	IMPROVE	<i>Chung and Seinfeld, 2002</i>
New York, Botanical Garden, USA	73°52'W	40°52'N	January- December 2000	3.41	PM2.5 Technical Assessment and Characterization study in New York – “PM2.5 Supersite” in New York	<i>Burkhard et al., 2008</i>
Pinnacle State Park, USA	77.21W	42.09N	January- December 2001	1.68	“PM2.5 Supersite” in New York	<i>Burkhard et al., 2008</i>
Whiteface Mountain, USA	73°54'W	44°22'N	January- December 2001	1.13	“PM2.5 Supersite” program in New York State.	<i>Burkhard et al., 2008</i>
Rochester, USA	77.67W	43.12N	January- December 2001	2.00	“PM2.5 Supersite” in New York	<i>Burkhard et al., 2008</i>
Buffalo, USA	78°52'W	42°53'N	January- December 2002	2.67	“PM2.5 Supersite” in New York	<i>Burkhard et al., 2008</i>
Arão, Portugal, northwestern coast	8°47'W	40°30'N	November 1993-August 1994	2.73		
Aveiro, Portugal	8°38' W	40°34'N	July – August 2002, May-August 2003, June 2004	3.47	Present and Retrospective State of Organic versus Inorganic Aerosol over Europe: Implications for Climate – EU Project CARBOSOL	<i>Gelencsèr et al., 2007</i>
			December 2002, January-February 2003, December 2003-January 2003	12.3		

Location	Longitude	Latitude	Time period	OC concentration, $\mu\text{g C}/\text{m}^3$	Field campaigns, Project or Program	Reference
Aveiro, Portugal	8°38'W	40°34'N	Summer 2003	2,6 – baseline period	EU Project CARBOSOL	<i>Pio et al</i> , 2008
				6,4 – very intense fires		
Aveiro, Portugal	8°38' W	40°34'N	summer (September 2002 – September 2004)	3.10	EU Project CARBOSOL	<i>Pio et al</i> , 2007 and <i>Legrand and Puxbaum</i> , 2007
			winter (September 2002 – September 2004)	7.50		
Puy de Dôme, France	2° 57'E	45°46' N	December 2002, January and December 2003	0.65	EU Project CARBOSOL	<i>Gelencsér et al.</i> , 2007
			June 2003	4.63		
Puy de Dôme, France	2° 57'E	45°46' N	summer (September 2002 – September 2004)	2.40	EU Project CARBOSOL	<i>Pio et al</i> , 2007 and <i>Legrand and Puxbaum</i> , 2007
			winter (September 2002 – September 2004)	0.79		
Schauinsland, Global Atmosphere Watch (GAW) station, Germany	07° 54'E	47°55'N	December 2002, January and December 2003	1.38	EU Project CARBOSOL	<i>Gelencsér et al.</i> , 2007
			June – August 2003	3.80		
Schauinsland, Global Atmosphere Watch (GAW) station, Germany	07° 54'E	47°55'N	summer (September 2002 – September 2004)	3.40	EU Project CARBOSOL	<i>Pio et al</i> , 2007 and <i>Legrand and Puxbaum</i> , 2007
			winter (September 2002 – September 2004)	1.37		
Sonnblick, Austria	12° 57'E	47°03'N	summer (September 2002 – September 2004)	1.38	EU Project CARBOSOL	<i>Pio et al</i> , 2007 and <i>Legrand and Puxbaum</i> , 2007
			winter (September 2002 – September 2004)	0.48		
K-Puszta, Hungary	19° 35'E	46°58'N	July-August 2002, May 2003, August-September 2003	4.52	EU Project CARBOSOL	<i>Gelencsér et al.</i> , 2007
			November-December 2002, February and December 2003, January-February 2004	8.91		
K-Puszta, Hungary	19° 35'E	46°58'N	summer (September 2002 – September 2004)	4.90	EU Project CARBOSOL	<i>Pio et al</i> , 2007 and <i>Legrand and Puxbaum</i> , 2007
			winter (September 2002 – September 2004)	7.40		
Illmitz, Austria	16° 46'E	47° 46'N	July – December 2002	5.320	EMEP EC/OC campaign, EMEP station – AT02	EMEP particulate matter data: http://www.nilu.no/projects/cc/c/emepdata.html
			January -July 2003	5.798		
Ghent, Belgium	3°43'E	51°03'N	July – December 2002	4.254	EMEP EC/OC campaign, EMEP station – BE05	EMEP particulate matter data
			January -July 2003	3.973		
Košetice, Czech Republic	15° 05'E	49° 35'N.	July – December 2002	3.855	EMEP EC/OC campaign, EMEP station – CZ03	EMEP particulate matter data
			January -July 2003	4.996		

Location	Longitude	Latitude	Time period	OC concentration, $\mu\text{g C/m}^3$	Field campaigns, Project or Program	Reference
Langenbrügge (Waldhof), Germany	10° 45'E	52° 48'N.	July – December 2002	4.535	EMEP EC/OC campaign, EMEP station – DE 02	EMEP particulate matter data
			January -July 2003	4.996		
Virolahti, Finland	27° 41'E	60° 31'N.	July – December 2002	2.373	EMEP EC/OC campaign, EMEP station – Fi17	EMEP particulate matter data
			January -July 2003	1.802		
Penicuil, United Kingdom	3° 14' 00"W	55 49' 00"	July – December 2002	1.392	EMEP EC/OC campaign, EMEP station – GB46	EMEP particulate matter data
			January -July 2003	1.667		
Mace Head, Ireland	09° 54'W	53° 20'N	July – December 2002	0.962	EMEP EC/OC campaign, EMEP station – IE31	EMEP particulate matter data
			January -July 2003	1.477		
Ispra, Italy	08° 38'E	45° 48'N.	July – December 2002	7.154	EMEP EC/OC campaign, EMEP station – IT04	EMEP particulate matter data
			January -July 2003	8.332		
San Pietro Capofiume, Italy	11 °37'E	44 ° 39' N	July – December 2002	6.069	EMEP EC/OC campaign, EMEP station – IT-08	EMEP particulate matter data
			January -July 2003	5.758		
Kollumerwaard, Netherlands	6° 17'E	53° 20'N	July – December 2002	2.95	EMEP EC/OC campaign, EMEP station – INL09	EMEP particulate matter data
			January -July 2003	2.252		
Birkenes, Norway	8° 15'E	58° 23'N	July – December 2002	1.027	EMEP EC/OC campaign, EMEP station – NO01	EMEP particulate matter data
			January -July 2003	1.059		
Braganza, Portugal	06° 46'W	41° 49'N	July – December 2002	2.899	EMEP EC/OC campaign, EMEP station – PT01	EMEP particulate matter data
			January -July 2003	5.304		
Aspvreten, Sweden	17° 23'E	58° 48'N	July – December 2002	2.168	EMEP EC/OC campaign, EMEP station – SE12	EMEP particulate matter data
			January -July 2003	2.07		
Stará Lesná, Slovakia	20° 17'E	49° 09'N	July 2002-July 2003	4.32	EMEP EC/OC campaign, EMEP station – SK04	<i>Yttri et al., 2007</i>
Lille Valby, Denmark	12°08'E	55°41'N	August-September 2009	2.1	Station Danish Air Quality Monitoring Programme (LMP), Secondary Organic aerosol in the NOrdic RurAL Environment study (SONORA)	<i>Yttri et al., 2011</i>
Urban, industrial						
Los Angeles, USA	118° 9'W	34° 3'N	January-December 1993	5.15	South Coast Air Quality Management District (SCAQMD)	<i>Hannigan et al., 1996</i>
Los Angeles, USA	118° 9'W	34° 3'N	January 1995-February 1996	7.74		<i>Na et al., 2004</i>
Mira Loma, USA	118° 29'W	33° 59'N	September 2001-January 2002	10.8		<i>Na et al., 2004</i>
St Louis, USA	90° 12' W	38° 35' N	January- December 2002	3.88	Supersite program in St. Louis Midwest Air Quality Study for the Pittsburg	<i>Bae et al., 2004</i>
Pittsburg, USA	79° 57' W	40° 27' N	January - February 2002	2.35		<i>Heald et al., 2008</i>
			July-August 2002	5.16		
Mexico City, the United Mexican States	99° 22' W	19° 03' N	November 2003, March 2004, November 2004	7.31 – 12.90		<i>Vega et al., 2011</i>
	99° 12' W	19° 24' N	March 2006	12.8		<i>Heald et al., 2008</i>
Sao Paulo, Brazil	46 ° 37' W	23° 32' S	July-September 1997	15.8		<i>Na et al., 2004</i>

Location	Longitude	Latitude	Time period	OC concentration, $\mu\text{g C}/\text{m}^3$	Field campaigns, Project or Program	Reference
Sihwa, South Korea	126° 44' E	37° 21' N	June 1998	4.9		<i>Park et al., 2001</i>
			February 1998 – November 1999	9.87		<i>Park et al., 2001a</i>
Gwangju, South Korea	126.85° E	35.16° N	July-August 2002	1.4		<i>He et al., 2004</i>
Gosan, South Korea	126° 48' E	34° 38' N	March-April 2001	3.1	Asian Aerosol Characterization Experiment (ACE-Asia) – North-West Pacific Ocean	<i>Bates et al., 2006</i>
			April 2001	7.0	Asian Aerosol Characterization Experiment (ACE-Asia)	<i>Simoneit et al., 2004</i>
Sapporo, Japan	141° 21' E	43° 4' N	April 2001	10.35	Asian Aerosol Characterization Experiment (ACE-Asia)	<i>Simoneit et al., 2004</i>
			June-July 2001	4.0		
			September 2001	1.5		
			January 2002	4.5		
Seoul, South Korea	126° 58' E	37° 34' N	June, 1999	10.30		<i>Park et al., 2001</i>
Beijing, China	116.4° E	39.9° N	July-August 2002	12.4		<i>He et al., 2004</i>
			January 2003	27.2		<i>Cao et al., 2007</i>
			June-July 2003	17.2		
Changchun, China	125.3° E	43.9° N	January 2003	39.2		<i>Cao et al., 2007</i>
			June-July 2003	12.5		
Jinchang, China	101.1° E	38.3° N	January 2003	23.0		<i>Cao et al., 2007</i>
			June-July 2003	8.1		
Qingdao, China	120.3° E	36° N	January 2003	26.6		<i>Cao et al., 2007</i>
			June-July 2003	5.0		
Tianjin, China	117.2° E	39.1° N	January 2003	38.9		<i>Cao et al., 2007</i>
			June-July 2003	16.5		
Xi'an, China	108.9° E	34.2° N	January 2003	102.3		<i>Cao et al., 2007</i>
			June-July 2003	27.3		
Yulin, China	109.8° E	38.3° N	January 2003	32.5		<i>Cao et al., 2007</i>
			June-July 2003	13.7		
Chongqing, China	106.5° E	29.5° N	January 2003	76.7		<i>Cao et al., 2007</i>
			June-July 2003	25.1		
Guangzhou, China	113.2° E	23.1° N	January 2003	41.1		<i>Cao et al., 2007</i>
			June-July 2003	10.6		
			August – September 2004	17.5	This project was supported by the Research Grants Council of Hong Kong (No. 40318003) and National Natural Scientific Foundation of China (No. 40590392).	<i>Duan et al., 2007</i>
			February -March 2005	23.9		
Hong Kong, China	114.1° E	22.2° N	November 2000- February 2001	5.52-10.16		<i>Ho et al., 2002</i>
			January 2003	11.2		<i>Cao et al., 2007</i>
			June-July 2003	7.3		
			August – September 2004	11.8	This project was supported by the Research Grants Council of Hong Kong (No. 40318003) and National Natural	<i>Duan et al., 2007</i>

Location	Longitude	Latitude	Time period	OC concentration, $\mu\text{g C}/\text{m}^3$	Field campaigns, Project or Program	Reference
			February -March 2005	11.4	Scientific Foundation of China (No. 40590392).	
Hangzhou, China	120,1° E	30.2°N	January 2003	30.6		<i>Cao et al., 2007</i>
			June-July 2003	17.1		
Shanghai, China	121,4° E	31.2°N	January 2003	28.6		<i>Cao et al., 2007</i>
			June-July 2003	13.3		
Shanghai, campus Shanghai University, China	121,29° E	31.14°N	October in 2005, January, April, and July in 2006	14.7		<i>Feng et al., 2009</i>
Wuhan, China	114,2° E	30.5°N	January 2003	38.2		<i>Cao et al., 2007</i>
			June-July 2003	14.2		
Xiamen, China	118,1° E	24.4°N	January 2003	16.5		<i>Cao et al., 2007</i>
			June-July 2003	4.8		
Kaohsiung City, Taiwan	120° 27'	23° 03'N	November 1998-April 1999	10.4		<i>He et al., 2004</i>
Kyoto, Japan	135°46' E	35°0' N	July-August 2002	5.0		<i>He et al., 2004</i>
Sapporo, Japan	141° 21' E	43° 4' N	May-July 2005	7.4		<i>Aggarwal and Kawamura, 2009</i>
			August 2005	3.5		<i>Aggarwal et al., 2011</i>
Ulaanbaatar (Ulan-Bator), Mongolia	106°54'E	47°55'N	July-August 2002	2.3		<i>He et al., 2004</i>
Madras, India	80,17°E	13.04°N	January-February 2007	9.12		<i>Fu et al., 2010</i>
			May 2007	3.65		
Colaba, Mumbai, India	72 °48' E	18 °54' N	2007-2008	20.4		<i>Joseph et al., 2012</i>
Dadar, west, Mumbai, India	72 °51' E	19 °1' N	2007-2008	28.4		<i>Joseph et al., 2012</i>
Khat west, Mumbai, India	72 °50' E	19 °4' N	2007-2008	31.3		<i>Joseph et al., 2012</i>
Mahul, Mumbai, India	72,89 E	19.02° N	2007-2008	26.13		<i>Joseph et al., 2012</i>

